PRECIPITATION CHANGES NEAR THREE GORGES DAM, CHINA

by

FANG ZHAO

(Under the Direction of J. Marshall Shepherd)

ABSTRACT

After Three Gorges Dam (TGD) was built in June 2003, the water level abruptly rose from 66 to 135 m. A second-order polynomial relationship between upstream water level and reservoir surface area is found using Landsat ETM+ images. The impact of TGD on regional precipitation is examined using NASA Tropical Rainfall Measuring Mission (TRMM) Multisatellite Precipitation Analysis (TMPA) from 1998 to 2009. Satellite estimates are found to have good quality after verifying with rain gauges following several methods. Monthly epoch analyses are performed. While composites of heavy rain days (top 25 percentile) do not show major distinguishable changes, composites of moderate rain days (mid 50 percentile) suggest that in the “Post Dam” periods, moderate precipitation is greatly reduced in the vicinity of the reservoir, while increased on both sides away from the reservoir. Overall, this analysis presents one of the most thorough and long-term analyses of TGD-hydroclimate relationships to date.

INDEX WORDS: Precipitation, TRMM, Three Gorges Dam, Climate, Land Use/Land Cover

# PRECIPITATION CHANGES NEAR THREE GORGES DAM, CHINA

by

FANG ZHAO

B.S., Peking University, China, 2009

A Thesis Submitted to the Graduate Faculty of The University of Georgia in Partial Fulfillment of the Requirements for the Degree

MASTER OF SCIENCE

ATHENS, GEORGIA

2011

PRECIPITATION CHANGES NEAR THREE GORGES DAM, CHINA

by

FANG ZHAO

| | |
|---|---|
| Major Professor: | J. Marshall Shepherd |
| Committee: | Thomas L. Mote |
| | Faisal Hossain |

Electronic Version Approved:

Maureen Grasso
Dean of the Graduate School
The University of Georgia
May 2011

# ACKNOWLEDGEMENTS

I would like to thank my thesis committee members for helpful advice, especially my major professor, J. Marshall Shepherd. He is always inspirational during our meetings, and I constantly benefit from his insightful guidance. It is such a joy to do research with him and make progresses in my master's study. I am lucky to study at UGA, and it is a great experience to have a very supportive advisor and a nice warm department. I would also like to thank my family and friends for their support. I thank my former research advisor Dr. Xinyi Zhao for sending me ground observation data. I acknowledge the UGA Graduate School for providing the funding for my research and study at UGA.

TABLE OF CONTENTS

Page

LIST OF TABLES

Page

LIST OF FIGURES

Page

# CHAPTER 1

# INTRODUCTION

Land surface changes such as expansion or contraction of lakes have a direct effect on the atmosphere through energy and moisture exchanges. Lakes absorb and store heat in the spring and summer, and release heat in the autumn and winter. The fluctuation of the lake areas plays a significant role in surface energy budget by altering surface albedo and energy partitioning [*Plank and Shuman*, 2009]. Besides altering local albedo and evaporation, Scott and Huff [1996] found the relatively cooler water of the Great Lakes can stabilize the atmosphere over the water in summer, thereby decreasing rainfall over the lake areas while increasing precipitation in the downwind direction. Although these studies are based on lakes, large reservoirs resulting from dam-driven inundation of land could impact local/regional climate with similar mechanisms. The notion that a large reservoir could be built to alter the natural precipitation patterns in the vicinity is not new [*Eltahir and Bras*, 1996]. More than sixty years ago, Jensen [1935] suggested such an idea to "engineer" rainfall. This notion has been debated by Holzman [1937] and Horton [1943]. Huntley et al. [1998] investigated vegetation adjacent to a reservoir in northern England and concluded that a major component of the vegetation changes observed can only readily be accounted for by an alteration in local climate due to the reservoir. More recently, Degu et al. [2011] have found evidence of altered precipitation and atmospheric stability parameters around large U.S. dams in certain climate regimes (arid/Mediterranean). Overall, the hydroclimatic effects of reservoirs are still inconclusive and region dependent. A better understanding of what a dam/reservoir might be doing to precipitation in its vicinity over the decadal timescales has implications for both the traditional dam planners/operators and the society.

## 1.1 Motivation

After Three Gorges Dam (TGD) was built in June 2003, the water level abruptly rose from 66 to 135 m (above sea level). This project in China has become the largest hydroelectric project in the world since the water level rose again to 156m in 2006. More than 600 $km^2$ of land, which were settlements, farmlands and forests, are now under water (Fig. 1.1). In October 2010, the water level upstream of the dam finally reached the designated 175 m, after two failed attempts at raising the water level to 175 m in 2008 and 2009 due to insufficient upstream discharge. Built on the main stream of the Yangtze River, the third longest river in the world, the unprecedented TGD is an interesting engineering achievement with profound influence. Millions of people have moved away from their homes; and the farmers who stayed have to work on newly resettled farms with steeper slopes and lower crop yields after the inundation. On the other hand, more people are using the cost-efficient hydroelectric power every day. Managers of the project need to control the water level in accord with climate conditions and achieve a balance between flood prevention and electricity generation. The research community is still debating the environmental cost and economic gain. A severe drought event occurred in Sichuan and Chongqing (upstream of the reservoir) in 2006, followed by an unusual flood in 2007. Although it is unlikely that the newly built project had such an immediate impact on climate, possible drought/flood events in the future have drawn much attention from the public. Therefore, hydroclimatic research on the effects of this project will be valuable for various stakeholders.

The resettled farmers, for example, would be concerned about precipitation changes. Resettlement problems have long been documented in this historically isolated and underdeveloped region where economic development is deterred by the harsh biophysical environment, overpopulation, and meager capital input [*Chau*, 1995]. A large part of the Three Gorges region was found to have already exceeded the population carrying capacity in 1985 [*Gao and Chen*, 1987]. This overcapacity problem is intensified by a significant portion of people who migrated to other regions returning. As reported by many news sources in 2009 (for example, as reported in http://news.ifeng.com/mainland/200912/1217_17_1477933.shtml), people had problems adapting to the

lifestyle far away from home with their limited skills and difficulty understanding the local language. It is therefore a very difficult situation for the resettled farmers, given that the new areas for farming are both limited in quality and quantity relative to the demand. Resettled farmers rely on their farms as the main source of income. These new farms rely on precipitation as a major water supply since irrigation systems are sparse and costly for the uphill terrace farms. A possible decrease in precipitation would further exacerbate the agricultural production of the resettled farmers. An increase in precipitation in these areas, however, would exacerbate landslide hazards in this mountainous region, especially as many forested areas are replaced by farmland and constructions. All these concerns make it interesting and of practical importance to examine the temporal patterns of precipitation and quantify if and how the project has altered precipitation since the water level rose. It is also useful to resolve the spatial patterns to ascertain how different regions will be affected with different precipitation trends.

While the Three Gorges Area is a research hotspot, little literature exists on the hydroclimatic effects of the reservoir, partly because these effects are less apparent, unlike landslides or reduction in downstream flow. A few previous observational and modeling studies have built a good foundation for understanding the hydroclimatic effects of TGD, but due to insufficient data and the complicated circulation patterns and topography of the Three Gorges Area, the influence of TGD on regional climate remains unclear. Previous studies relied on limited sources of data, which are different from one another, and they reached contradicting conclusions. Such disagreements highlight the need for more observational and modeling research in this area.

Miller et al. [2005] performed two simulations, control and land use change, for an eight week period (2 April – 16 May 1990) to determine the sensitivity of the local climate around the Three Gorges Dam. Results indicated that strong evaporation was offset by sinking moist air diverging away from the region, and no net change in precipitation was found (Fig. 1.2). They conceded that simulations at 10 km were not fine enough and suggested that 1 km multi-year simulations were needed. Their simulations were limited to the resolution of their model, accuracy of input data and reliability of parameterization. Wu et al. [2006] examined the effect of the TGD on the regional precipitation around the vicinity of the TGD by

analyzing the Tropical Rainfall Measuring Mission (TRMM) Multisatellite Precipitation Analysis (TMPA) rain rate data for an eight-year period (January 1998 to January 2006), and they concluded that after the TGD water level rose abruptly, rain rate had increased in the northern part of the region between the Daba and Qinling Mountains and had decreased in the vicinity of the TGD (Fig. 1.3). Their study considered the climatic effects of the TGD at the regional scale (~100km) rather than at the local scale (~10km). A quick analysis of the changes of TMPA rain rate for the two periods January 1998–January 2003 and January 2004–January 2009 is performed. Fig. 1.4 shows the resulted spatial pattern overlaying topography heights. This pattern was hypothesized to be related to the effects of Three Gorges Dam–reservoir system. The first drawback of their study is that they did not use point-source observation data to assess the accuracy of satellite data in this region. Also, the 2003 El Nino likely affected the precipitation variability in the region as well. Furthermore, a recent study by Xiao et al. [2010] pointed out that the precipitation change observed before and after the reservoir filling might have been caused by natural variability because a similar change of precipitation was observed before and after 1980 (Fig. 1.5). Xiao et al. [2010] analyzed the decadal variation of annual precipitation in the vicinity of the TGD using daily data from 27 rain gauges from 1960 to 2005, and they concluded that the variation in precipitation around the TGD shown by Wu et al. [2006] is part of the natural interannual oscillation of precipitation. However, the sparse observational records Xiao et al. used may not accurately depict climate conditions in this region, because the point-sampling of rain gauges may not truthfully represent the spatial distribution of precipitation in an area with complicated topography, which happens to be the case in this region. Besides, their observed phenomenon might result from factors like instrumental errors, interpolation methods and replacement of old rain gauges by new ones. Even if the pattern they observed is accurate, it does not directly answer the unresolved question whether the TGD has any effects on rainfall, or if the precipitation change is completely related to natural variation.

Obviously, previous studies could be more convincing if they had not relied on a single source of data. The lack of consensus in previous research and the huge concerns on the TGD highlight the importance of this study. Besides using a longer study period and multiple data sources, this study also

addresses the noticeable changes in water level of the Three Gorges Reservoir occurring in recent years. In addition to two abrupt changes in 2003 and 2006, there are also seasonal variations. Unlike a natural river in a region where rainfall is abundant in warm season, the water level of the reservoir is low in summer and high in winter. During 2008-2010, the water level was approximately 145 m in summer and 170 m in winter, respectively. This variation results in fluctuation of water surface area and influences the energy and water balance. This important but possibly under-addressed phenomenon will be analyzed in this study.

## 1.2 Research Objectives

The primary objectives of this research are as follows:

1. Quantify the relationship between annual and seasonal water level change and the fluctuation of the Three Gorges Reservoir area.
2. Assess the spatial-temporal trend of rainfall based on observation-verified TMPA data as water level of the reservoir changes.

The first objective seeks to quantify the relationship between annual and seasonal water level change and the fluctuation of the Three Gorges Reservoir water surface area. The water level upstream of the dam has exhibited several jumps and stable stages since it was first monitored in 2002 (Fig. 1.6), and the current management practice keeps the water level low in summer and high in winter, indicating varied seasonal effects. It is hypothesized that there is some type of second-order polynomial relationship between the area of Three Gorges Reservoir (TGR) and measured water level upstream of TGD. Based on data from numerous reservoir/sedimentation survey reports from the U.S. Bureau of Reclamation (http://www.usbr.gov/pmts/sediment/projects/ReservoirSurveys/index.html), the relationship is formulated as

$$y = a_1 + a_2x + a_3x^2$$

where y is reservoir area, x is water level/elevation, $a_1$ is an intercept, and a2 and a3 are coefficients. To simplify the problem and use fewer Landsat scenes, the reservoir area in this study is defined not to

include the tributaries. Landsat images at five different stages are used to determine the respective reservoir surface area, and the calculated reservoir areas at the five stages are then correlated with the corresponding water level upstream of the dam.

The second objective is to assess the spatial-temporal trend of rainfall based on observation-verified TMPA data as the reservoir changes. With this study, we provide the longest study record to date and capture multiple El Nino cycles, which previous studies lacked. The hypothesis is that (1) the TMPA estimates will be relatively well correlated with point-sources rain gauge estimates and (2) rain rate decreases near TGR and increases in the climatological downwind direction as the reservoir expands. NASA's Tropical Rainfall Measuring Mission Multisatellite Precipitation Analysis (TMPA) rain rate data from 1998 to 2009 are used. This study is the first to verify the satellite estimates with rain gauges in this region. After multiple verification procedures, an epoch analysis is designed to assess the regional hydroclimatic effects of the dam. Monthly 700 hPa and 850 hPa geopotential height composite maps for the 12 years are generated to assess the large-scale synoptic environment and primary wind direction. For each month in the rainy season (April-October), the geopotential height map of each year is compared with the composite of that month, and years with abnormal synoptic conditions (i.e., primary wind direction not in the same quadrant with and 45 degrees away from that of the composite, position of high and low height centers, etc.) are marked and excluded. Based on the water level data, the remaining years are divided into three epochs: "pre-dam", "post-dam" and "post-dam II" (post dam with further water level rise while reaching the designated 175 m water level). Heavy rain days (top 25 percentile) and moderate rain days (mid 50 percentile) for the whole area are selected from each epoch, and composite analyses will be applied. Light rain days (bottom 25 percentile) mostly have an average rain rate below 1 mm $d^{-1}$, and satellite-based precipitation estimates at this magnitude of rainfall have a much larger uncertainty (Tian and Peters-Lidard [2010]). Therefore, the composite of light rain days may not provide reliable interpretations.

The hydroclimatic research on the effects of TGD has implications in many aspects. Previous studies on this topic have shortcomings, and there is no consensus in their conclusions. This work seeks to acquire a better understanding on the spatial-temporal changes of rainfall in the study area after the water level rises. Also, the relationship between the upstream water level change and the fluctuation of reservoir surface is examined.

**Fig. 1.1**. A Yangtze River village that is now underwater as the water level rose. It is on a small island of the Lesser Three Gorges River which is a tributary of the Yangtze River. Photograph taken by Hershel Gattis on July 7, 2005 (http://www.flickr.com/photos/tnwanderer/223645928/).

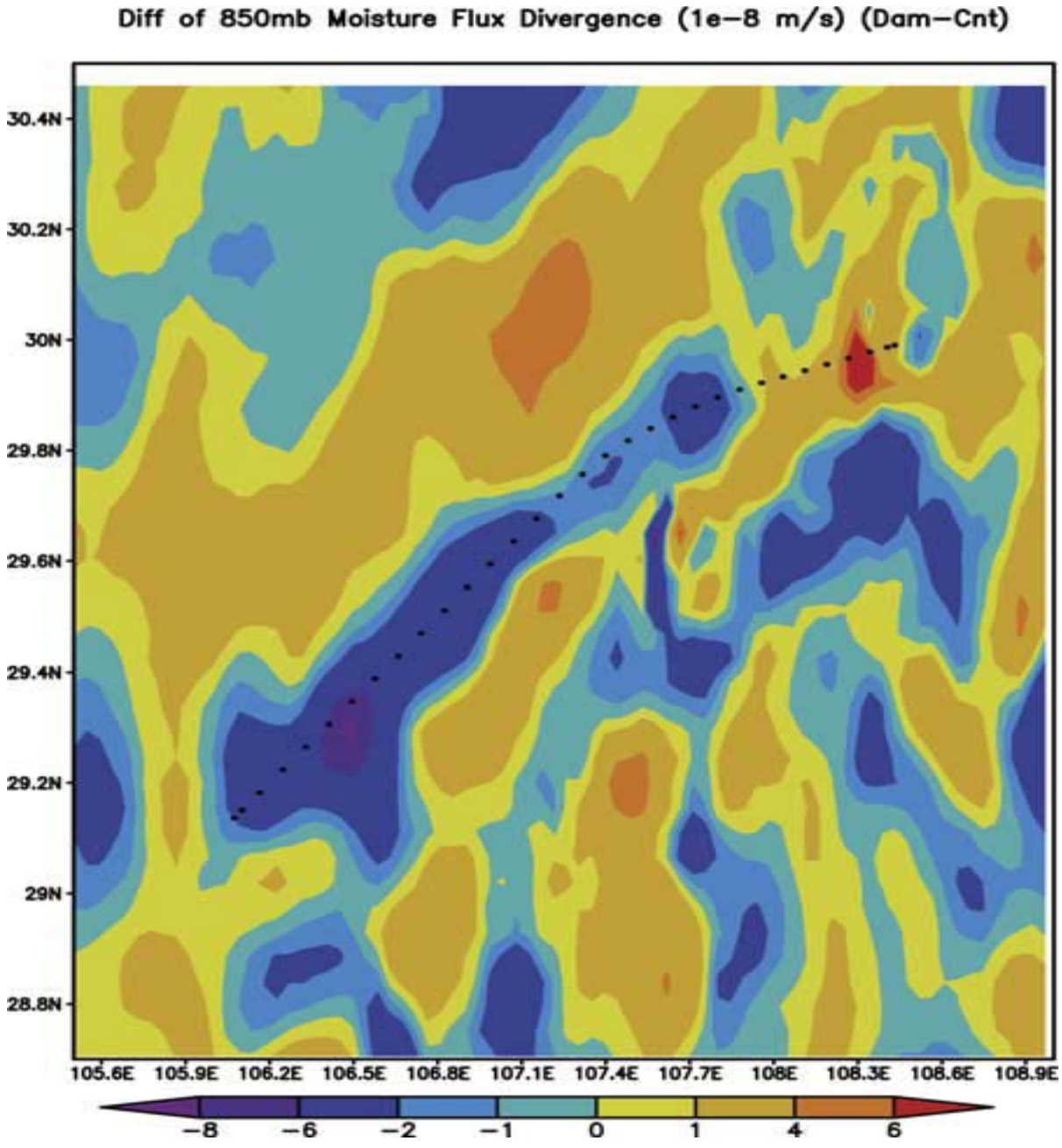


**Fig. 1.2**. The 850 mb moisture flux divergence ($10^{-8}$ m $s^{-1}$) difference between the change due to the Three Gorges Dam and the control simulation (from Miller et al. 2005).

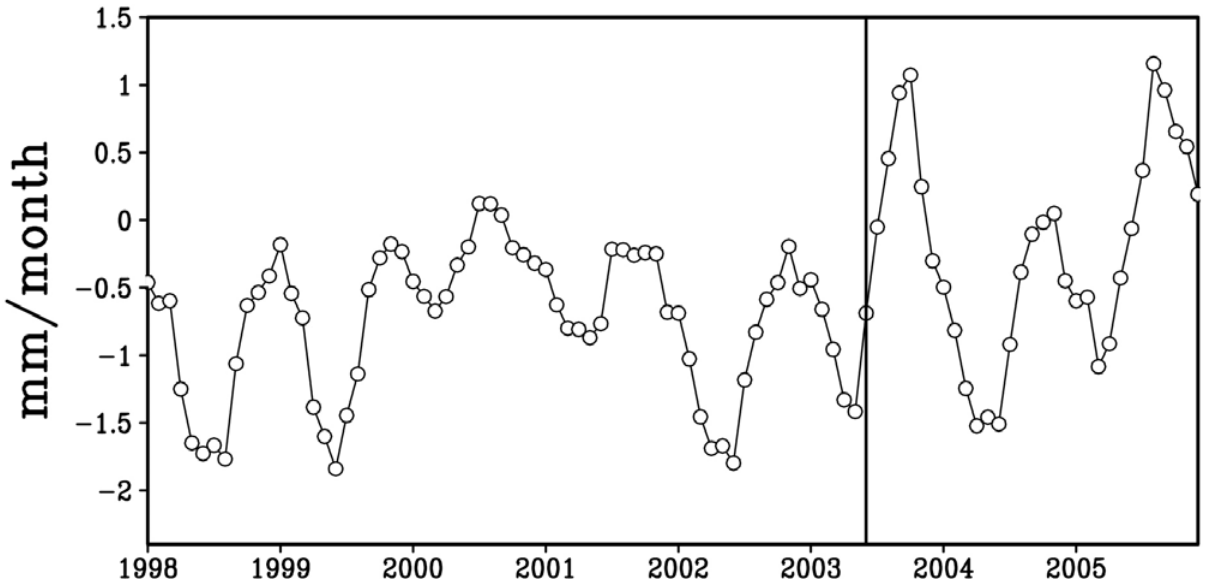


**Fig. 1.3**. Time series of the difference of the TMPA rain rate between the region north of the Yangtze River (31.0–34.0°N, 107.0–111.0°E) and the whole TGD area (28.0–34.0°N, 107.0–111.0°E). The vertical line indicates when the TGD water level rose to 135 m (from Wu et al. 2006).

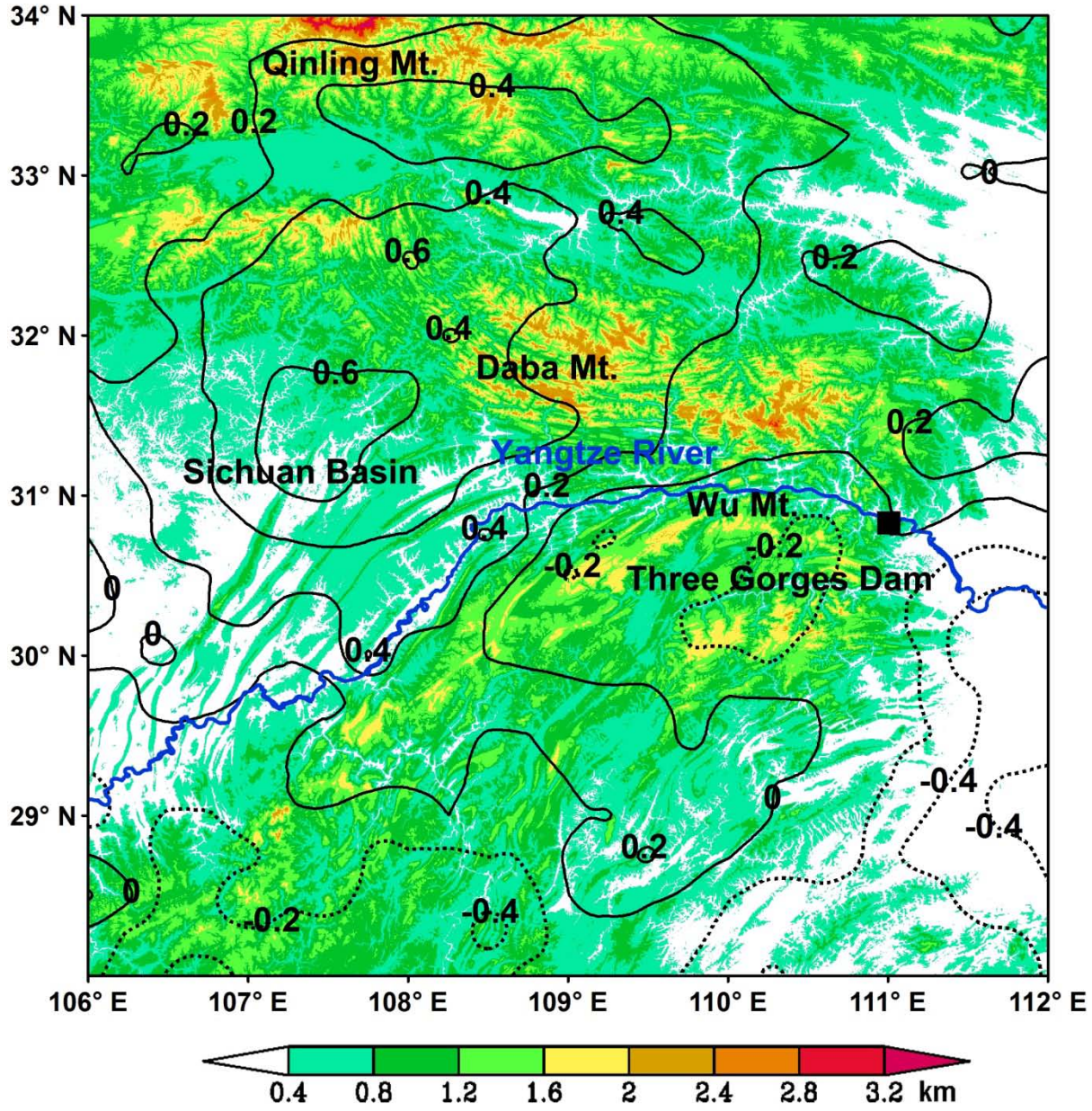


**Fig. 1.4**. Changes of the TMPA rain rate (mm day$^{-1}$, contours) after the TGD water level rose to 135 m, derived from the two five-year periods: January 1998–January 2003 and January 2004–January 2009. Topography data is from the U.S. Geological Survey (USGS) 30-second global data set (http://eros.usgs.gov/#/Find_Data/Products_and_Data_Available/GTOPO30).

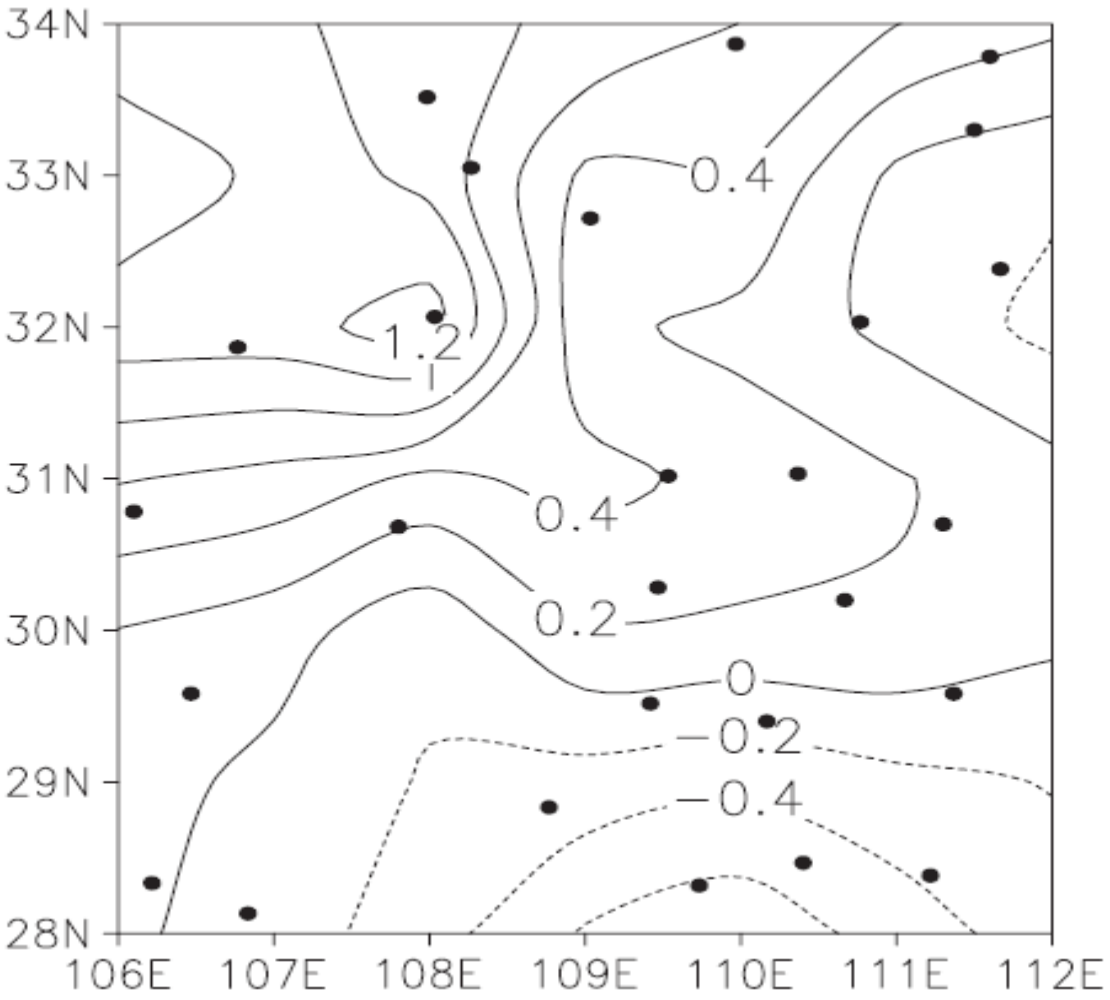


**Fig. 1.5**. Difference of the mean annual precipitation (mm day$^{-1}$) derived from the two periods between 1981–1984 and 1977–1980. Black dots denote station locations (from Xiao et al. 2010).

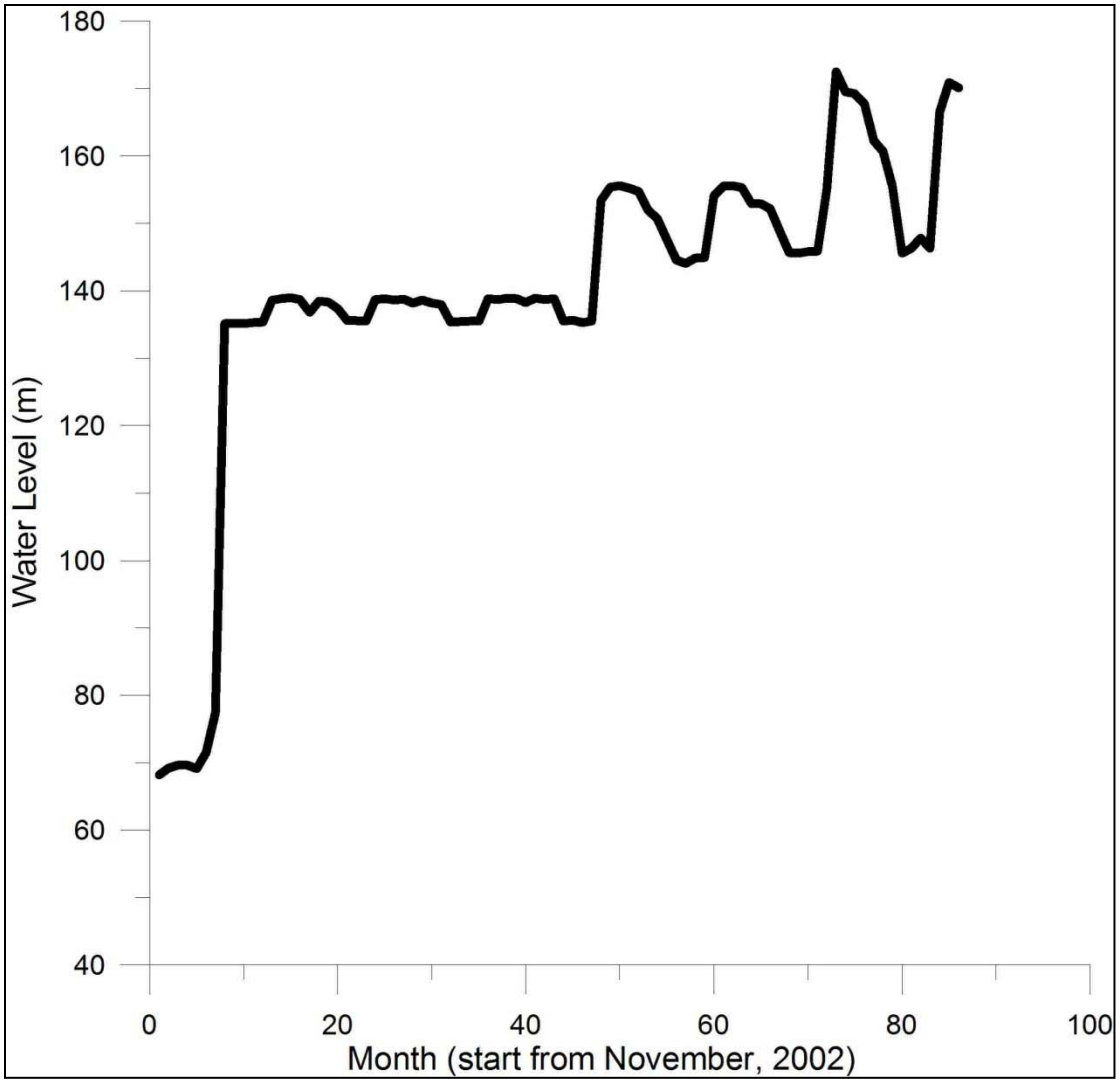


**Fig. 1.6**. Monthly variation of the water level upstream of the dam from November 2002 to December 2009. Water level in each month is represented by the reading at 2 UTC on the 15$^{th}$ day of that month. Data accessed online from the official website of China Three Gorges Corporation (http://www.ctgpc.com.cn/en/index.php).

# CHAPTER 2

# LITERATURE REVIEW

## 2.1 Precipitation

Anthropogenic influence on climate has drawn many concerns globally, and it is extensively addressed in the Intergovernmental Panel on Climate Change (IPCC) Fourth Assessment Report [*Trenberth et al.*, 2007]. Most attention, however, is given to temperature change rather than precipitation variation, because precipitation changes are much less spatially coherent and statistically significant compared with temperature change [*Alexander et al.*, 2006]. Over the 20th century, some regions have seen an increase in annual precipitation, such as in the U.S. [*Karl et al.*, 1995; *Karl and Knight*, 1998; *Trenberth*, 1998; *Kunkel et al.*, 1999; *Easterling et al.*, 2007], Japan [*Iwashima and Yamamoto*, 1993], northwestern Australia [*Rotstayn et al.*, 2009], South Africa [*Mason et al.*, 1999] and northern Europe [*Scho¨nwiese and Rapp*, 1997; *Førland et al.*, 1998]. Decreasing trends are evident in southern Europe [*Scho¨nwiese and Rapp*, 1997], eastern and southwestern Australia [*Murphy and Timbal*, 2008; *Taschetto and England*, 2009].

Changes in extreme precipitation events, however, are likely to increase and to be disproportionately large (Fig. 2.1) compared to any change in the total precipitation if the shape of the precipitation distribution does not change [*Groisman et al.*, 1999, 2005]. Both climate models under enhanced greenhouse conditions [*Semenov and Bengtsson*, 2002; *May*, 2008; *Rocha et al.*, 2008] and observations [*Jung et al.*, 2002; *Fuhrer et al.*, 2006; *Ramos and Martinez-Casasnovas*, 2006] suggest an increase in heavy precipitation frequency over most areas [*Trenberth et al.*, 2007].

However, it remains a challenge to ascertain what precipitation changes may be the result of large-scale climate changes associated with greenhouse gases, particularly when other forcing mechanisms (e.g., land surface changes, monsoonal variability, aerosols, etc.) may be a factor too.

## 2.2 Monsoon and Aerosol Changes

There is consensus in recent literature that the East Asian summer monsoon has weakened since the end of the 1970s [*Wang*, 2001; *Ding et al.*, 2008, 2010]. This change in monsoon regime has been linked with the inter-decadal variability of precipitation in East Asia [*Jiang et al.*, 2007]. Prolonged droughts occurred in North China and, at the same time, marked flooding conditions occurred in the Yangtze River basin and South China in the period from the end of 1970s to the beginning of the 21$^{st}$ century, and the rainfall regime underwent an abrupt shift in late 1970s. This monsoon-rainfall relationship is likely explained by the significant weakening of northward moisture transport and convergence of the East Asian summer monsoon since 1978. As a result, there is a large deficiency of moisture supply for precipitation in North China, and major moisture convergence, which induces more precipitation in South China including the Yangtze River basin [*Ding et al.*, 2008].

The monsoonal change has been associated with several mechanisms. The first one invokes the inter-annual and inter-decadal variations on the sea surface temperature in the Pacific and Indian Ocean [*Ju and Slingo*, 1995; *Hu*, 1997; *Weng et al.*, 1999; *Chang et al.*, 2000; *Yang and Lau*, 2004]. Another physical explanation is the correlative relationship between the Tibetan Plateau winter and spring snowpack and the Asian summer monsoon circulation and rainfall [*Zwiers*, 1993; *NCC*, 1998; *Liu et al.*, 2003, 2004; *Qian et al.*, 2003; *Wu and Qian*, 2003; *Zhang et al.*, 2004]. Since the late 1970s, the significant inter-decadal increase in sea surface temperature anomaly has greatly reduced the land-sea thermal contrast between the Asian land area and tropical Pacific and Indian oceanic regions. At the same time, the rapid increase in the preceding winter and spring snowpack over the Tibetan Plateau has considerably reduced the atmospheric heating over the large-scale land area in the subsequent spring and summer, due to increased albedo and less solar radiation absorbed at the surface. The combined effects

lead to significant reduction of the land-sea thermal contrast and the tropospheric meridional and zonal temperature gradients in the Asian monsoon region, which is responsible for weakening of the Asian summer monsoon, as illustrated in Fig. 2.2 [*Ding et al.*, 2009].

Research on aerosol effects on precipitation in East Asia has been limited, and the influence of aerosols does not seem to be as large as that of the monsoon. Only a few modeling studies investigated the direct effects (radiative forcing) of black carbon aerosol changes on precipitation in East Asia [*Wu et al.*, 2008, 2009], and the simulation results (precipitation increases in most North China and deceases in South China) contradict recent trends of flooding in the south and drought in the north.

## 2.3 Land Surface Effects on Atmosphere

Precipitation patterns in different regions are affected by variant human activities. Land Use/ Cover Change (LUCC) is a major anthropogenic influence, and its biogeochemical and biogeophysical impacts have been well documented [*Feddema et al.*, 2005; *Mahmood et al.*, 2010]. Ray et al. [2009] states that land cover conversion results in atmospheric changes because the dynamic, thermodynamic, and radiative processes that couple the Earth surface with the atmosphere are land cover specific. LUCC is highlighted as a major climate forcing by the National Research Council [2005]. It is even considered as a first order forcing, at least as large as the radiative effect of the human addition well-mixed greenhouse gases [*Pielke et al.*, 2007].

Various field programs have been undertaken with a focus on land surface-atmosphere interactions in places like the U.S., Canada, Europe, Africa and the Amazon region [*Pielke et al.*, 1997]. Recent papers have examined such topics as conversion of forest to farmland [*Bounoua et al.*, 2000], conversion of grassland to agricultural land [*Chase et al.*, 1999], conversion of natural vegetation to urban and agricultural land [*Pielke et al.*, 1999; *Shepherd et al.*, 2010] and aforestation [*Jackson et al.*, 2005]. Modeling is often used to assess the influence of LUCC on the regional hydroclimate (See Fig. 2.3 for example), but the accuracy of such work is affected by the accuracy of initial and boundary condition including land cover. This, unfortunately, is not easy to acquire due to the rapid change of land cover and

lack of adequate data. Robust accuracy assessment is only found in a few studies, and the literature suggests that detailed atmospheric information is more crucial in improving simulation accuracy than land cover information [*Ray et al.*, 2009]. Moreover, the same type of conversion can have different impacts on different regions [*Pielke et al.*, 2007], making it more difficult for modeling efforts.

## 2.4 Dams and Their Effects

Dam construction on rivers is an important human activity, which dates back to 5000 years ago in Jordan [*Garbrecht*, 1986]. Around the world, the World Commission on Dams (WCD) reports that there have been at least 45,000 dams built since the 1930s, and half of the world's rivers have at least one dam [*WCD*, 2000]. Dams and their impounded reservoirs can trigger a series of LUCC. More land may be brought under irrigation, natural vegetation may be converted to agricultural land due to inundation of the reservoirs, and the downstream regions may become more urbanized due to a reduced risk of flooding and possible migration [*Hossain et al.*, 2010]. Some of these effects have impacts on local energy and moisture balances.

Observed data and modeling studies support the notion that atmospheric moisture added by irrigation can alter precipitation distributions if mesoscale conditions are appropriate [*Stidd*, 1975; *Barnston and Schickedanz*, 1984; *Lohar and Pal*, 1995; *DeAngelis et al.*, 2010]. If dam-driven land cover change can trigger changes in precipitation patterns, then it will mostly likely also change the patterns of extreme precipitation [*Avissar and Liu*, 1996]. Related studies on the mechanisms with which large dams affect extreme precipitation patterns are summarized in Hossain et al. [2009] (Fig. 2.4). Eltahir and Bras [1996] described the notion of precipitation recycling that after water vapor evaporates from the surface, part would be transported away, and the remainder would be recycled back to the surface of the region from which it was then evaporated in the form of precipitation. Precipitation recycling depends on the probability of precipitation being recycled from local evaporation, a factor that increases with the size of the region or the basin. When it comes to water level rise in a large river basin, the effect of precipitation recycling on the rainfall regime cannot be ignored. After dams impound large reservoirs, it is physically

plausible that the increased evaporation from the open water surface might alter both average and extreme precipitation patterns through a feedback mechanism of the precipitation recycling.

Another important mechanism is local circulation over reservoir water and adjacent land, which is similar to the process shown in the sea/lake breeze schematic diagram (Fig. 2.5, Sills [1998]). Various types of sea/lake breeze-like local circulations are summarized in Segal and Arritt [1992], including irrigation and vegetated land. The difference in sensible heat fluxes is speculated to be the reason for the sea/lake breeze thermal forcing in early studies [*Arritt*, 1987]. In summer, a large land-water temperature difference develops within the lower atmosphere and the corresponding pressure gradient produces the local circulation. Air over the reservoir is cooler and subsidence dominates. Therefore, sinking air over reservoir creates a local high pressure, and the air would diverge away from water surface. The cool air would push the warm air as it advances into land and generates updrafts at some distance from water. As a result, precipitation could be suppressed over the water surface and enhanced over land at some distance away from water.

In reality, the lake breeze effect described above may interact with other mechanisms (topography, large-scale flow, etc.). As a result, previous observational studies did not find a consistent lake breeze induced pattern. Contrary to Scott and Huff's [1996] conclusions regarding the Great Lakes, rainfall over Lake Victoria in East Africa is higher than surrounding land areas from TMPA estimates, which is consistent with modeling results [*Anyah et al.*, 2006]. The rainfall increase over Lake Victoria is attributed to the enhanced over lake evaporation. Another study investigated the impact of the Itaipu Lake (artificial reservoir on the Brazil-Paraguay frontier, approximately 170 km long and 7.5 km wide) on the climate and local circulations. It concluded that the temporal pattern of the precipitation over the region does not indicate any consistent modification in the rain regime after the lake formation [*Stivari et al.*, 2005]. They did, however, find the presence of a local circulation with lake breeze characteristics showing horizontal wind divergence over the lake during daytime and convergence during nighttime from the surface wind data.

Modeling simulations have provided a partial explanation for the observed case-specific lake breeze effects. In a recent review of numerical studies on sea/gulf/lake/river breezes (referred to as sea breeze in section 2.4, in consistency with the cited literature), Croseman and Horel [2010] listed ten geophysical variables affecting the characteristics of sea breezes. The fundamental driver of sea breezes is the differential sensible heating between the land and water surfaces. Variations in land-surface sensible heat flux, background geostrophic wind, and atmospheric stability have a pronounced effect on the intensity of sea breezes at a given location. Water body dimensions, Coriolis force, terrain height and terrain slope may explain differences in sea breezes around the world. The impacts of shoreline curvature, roughness length and atmospheric moisture on sea breezes are generally smaller. Influences of some of the various factors on the areal extent (inland penetration) of sea breeze effects are listed below:

- Increasing the land surface sensible heat flux tends to increase the overall intensity of sea breezes, which acts to increase the inland penetration of sea breezes. However, as the land-surface sensible heat flux increases, turbulent convection also increases, which acts to destroy the thermal gradient along the sea-breeze front. This process, known as turbulent frontolysis, decreases the inland penetration of the sea-breeze front through a weakening of the horizontal temperature gradient during peak daytime heating and increasing drag [*Simpson et al.*, 1977; *Abbs and Physick*, 1992; *Ogawa et al.*, 2003].
- Sea-breeze characteristics may also be weakened or strengthened by interactions (e.g., frictional retardation, thermal coupling) with an urban heat island circulation. The size of the urban area, distance between the urban area and the coast, and surrounding topography modulate these highly variable (in both sign and magnitude) interactions [*Yoshikado*, 1990; 1992; *Kusaka et al.*, 2000; *Ohashi and Kida*, 2002; 2004; *Lemonsu et al.*, 2006; *Freitas et al.*, 2007; *Thompson et al.*, 2007; *Cheng and Byun*, 2008; *Dandou et al.*, 2009; *Shepherd et al.*, 2010].
- Lakes in deep valleys may be more sensitive to lake temperature variations due to interactions between boundary-layer stability and topography [*Segal et al.*, 1983].

- For offshore geostrophic flows of 1–2 m $s^{-1}$, inland penetration is on the order of 50 km, while inland penetration is on the order of 10 km for offshore geostrophic flows of 4–5 m $s^{-1}$ and onshore penetration occurs later in the afternoon [*Arritt*, 1993; *Tijm et al.*, 1999; *Porson et al.*, 2007a].
- Increasing stability leads to slightly weaker winds near the shoreline and increased inland extent [*Walsh*, 1974; *Rotunno*, 1983].
- Little is known about the dependence of inland penetration on the magnitude of the water body dimensions except that smaller water body dimensions tend to lead to smaller inland penetration [*Physick*, 1976; *Zhong et al.*, 1991].
- Topography can enhance sea breezes through elevated heating and cooling, which drives slope flows that combine with sea breezes, or suppress them by mechanically blocking the onshore flow [*Atkinson*, 1981; *Abbs and Physick*, 1992]. Porson et al. [2007b] were the first to systematically vary atmospheric stability, slope angle and slope length. They found that inland penetration is highly dependent on both terrain slope and atmospheric stability. A secondary effect of topography on sea breezes is channeling, which can locally enhance inland penetration [*Abbs*, 1986; *Abbs and Physick*, 1992; *Segal et al.*, 1997].
- The effect of the Coriolis force on late afternoon sea-breeze strength is significant (Coriolis effects are minimal through the early afternoon hours), and increases with increasing latitude [*Yan and Anthes*, 1987].

Because all or some of these factors would be largely different in different regions, the seemly inconsistent effects in observations could be readily reconcilable. Despite the extensive number of scientific studies devoted to understanding the influence of geophysical parameters on sea breezes, gaps remain, and are largely due to numerical and computational limitations such that a limited range of parameter values have been examined [*Crosman and Horel*, 2010]. Nonetheless, numerical studies have the advantage of directly examining sea breeze effect, and researchers continue to conduct region/case-specific simulations in recent years [*Stivari et al.*, 2003; *Tomassetti et al.*, 2003; *Anyah et al.*, 2006].

## 2.5 Background of Three Gorges Project

The idea of building a large dam across the Yangtze River originated in the 1950s. Since the National Congress of China officially approved the Three Gorges Project (TGP) in 1992, the Three Gorges Area has seen many debates and rising concerns in a variety of fields. The influence of this project is felt on the natural and social environments in the reservoir area. In addition to inundating 19 towns and counties (Fig. 2.6) and 24,000 hectares of arable land, the project destroyed a tourist region not unlike the Grand Canyon in the U.S. [*Gwynne and Li*, 1992]. Over a million people had to move away from fertile farmland, and some resettled in much less desirable areas nearby. This change would have serious secondary environmental impacts [*Tan and Yao*, 2006]. The project fragmented large, continuous habitats into smaller patches. It reduced biodiversity, changed ecological processes like nutrient and water cycling, and eventually will cause irreparable ecological damage [*Edmonds*, 1992; *Shen and Xie*, 2004]. Other issues include the sedimentation problem, reservoir induced earthquakes and landslides [*Wang*, 2002]. Despite the huge debates and reported negative effects, the Three Gorges Dam (TGD) was eventually built for the purpose of hydroelectric power generation, flood control and navigation.

There has been a huge ongoing interest in hydroelectric power in China for about 30 years. Although the U.S. has the largest number of dams in the world, China is now the largest producer of hydroelectricity (followed by Canada, Brazil and the U.S.), and untapped hydroelectric power resources are still abundant in southwest China. While net hydroelectric power generation decreased in the U.S. compared to 30 years ago, there has been a sevenfold increase in China during the same time (Energy Information Administration, http://www.eia.doe.gov/emeu/international/electricitygeneration.html). With a total installation of generating capacity of 18,200MW, and an average annual output of 84.7 trillion watt hours, Three Gorges Project is the largest hydropower plant in the world. (TGP claimed that title from the Itaipu power plant, jointly owned by Brazil and Paraguay.) It was planned to supply electricity to east, central and south China where 600 million people live [*Wang*, 2002].

Besides producing hydroelectricity, dams are considered very important for flood prevention. In China, flood events occur almost twice every year, and an area of about 90,000 km is affected each year. Previous studies have also shown that the frequency of extreme events may have increased in recent decades in various regions across China [*Zhai et al.*, 2005]. These events are most pronounced in the Yangtze River Basin, which is characterized by a typical monsoon climate. As the Yangtze River flows from west to east, the transmeridional rain belt (which moves from south to north, then moves back south in China from April to October) stalls and causes heavy rainfall. The huge river system receives water from all flanks and the water level rises rapidly. Meanwhile, the relatively dense and urbanized population along the river makes the floods more deadly and costly [*Zhu*, 1999]. With about 22.15 billion $m^3$ of flood control storage capacity in TGR, the flood risks in the downstream areas are greatly reduced [*Wang*, 2002].

The TGD significantly increases both reliability and capacity of the 660 km long waterway from Yichang City to Chongqing Municipality, resulting in a direct stimulus to economic growth [*Peng et al.*, 2010]. It is possible now for 10,000 tons of barge fleet to sail directly to Chongqing harbors. It is estimated to increase annual one-way navigation capacity from 10 million tons to 50 million tons, and decrease navigation cost by 35-37% [*Wang*, 2002].

TGP has profound influence in many aspects. The research on this large project contributes to previous research on the effects of land surface change on the atmosphere. Recent literature suggests that there are no major shifts in monsoon or aerosol over this region in the first decade of the new century. Therefore, it is easier to observe the possible effects of TGP on precipitation.

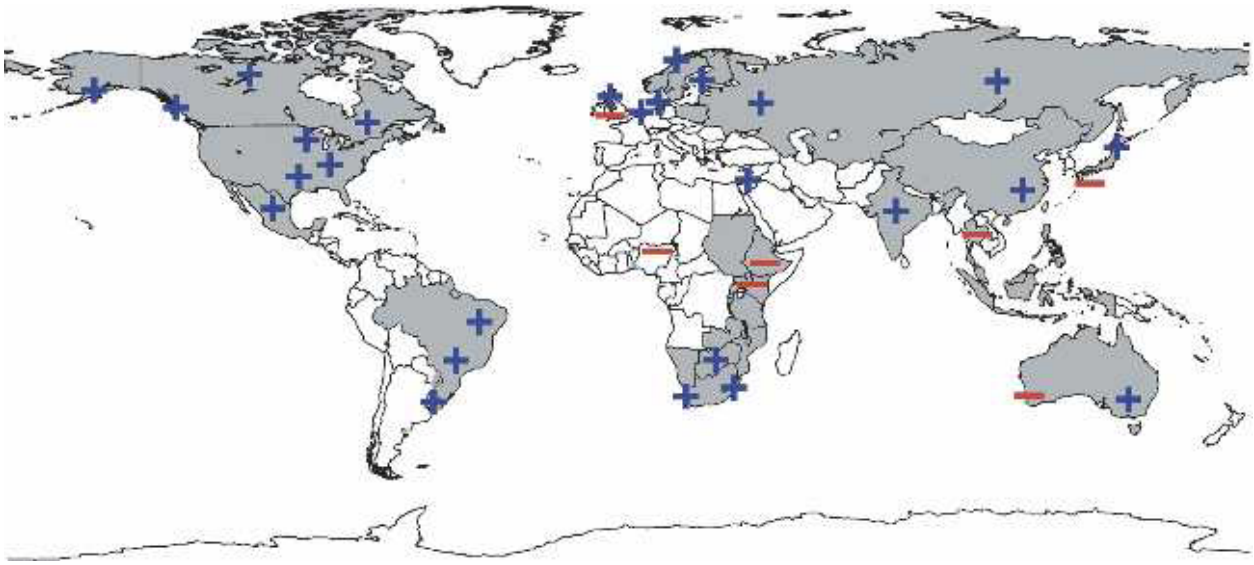

**Fig. 2.1**. Regions where disproportionate changes in heavy and very heavy precipitation during the past decades were documented compared to the change in the annual and/or seasonal precipitation (from Easterling et al. 2000, substantially updated). Thresholds used to define heavy and very heavy precipitation vary by season and region. However, changes in heavy precipitation frequencies are always higher than changes in precipitation totals and, in some regions, an increase in heavy and/or very heavy precipitation occurred while no change or even a decrease in precipitation totals was observed (from Groisman et al. 2005).

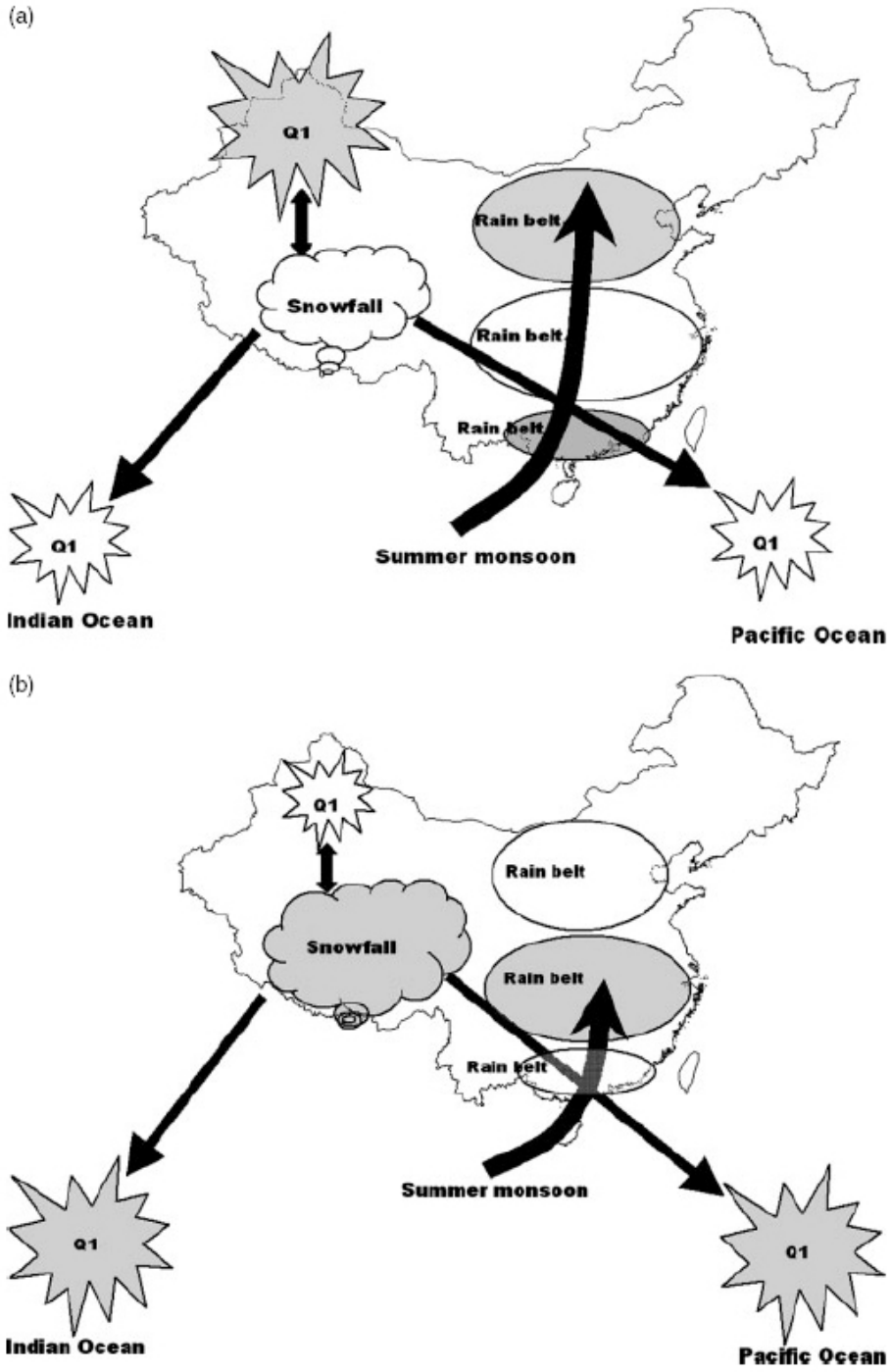


**Fig. 2.2**. Schematic diagram of the possible cause of weakening of the Asian summer monsoon. The anomalously strong (weak) Asian summer monsoon condition is illustrated by (a) and (b), respectively. Shaded areas indicate abundant snow, high sea surface temperature anomaly, intense atmospheric heating and ample precipitation. Bold arrows represent the summer monsoon airflow (from Ding et al. 2009).

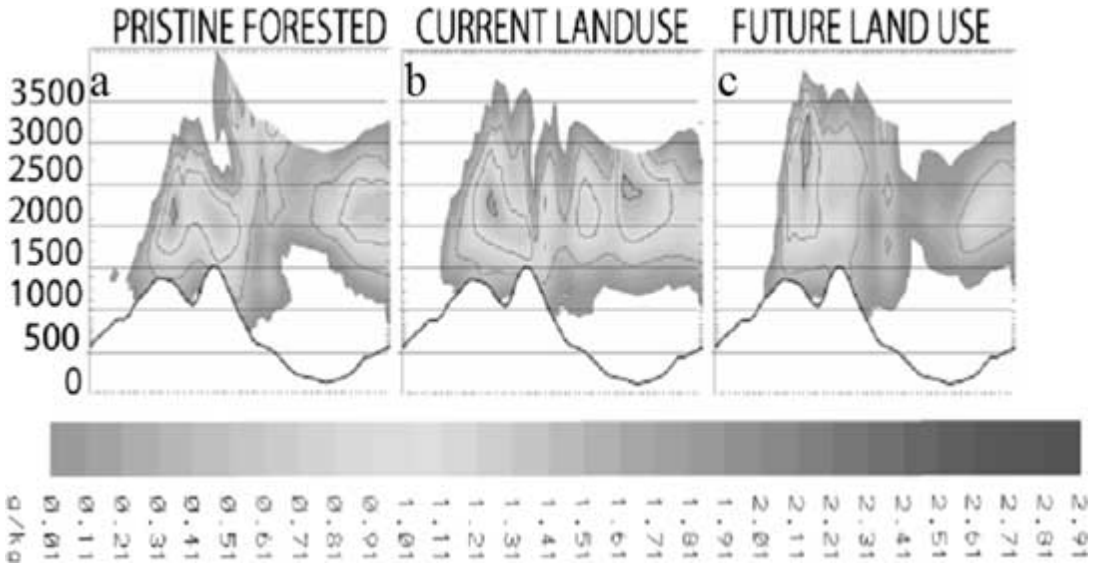


**Fig. 2.3**. Numerical simulation of orographic cloud formation for three lowland deforestation scenarios in Northern Costa Rica: a) pristine forests; b) current land-use; c) complete deforestation of the lowlands. East-West cross sections of cloud water mixing ratio, simulated by the Regional Atmospheric Modeling System, show orographic cloud bank formation at lower elevation when there is forest cover in the lowland areas (from Nair et al. 2006).

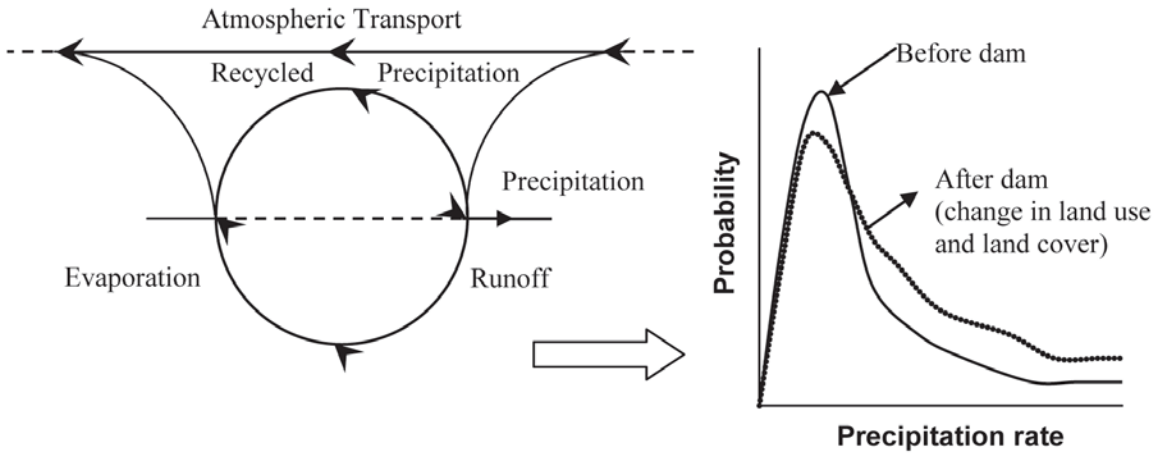


**Fig. 2.4**. (a) Schematic conceptualization of man-made alteration of extreme precipitation by a reservoir (from Eltahir and Bras, 1996). The dashed line through the circle represents the land-atmosphere interface. (b) Graphical depiction of the alteration in extreme precipitation frequency due to dams (from Hossain et al. 2009).

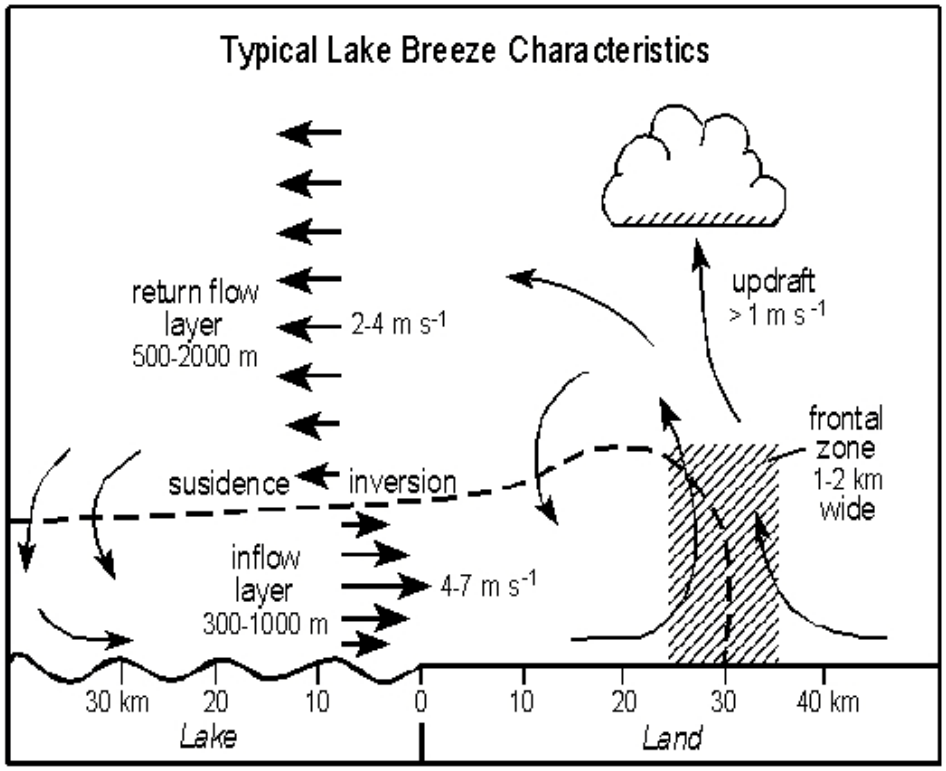


**Fig. 2.5**. Idealized illustration of a typical lake breeze circulation and its associated front. Common features are labeled. The dashed line represents the outer boundary of the inflow layer. The frontal zone is not shown to scale (from Sills 1998).

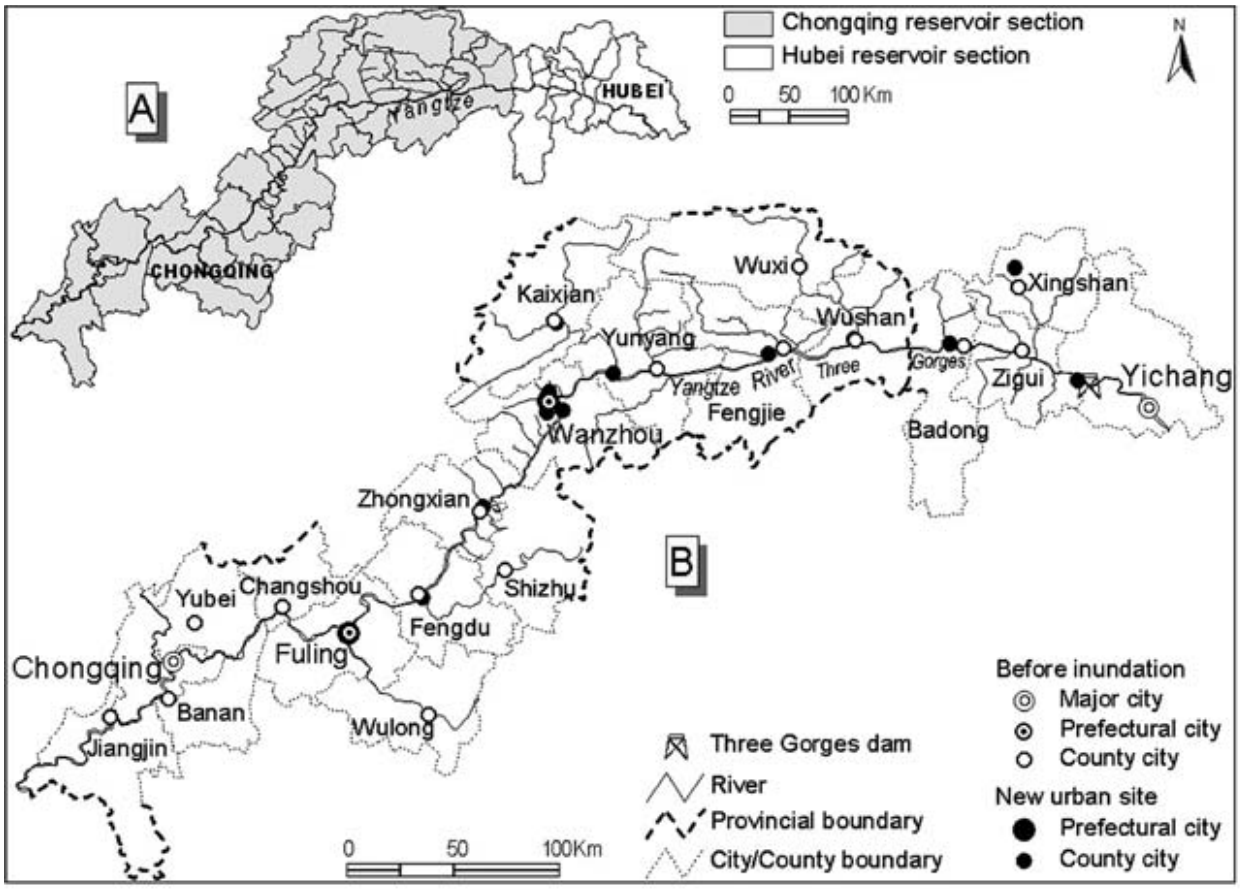


**Fig. 2.6**. (a) Two sections constituting the Three Gorges reservoir area: Chongqing and Hubei. (b) Various cities and counties in the reservoir section, some of which are completely submerged and others affected by the construction of the Three Gorges dam (from Tan and Yao 2006).

# CHAPTER 3

# RESEARCH DESIGN AND METHODOLOGY

## 3.1 Study Area and Period

The Three Gorges Reservoir region is located in the middle part of the Yangtze River Basin. It has an area of about 56 000km$^2$ and stretches along the Yangtze River from the Jiangjin District of Chongqing to Yichang City of Hubei (refer to Fig. 2.6). The elevation ranges from over 1000 m to 50 m in the east. The mountainous areas are located in the middle of the region, while other parts of the region are mostly hilly areas, with a few plains (refer to Fig. 1.4). The area is dominated by a subtropical monsoon climate, and precipitation varies both in time and space. Mean annual precipitation is 1200 to 1400 mm in the middle mountainous areas, and 900 to 1100 mm in the hilly and plain areas. About 85% of annual precipitation falls from April to October, more than half of which falls from May to July. A previous climatological study on this region found that summer (JJA) precipitation and heavy rain (>25 mm day$^{-1}$) near the reservoir are significantly correlated with the ridge position and intensity of the West Pacific Subtropical High [*Fang et al.*, 2010] (Fig. 3.1).

The Three Gorges study area is defined in the vicinity of TGD (28-34°N, 106-112°E). The area is chosen to position the reservoir in the middle and to include major adjacent topographic features that might interact with the reservoir in precipitation processes. This study area is identical to previous studies by Wu et al. [2006] and Xiao et al. [2010], which makes it convenient to compare with their results. Daily precipitation data from 34 China national meteorological monitoring stations (including the 27 stations used in Xiao et al. [2010]) in the area provide sufficient coverage for TMPA rainfall validation purposes in this research. The time period for this study spans 1998-2009 in accordance with available TMPA data.

It is the longest study record to date, and the 2003 abrupt water level rise occurred in the middle of this period. This time period also allows an epoch analysis with several years in each epoch.

## 3.2 Water Level and Landsat Data

### 3.2.1 *Water Level*

Hourly water level data of the reservoir measured upstream of the dam from November 2002 until now are available online from the website of China Three Gorges Cooperation (http://www.ctgpc.com.cn/sx/sqsk.php). This state-owned cooperation posts various hydrological information of the reservoir on its website, and a query of water level upstream of the dam at any time (hourly) since November 2002 could be easily performed (Fig. 3.2). The readings at 2 UTC (about the time when the Landsat satellite passes over this area) on the 15$^{th}$ day of each month are first retrieved to identify periods of relatively stable water level. Precautions are taken for months with drastic water level changes. Table 3.1 categorizes the time periods for the five different water levels determined for reservoir area interpretations from Landsat images (until May 2010).

Table 3.1 Five stages of water level upstream of the dam

| Stage | Water Level | Periods |
|---|---|---|
| 1 | 68.15-77.35 m | Before 5/2003 (water level measurements started after 11/2002) |
| 2 | 135.10-138.94 m | 6/2003 - 9/2006 |
| 3 | 145.61-148.76 m | 5/2007-9/2007, 5/2008-9/2008, 6/2009-9/2009 |
| 4 | 150.75-156.9 m | 10/2006-4/2007, 10/2007-4/2008, 10/2008, 5/2009, 3/2010-5/2010 |
| 5 | 166.53-172.45 m | 11/2008-2/2009, 10/2009-1/2010 |

### 3.2.2 *Landsat Imagery*

Landsat images are appropriate for the study due to the distinct character of the reservoir, which is over 600 km long but quite narrow. After the impoundment, it is on average over 1 km wide. The ideal data source would cover the whole reservoir with a few scenes while having adequate resolution to resolve the narrow reservoir width. Images like MODIS would be so coarse spatially that the width of the

reservoir only equals to two or three of its pixels. On the other hand, it would require too many scenes for data with higher spatial resolution to cover the reservoir. Besides, these sources usually suffer from poor temporal resolution thus reducing the chance of having cloud-free images (especially considering the cloudy nature of the region) in a time window as small as seven to eight months (Table 3.1). Landsat images have a nice balance of temporal and spatial resolution. Spatially, the 1 km width equals to 40 pixels in the Landsat data. Temporally, the 16-day return period allows a better choice of cloud-free images. Furthermore, Landsat images could be freely obtained, and they have been widely used in land cover studies [to gives some examples, *De Fries et al.*, 1998; *Vogelmann et al.*, 1998; *Kiage et al.*, 2007; *Ruelland et al.*, 2008; *Xian et al.*, 2009].

This analysis relies on Landsat ETM$^+$ data from 2000 (before the abrupt water level rise in 2003, water level is relatively constant in similar seasons) to 2010 to interpret the areas of Three Gorges Reservoir at five different water level stages. Six scenes of Landsat data are selected to cover the whole reservoir (Fig. 3.3, labeled by path/row identifiers). The Landsat data are retrieved from Landsat archive (Landsat 7) using the USGS Earth Explorer (http://edcsns17.cr.usgs.gov/EarthExplorer/). A problem with Landsat is that on May 31, 2003, the Scan Line Corrector (SLC) failed, which had compensated for the forward motion of Landsat 7. As a result, there are data gaps (shown as black strips) with width that increases toward the scene edge on the images afterwards (Fig. 3.4). The maximum width of data gaps along the edge of image is approximately 390 to 450 meters (http://landsat.usgs.gov/products_slcoffbackground.php). To correct this problem, one or two additional scenes with similar water level are used in addition to the images for classification. The data gaps of the classification images and correction images need to have minimum overlap. Mask files are acquired for the data gaps. These files are applied on the correction images, and after that the resulted strips are mosaiced with the classification images to create nearly seamless images for reservoir extraction. Cloud-free (or minimal cloud, here a scene is considered “cloud-free” if there is no cloud covering the reservoir, because only the reservoir area is of concern) scenes are chosen both for extracting reservoir area and filling in SLC-induced gaps. Overall, five sets of 30 images are used for area extraction and another 30 or

more images for gap correction. If there is no cloud-free image available for any scene, a cloud-free scene with the closest water level is used instead. Such replacements are made only twice out of 30 images. The scenes that are replaced are far from the dam, and they are expected to have a small impact on the extracted area. Table 3.2 lists all the images used for area extraction.

Table 3.2 Dates of all Landsat Images used for reservoir area extraction

| Path/Row / Stage | P125R39 | P126R38 | P126R39 | P127R39 | P128R39 | P128R40 |
|---|---|---|---|---|---|---|
| 1 | 12/30/02 | 11/03/02 | 11/03/02 | 11/04/00 | 03/25/03 | 04/02/03 |
| 2 | 08/27/03 | 10/21/03 | 08/02/03 | 04/24/05 | 07/31/03 | 04/02/06 |
| 3 | 09/28/09 | 07/01/09 | 08/18/09 | 09/10/09 | 09/01/09 | 09/01/09 |
| 4 | 11/07/06 | 10/13/06 | 10/13/06 | 05/21/09 | 10/11/06 | 10/11/06 |
| 5 | 01/15/09 | 01/22/09 | 01/22/09 | 11/10/08 | 10/11/06* | 10/11/06* |

* No good cloud-free images available. Use previous stage's images as replacements.

## 3.3 Precipitation Data

### 3.3.1 *Ground Observations*

Thirty-four China national meteorological monitoring stations within our study area have been selected, six of which are located along the Yangtze River. The datasets are from the official source of the homogenized dataset of China Meteorological Administration's National Climate Center (CMA NCC), and they are available on the China Meteorological Data Sharing Service System (http://cdc.cma.gov.cn/). The daily precipitation is recorded by manual observations at 6-hour intervals. The error of the rain-gauge data is less than 0.1 mm, which would not affect the validation purpose of this study. Further details of quality control, instrumentation used and data processing are given in Appendix A. Daily values from 1998 to 2009 for all stations are used for validation, and there are no missing data or changes of site location in this time period. Daily values from 1961-1990 are used to construct a climatology. Note that even when aggregating satellite data into 1-degree cells, the goal of having at least one station in each grid cell is still not satisfied. Obviously, satellite estimates of rainfall would be useful in this poorly

gauged region. For the validation purpose, a Thiessen-polygon based approach (discussed in 3.5.2) is used to compensate for the number of available rain gauges.

3.3.2 *TMPA Estimates*

Satellite-based daily rainfall amounts from NASA's Tropical Rainfall Measuring Mission (TRMM) Multisatellite Precipitation Analysis (TMPA) from 1998 to 2009 are acquired from NASA's Goddard Earth Sciences Data and Information Services Center (GES DISC, http://mirador.gsfc.nasa.gov). TMPA is a 3-hourly, 0.25-degree (~25 km) product described in Huffman et al. (2007). This study employs the merged TMPA_3B42 3-Hourly and TMPA_3B43 monthly version of the TMPA, composed of available microwave (e.g., TRMM microwave imager, Special Sensor Microwave Imager (SSM/I), Advanced Microwave Scanning Radiometer (AMSR) and Advanced Microwave sounding Unit (AMSU)) and calibrated infrared (IR) estimates.

Note that the merged products like TMPA are so relatively new that there is a lack of inter-comparison/validation studies in the literature. This makes our study a valuable contribution in itself. Hand and Shepherd [2009], in a 9-year study around the Oklahoma City, showed that satellite precipitation estimates capture spatial rainfall variability as well as traditional ground-based resources of the Oklahoma mesonet. However, TMPA estimates may not perform equally well in different regions. For example, low values of rain rates in interior tropical Africa, central Asia, and the Great Plains in the U.S., as well as higher values in equatorial Amazonia and along the southwestern coast of India are consistent with known issues with microwave-based estimates in those regions [*Huffman et al.*, 2007]. It would be interesting to know how well/poorly the TMPA estimates perform, and if the bias is underestimation, overestimation, or mixed in the study area. Herein, we describe a research version of the TMPA that contains a gauge adjustment. The gauges used for the adjustment may contain some of the gauges used for validation in this study, which would influence the correlations between TMPA and gauge estimates. The gauge adjustment is included in the TMPA for the very reason of improving the product and extending it spatially where gauges are not present. It is worth noting that there is also a real time version of TMPA available for more immediate analysis, and it does not contain a gauge adjustment.

The resolution of the gauge network is coarse (e.g., the 2.5° Global Precipitation Climatology Center monthly gauge dataset described by Rudolf et al. [1994]), and so it would be encouraging if, even with this coarse adjustment, our results using 0.25° data products are still accurate.

### 3.4 NCEP Data

National Centers for Environmental Prediction (NCEP) Reanalysis data are used to determine the large-scale atmospheric condition for each month. The NCEP/NCAR Reanalysis 1 project is using a state-of-the-art analysis/forecast system to perform data assimilation using past data from 1948 to the present (Kalnay, 1996). For this study, monthly 700 hPa and 850 hPa geopotential height (GPH) fields are obtained from the NOAA/OAR/ESRL PSD (http://www.esrl.noaa.gov/psd/). It is assumed that the synoptic condition of an individual year is not anomalous if its 700 hPa and 850 hPa GPH are similar with the 12-year composites. 700 hPa and 850 hPa GPH were considered to be adequate to portray large-scale atmospheric features [*Camberlin*, 1997], and they could be used to estimate low level primary wind direction.

### 3.5 Research Methodology

#### 3.5.1 *Reservoir Extraction*

The purpose of correlating water level with reservoir area is to use the high temporal resolution water level data to estimate reservoir area at an hourly timescale, which would be valuable for future modeling simulations. The assumption is that for the same water level at different times, the reservoir area would be constant. This assumption seems valid because there are no major landform (bank shape) changes adjacent to the reservoir over the past few years. This assumption allows for a larger selection of cloud-free images within each time frame for different water level stages. The results of reservoir area interpretations could be merged to retrieve the whole reservoir area related to a certain water level stage.

For area extraction, images are first preprocessed in Erdas Imagine 9.3 to address the SLC problem, and the procedures include layer stack, subset image, histogram equalization, mask and mosaic. Although

the color display between the classification and data gap correction images is not balanced or uniform, the differences are shown to be insignificant for the classification of water. After preprocessing, the nearly seamless subset images containing the reservoir area are classified using Feature Analyst (FA) in ArcGIS 9.3. Feature Analyst's machine learning approach to automated feature extraction incorporates software agent technology which "learns" to find features like hydrology, vegetation, and other land cover features based on user-specified examples. The software provides object-specific feature capture technology using spatial context and advanced machine learning techniques that allow controlling of feature extraction process rather than using hard-coded rule base (FA manual, http://www.featureanalyst.com/feature_analyst/publications/manuals/FA_4.2_RELEASE/FA_4.2_Reference_arc_040908_RELEASE.pdf). These features enable the software to fully utilize the spatial and spectral information to extract the river-shaped reservoir well. Feature Analyst based classifications of water body are processed after creation of training sets including polygons, which represents the shape and spatial distribution of the reservoir. Then the classified reservoir polygon in each scene is manually modified to make the result more accurate. After that, the classified reservoir polygon has accuracy comparable with what could be achieved by hand digitizing, and no further evaluation is necessary. An example of a classified image is shown in Fig. 3.5. Once all six parts of the reservoir polygon at one stage are obtained, they are merged together to get the full extent of the reservoir. In this study a narrow definition of the Three Gorges reservoir is employed. The tributaries of the reservoir are cut because of the limited coverage of each scene, although they do expand as the water level rose. The premise here is that the expansion of the tributaries is proportional to that of the main stream. Therefore, the reservoir area extracted from the main stream could represent the overall effects of the reservoir including the countless tributaries. The longitude of 106°E is chosen as the left border of the reservoir to match the study area extent. The water level rise has negligible effects on the Yangtze River channel upstream (west) of 106°E.

The exact water level is consulted online for the date of each scene used at 2 UTC (about the time Landsat images are captured). Then the approximate mean water level for each set of scenes is calculated

taking into account the relative portion of reservoir area in each scene. In this way, five water level-reservoir area data pairs are determined. Then in Microsoft Excel 2007, linear, power, exponential, logarithmic and second-order polynomial trend line fittings are performed, to determine the best description for the water level-reservoir area relationship.

3.5.2 *Validation of TMPA*

It is hypothesized that the TMPA estimates will be relatively well correlated with point-source rain gauge estimates. The region is poorly gauged in the first place. Even if there are many more gauges, point-source gauge methods may not be appropriate for analysis of spatial distributions of rainfall, which, unlike temperature or moisture fields, tends to be highly variant. The point-source/area-average problem is well known in precipitation remote sensing communities and is an ongoing area of research [for example, *Hand and Shepherd*, 2009].

Comparisons between satellite-estimated precipitation and rain gauge data have typically used linear regression analysis as the main analytic tool for assessment [*Barrett et al.*, 1994]. Multiple validations are performed to examine the quality of TMPA estimates both temporally and spatially. The first set of correlation analyses are conducted for this study to establish the relative accuracy of areal average point-source (gauge) versus areal average satellite (TMPA) rainfall estimates. Areal averages of both estimates for the 144 months from 1998 to 2009 within the 6°×6° latitude-longitude region are calculated. For TMPA estimates, rainfall per month is averaged from the 576 data grids (0.25°×0.25° grids). For gauge estimates, averages are derived from all 34 gauges. Then Pearson's correlation between the 144 data pairs is calculated. In addition to TMPA's performance throughout the year, the 144 pairs are divided into four groups by season, and seasonal correlations are examined. Compared with other validation studies [*Hand and Shepherd*, 2009], a possible shortcoming of this approach is that the large study area would inflate correlation coefficients for these highly-aggregated data. One possibility is that the study area could be divided into sub-regions which have distinct precipitation patterns. TMPA data might have large positive biases in some sub-regions and negative biases in some others, and these biases might cancel out and result in high correlations for the average values of the whole study area. Thus it is

important to divide the whole area into sub-regions within which the rainfall characteristics are similar, and then compare the areal averaged TMPA estimates with gauge estimates in each sub-region. The empirical orthogonal functions (EOFs) obtained from the annual standardized 12-year TMPA precipitation data (576 0.25°×0.25° data grids) allow recognition of the sub-regions with different precipitation regimes. EOF analysis is an efficient method widely used in research areas including atmospheric science (please see review by Hannachi et al. [2007] for more information). For this study, EOF analysis is used only for the purpose of determining sub-regions. The daily scale cumulative rainfall and frequency distributions of occurrence of daily rainfall for the whole region are also compared.

The next set of correlation analyses aim to examine how accurate TMPA estimates are spatially. It is most convenient to divide the whole area into 36 1°×1° cells which is close to the number of rain gauges. In studies where multiple rain gauges are contained in one cell (Hand and Shepherd 2009), their approach is to average the stations within each cell. However, this approach could not be replicated here since there are only 34 gauges. An alternative and possibly better approach is to use the Thiessen Polygon method [*Thiessen*, 1911], which is also adopted in Han et al. [2010], to divide the whole region into polygons surrounding the rain gauges. This method first connects all the rain gauges by dashed lines (Fig. 3.6). Next, perpendicular bisectors of the straight lines are constructed. The bisectors meet at a common point inside or outside of the triangle. The resulting polygons around each rain gauge are known as the Thiessen polygons [*Bedient and Huber*, 2002]. By using this approach, each rain gauge would be in the center of the polygon surrounding it. In this way, the whole region is separated into many polygons, and any place in each division is closer to the central rain gauge than any other gauges. In other words, each of the 34 gauges would be best to represent the precipitation in its surrounding polygon area. Then the polygons are overlaid on the 1°×1° grids (Fig. 3.7), most cells are covered by several parts of the polygons surrounding different rain gauges. As a result, each TMPA 1°×1° grid could be related with one or more rain gauges. TMPA data are resampled to each 1°×1° cell, and the related 1°×1° area-weighted average rain gauge data are derived. Annual and seasonal averages from 1998 to 2009 are calculated for each cell for the two data sources. Scatter plots of mean monthly rainfall estimates from the 36 TMPA

1°×1° grid cells versus the corresponding estimates from the gauge stations for all seasons are prepared to determine how well (or poorly) the rainfall distribution from the TMPA data performs.

3.5.3 *Determining Epochs*

The epoch analysis seeks to examine the precipitation changes when all influencing factors other than the reservoir surface area are held similar. Ideally, this approach would replicate modeling simulations, and the "true" results instead of uncertain modeling output would be observed. It is obvious that the replications could never be perfect, but it is the goal of this study that the epochs would be determined as similar as possible in other conditions. First, the study focused on the rainy season in this region, which is objectively determined by analyzing the distribution of monthly rainfall in both sub-regions and the whole region, using 1961-1990 gauge data as an indication of regional climatology. Results show that rainfall peaks earlier in the south sub-region than the north, which is associated with the south-to-north shifting of the transmeridional rain belt in early rain season. Overall, April to October seems to be a proper definition of the rainy season for the whole region, comprising 85% precipitation (Fig. 3.8). Epoch analyses are performed for each month in the rainy season. Determined from the water level plot (refer to Fig. 1.6), the two abrupt water level jumps in 6/2003 and 10/2006 divide the 12 years into three periods: "pre dam" (1/1998-5/2003), "post dam" (2003.6-2006.9) and "post dam II" (10/2006-12/2009). Take July as an example, the 12 Julys in 1998-2009 are initially divided into three epochs: 1998-2002, 2003-2006 and 2007-2009. Depending on the water level data, other months may have different divisions of epochs. After the initial division, the next step is to keep the large-scale condition similar within each epoch. 700 hPa and 850 hPa geopotential heights (GPH) are good indications for the synoptic condition. The average GPH for July (Fig. 3.9) is easily composited using the online composite tool (http://www.esrl.noaa.gov/psd/cgi-bin/data/composites/printpage.pl). Then the 700 hPa and 850 hPa GPH of each of the 12 Julys are compared with the average July GPH. A July is included in the epoch if the primary wind direction inferred from the GPH falls in the same quadrant or is within 45 degree of the composite wind direction in the 700 or 850 hPa GPH. The positions of high and low height centers are

also considered. Similar procedures are performed for other months. The final divisions of epochs are listed in Appendix B.

3.5.4 *Epoch Analysis*

Once the epochs are determined for each month, rain rate composites of the top 25 percentile rain days (representing heavy rain condition) from the TMPA data (given that the validation results suggest TMPA data have good quality in this region) are calculated. Then the percent changes of the two "post-dam" composites are derived by comparing with the "pre-dam" composite. Some literature suggests that mesoscale influences would be more apparent under weak synoptic condition [*Shepherd*, 2005; *Mote et al.*, 2007], while heavy rain days are more likely to associated with strong synoptic conditions in this region with strong monsoon influence. Therefore, rain rate composites of the mid 50 percentile rain days are also retrieved and analyzed in similar procedures.

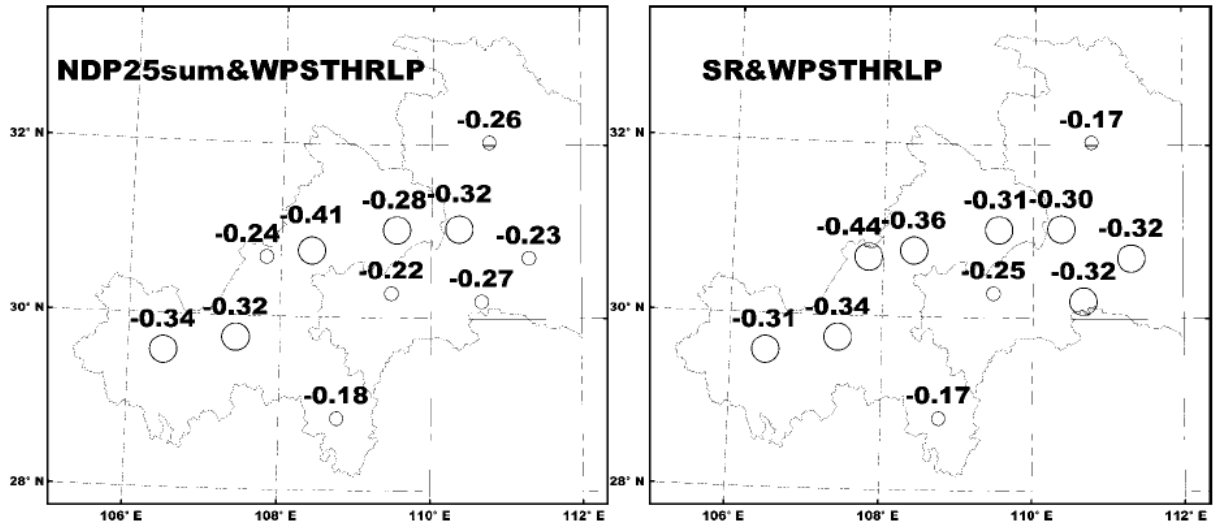


**Fig. 3.1**. Correlations between cumulative precipitation for days with rainfall exceeding 25 mm (NDP25sum), summer (JJA) rainfall (SR) and West Pacific Subtropical High ridge line position (WPSTHRLP). Correlation coefficients are shown next to the stations. Large circles denote that the correlation is significant ($p < 0.05$). Stations with significant correlations are along the reservoir, which is located in the middle of the region (not shown) (From Fang et al. 2010).

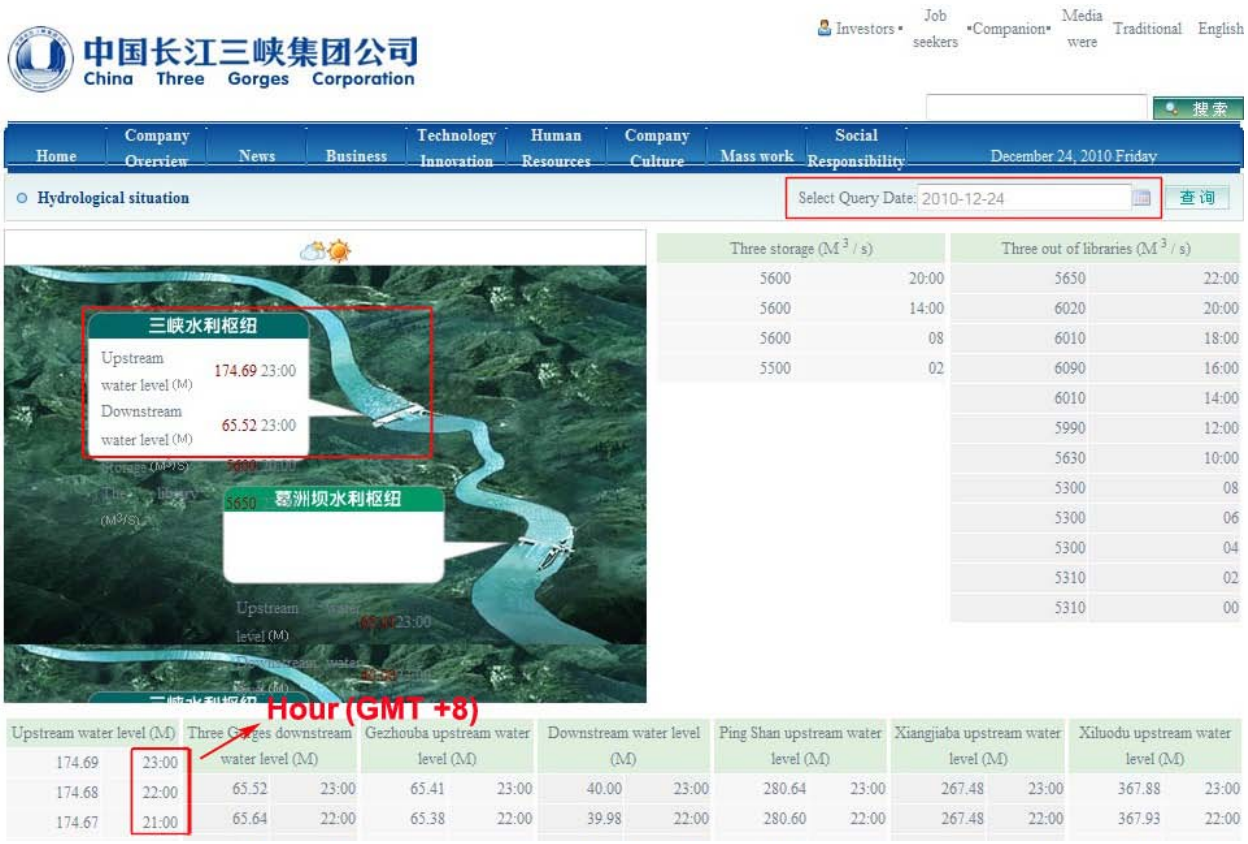


**Fig. 3.2**. The official website of the State-owned China Three Gorges Corporation (Google Translated). It is the source for hourly upstream water level data.

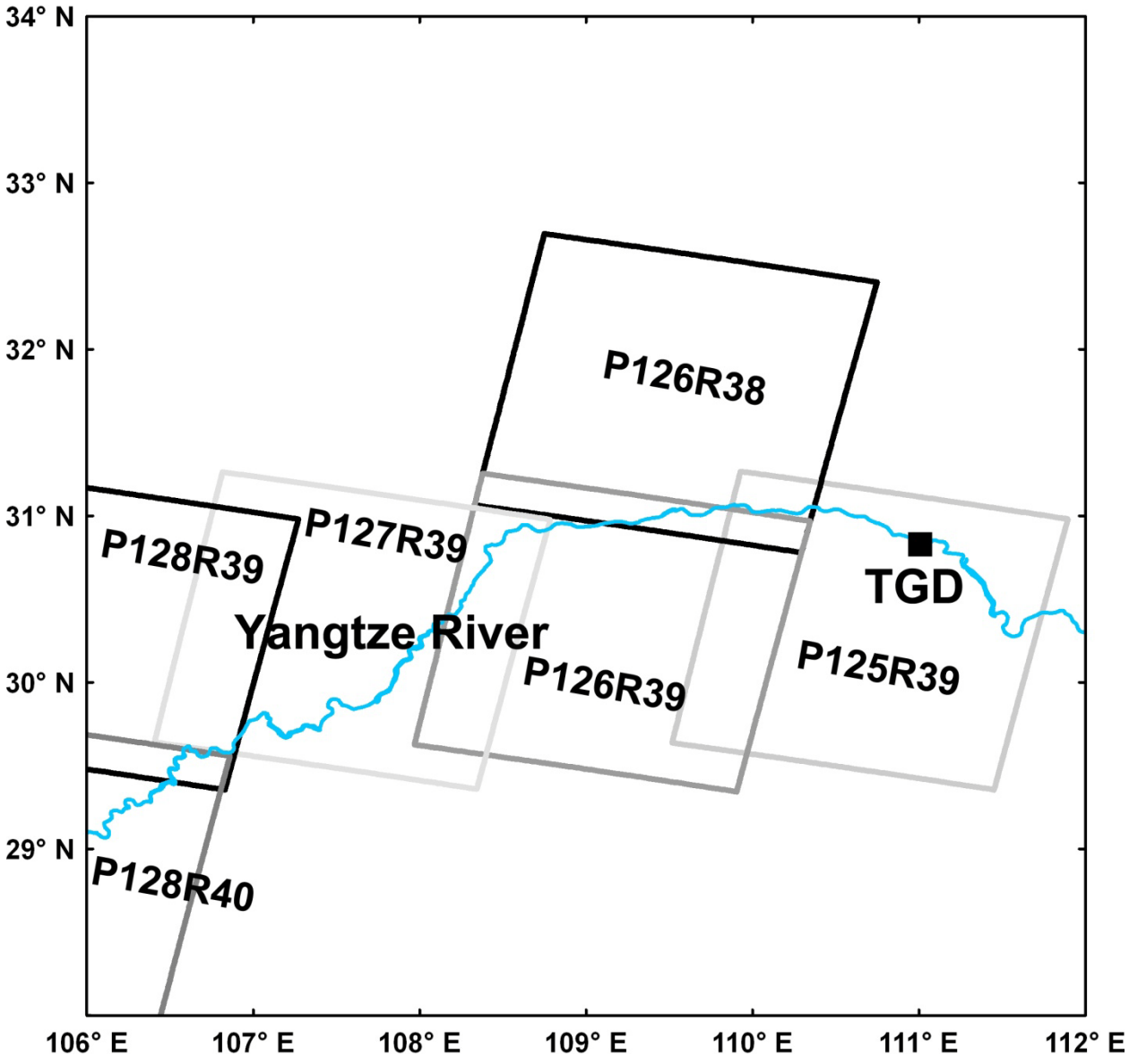


**Fig. 3.3**. Locations of the six scenes covering the whole reservoir area (shown in blue on the left of the TGD) depicted as boxes with their path/row numbers.

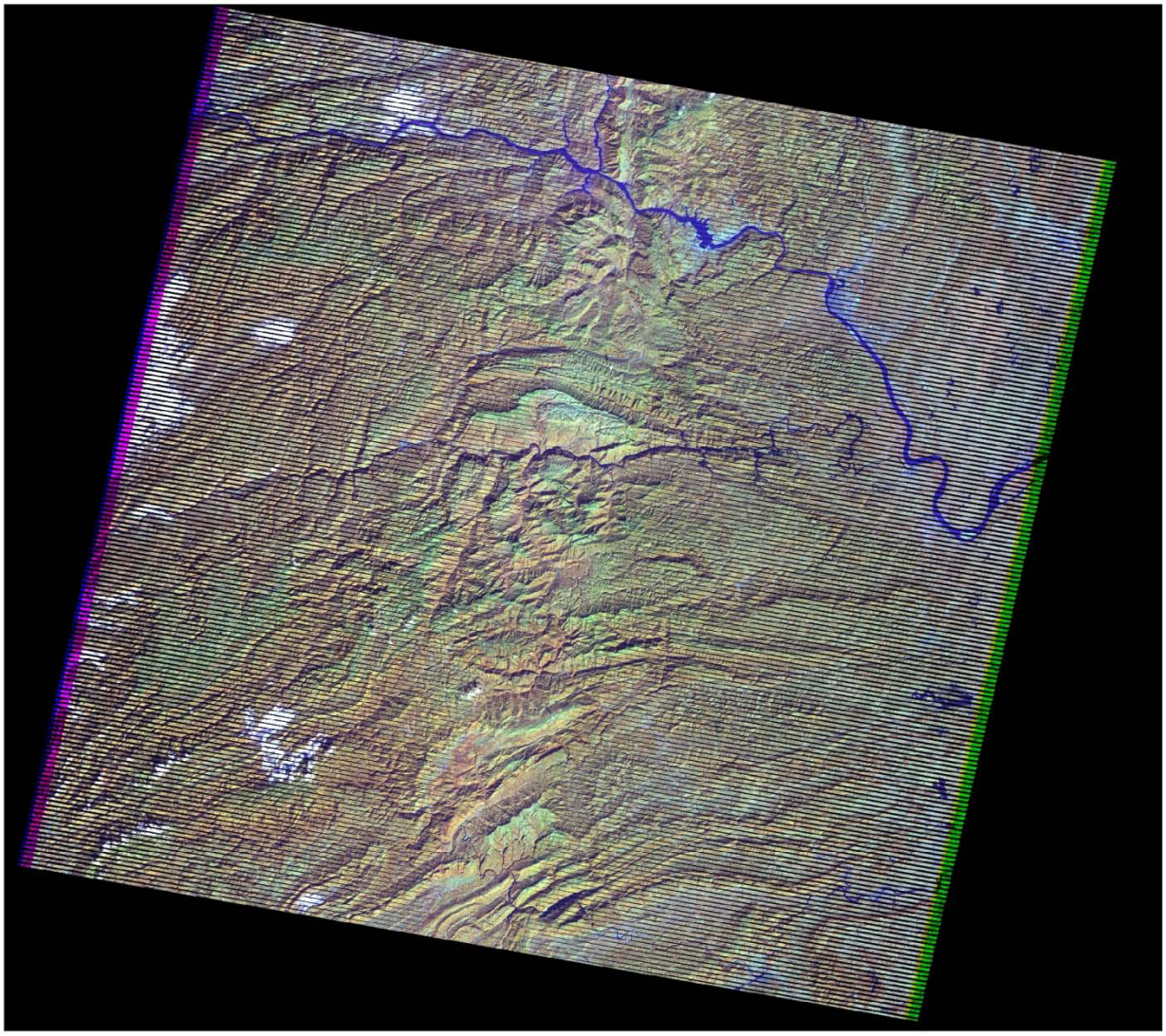

**Fig. 3.4**. An example of one of the original scenes which has the SLC problem. The data gaps are shown as black strips, which are widest near the left and right borders. The gaps are reduced near the central part of the image.

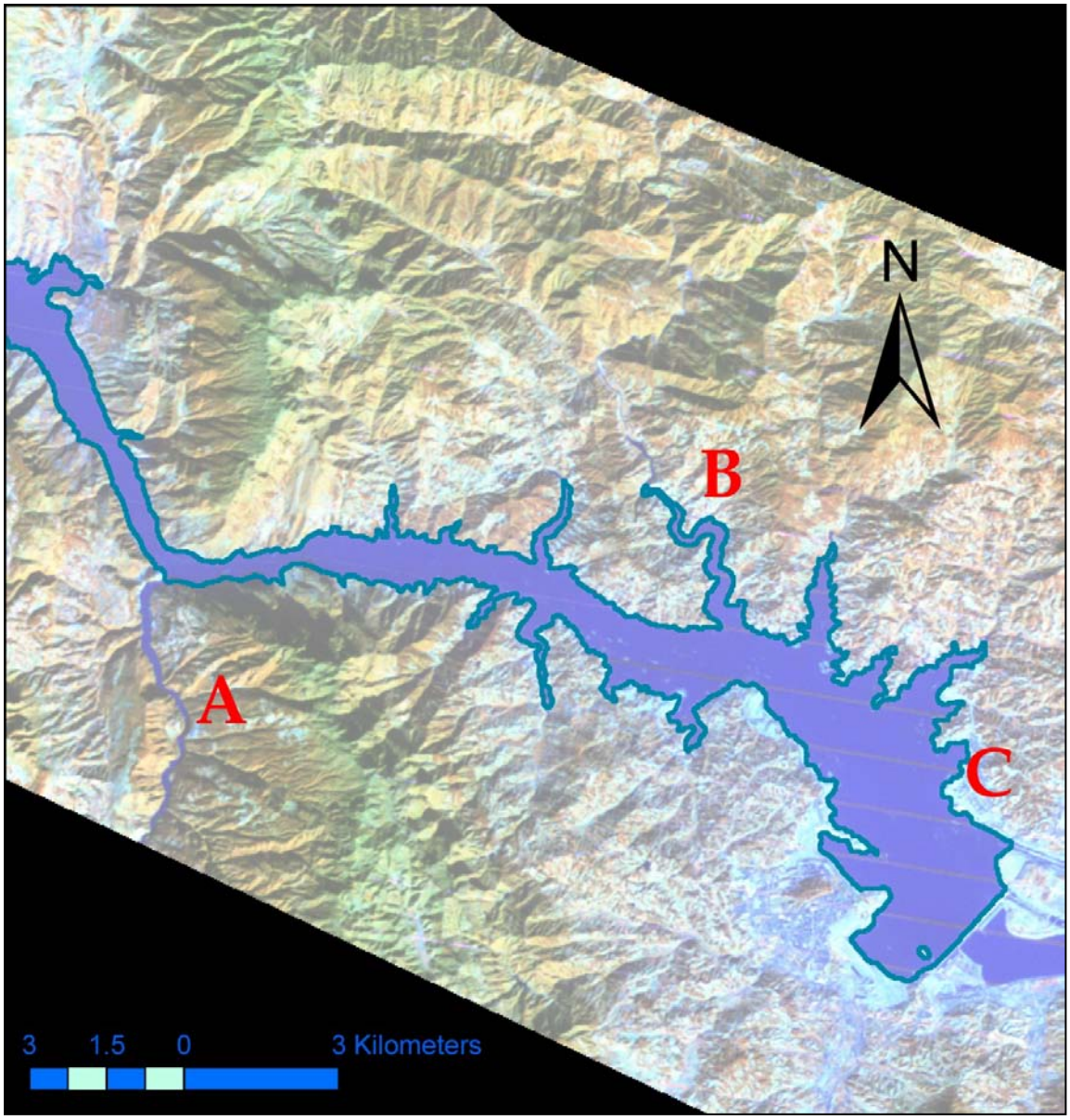


**Fig. 3.5**. An illustration showing the starting part of extracted reservoir area polygon at stage 4. Water level is marked with dark blue line. The image is a composite of band 4, 5 and 3, depicting a good contrast between land and water. A is considered a tributary and not included because it stretches out to the border, and B is reckoned part of the reservoir as defined since most of it is confined within a short distance from the trunk. The horizontal light grey strips at C are mosaic data which fills the data gaps of the original scene.

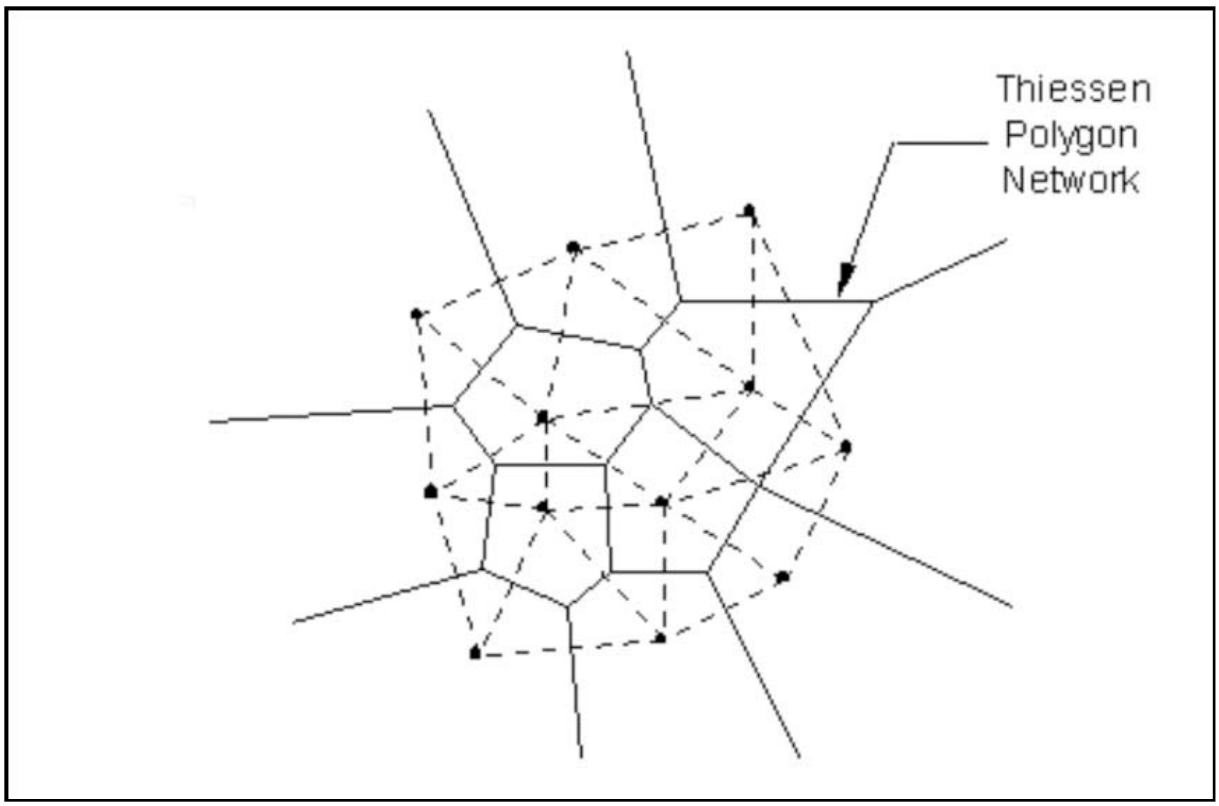


**Fig. 3.6**. Conceptual illustration of the Thiessen Polygon Network (http://www.ems-i.com/smshelp/Data_Module/Interpolation/Natural_Neighbor.htm).

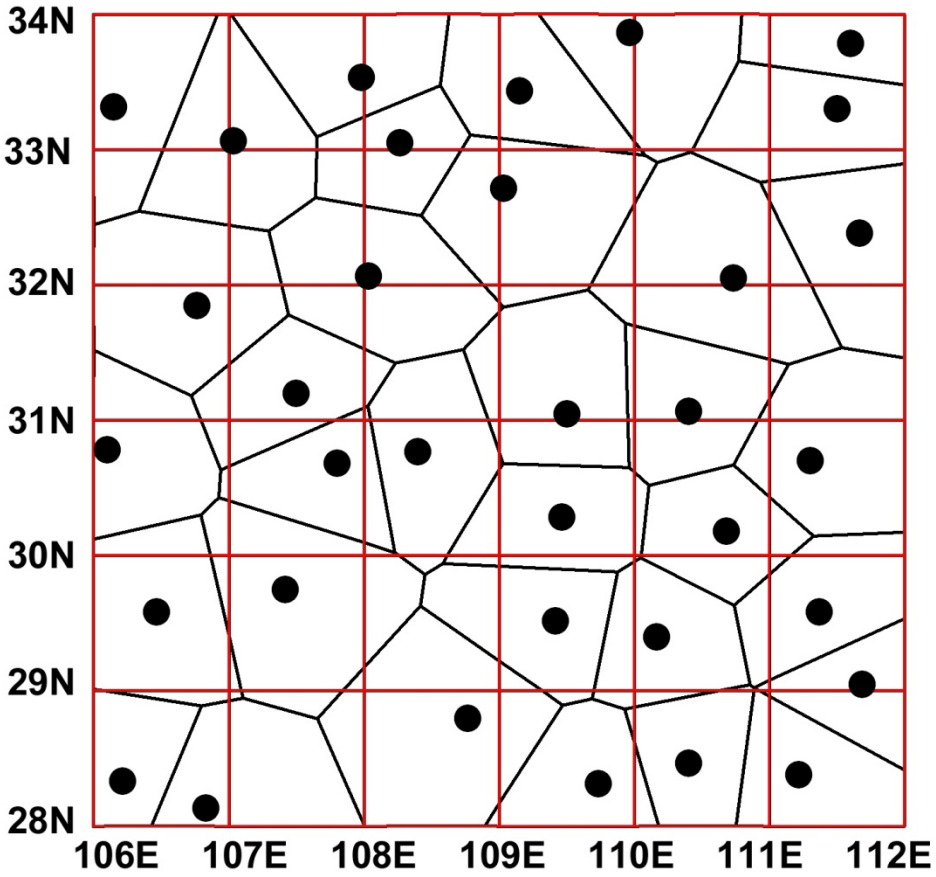


**Fig. 3.7**. Location of the 34 rain gauges (black dots) and Thiessen polygons (black) superimposed on the 36 one-degree cells (red).

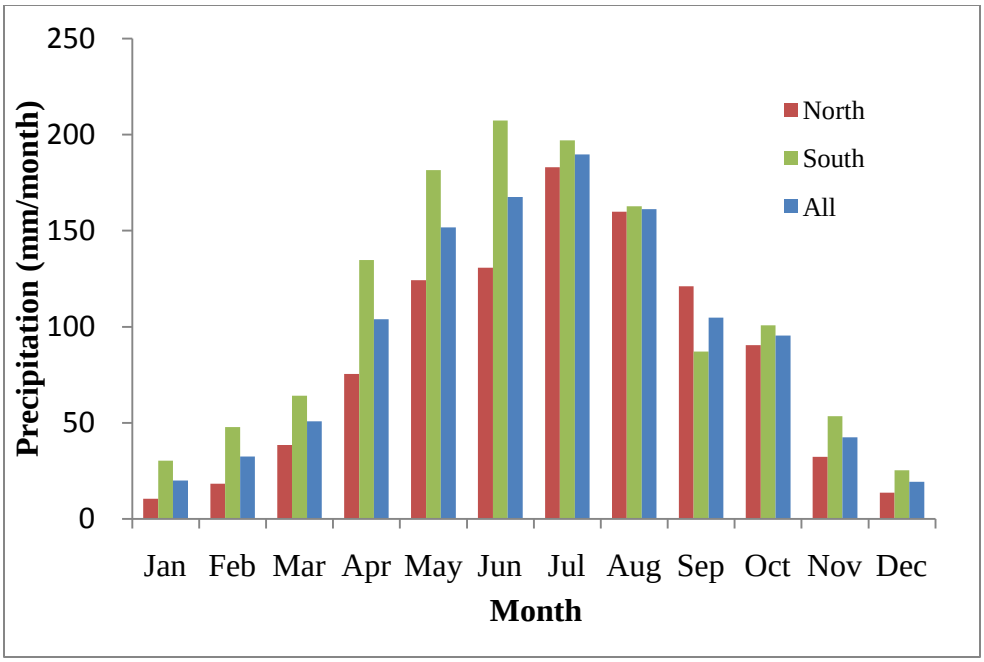


**Fig. 3.8**. Distribution of monthly precipitation over the whole region and the two sub-regions using 1961-1990 observation data from 34 China national rain gauges.

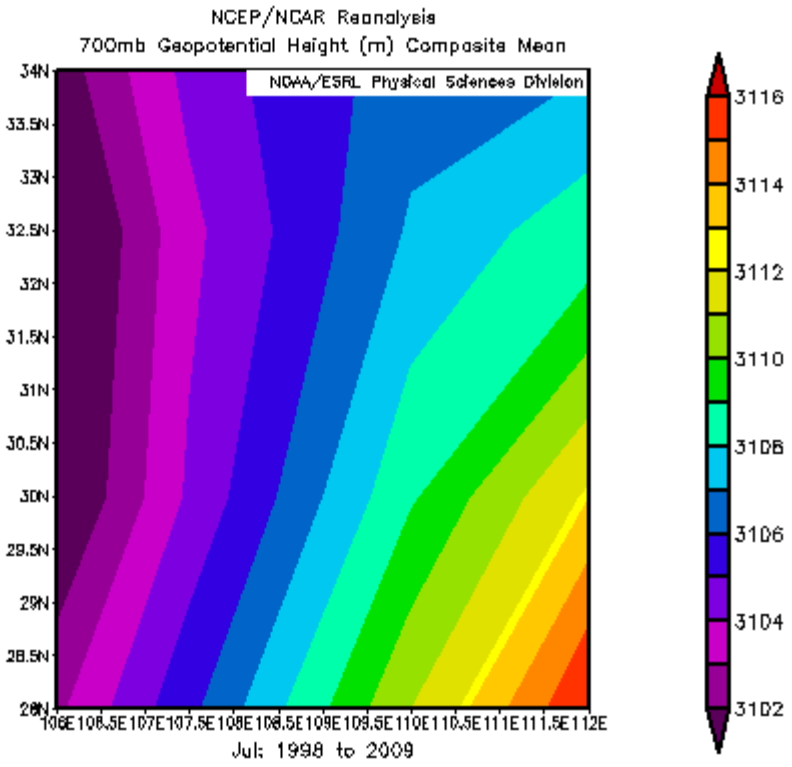


**Fig. 3.9**. An illustration of 700 hPa Geopotential Height (m) composite mean for July.

# CHAPTER 4

# RESULTS AND DISCUSSIONS

In this chapter, the results of water level-reservoir area relationship and validations of TMPA data are presented. Heavy and moderate precipitation composite maps of July are given as examples for the epoch analysis. The implications and possible mechanisms associated with the results are also discussed.

## 4.1 Water Level – Reservoir Area

The five water level-reservoir area pairs are plotted and fitted in Fig. 4.1. A second-order polynomial trend line is found to have a lower RMSE (RMSE = 9.96 $km^2$) than that of a linear, power, exponential or logarithmic relationship. The reservoir area as defined in this study expands from below 400 $km^2$ to about 750 $km^2$ as the water level rose from about 69 m to near 164 m (above sea level) upstream of the dam. At any water level (x, 69-164, m), the defined reservoir area (y, $km^2$) could be estimated from

$$y = 0.038x^2 - 5.165x + 557.4$$

Another important characteristic is that the width of the reservoir surface does not expand uniformly. At various distances upstream of the dam, the reservoir expansions at different water level stages are shown in Fig. 4.2. The expansion is largely dependent on the characteristics of the border and islands of the reservoir. If the border is steep, then little expansion occurs. In other cases, the water can inundate more low elevation land. As the water level rises, many islands in the river become much smaller, or fully inundated. For the region about 100 km to 250 km upstream, the reservoir did not expand much beyond the 146 m water level, because that part of the region is very mountainous (refer to Fig. 1.4) with steep river banks. The reservoir also did not expand much beyond the 146 m water level for the region 530 km upstream. The influence of rising water level is limited because this region might be too far from the dam,

or this region is more developed and people construct higher banks to prevent the reservoir from expanding. All these spatial heterogeneities of the reservoir could provide useful information in future interpretation of various reservoir impacts.

The attempt to compare the estimated values with the available published data was not possible due to different definitions of the reservoir. The area extraction of the reservoir in this study only focused on the mainstream, and the area of the mainstream is likely the most important mesoscale attribute for climate impact analysis. The detailed official reports may have a much wider definition of the reservoir including inundation of the tributaries, because they are interested in how much area is inundated. The information about how the official data were obtained, datasets used, and the methodology and assumptions (if any), of these reports are largely unavailable. Limited information from news reports and the Chinese Embassy in the U.S. are: at the water level of 175m, the length of the reservoir is 663 $km^2$, the reservoir covers an area of 1045 $km^2$, and the inundated slant area is 632 $km^2$ (http://www.china-embassy.org/eng/zt/sxgc/t36512.htm). A previous study has utilized the Shuttle Radar Topography Mission (SRTM) digital elevation model (DEM) data to compute the total and inundated reservoir surface areas, as well as the water volume and length of the reservoir at water levels between 135 and 175 m [*Wang et al.*, 2005]. Their computation is based on the bathymetry in a study area that they delineated, which is also different from, and larger than the definition of the reservoir in this study. They calculated the surface area at 165 m water level to be 903 $km^2$, which is about 150 $km^2$ larger than the result from a comparative water level in this study. They speculated that the SRTM DEMs have voids in shadow areas where there are no backscatters to the radar, phase unwrapping anomalies, or other radar-specific causes (e.g. low coherence). The SRTM DEMs also have a coarser resolution (90 m). The authors stated that ground truthing might be impossible due to the larger areal extent and cost, and Landsat 7 data suffers from the SLC failure problem. With the data processing procedures in this study however, the SLC problem seems to be a minor issue after mosaicing of the data gaps. Lack of cloud-free images, especially at higher water level, appears to be a bigger problem and may have affected the result in this study. The methodologies of using remotely sensed data as described in this study could be of value for future

verifications when there are sufficient cloud-free scenes for better interpretations of reservoir areas at higher water levels.

## 4.2 TMPA Temporal Validation

### 4.2.1 *Region-Wide Validation*

Areal mean monthly rainfall estimates from the 576 TMPA 0.25° (~25 km) grid cells are compared with the areal averages from the 34 gauges to determine how well the rainfall distribution from the TMPA data correlates with the gauge data. Validations over the whole region yield high correlations both annually and seasonally. The correlation between TMPA (y) and gauge (x) data over the 144 months (1998-2009) is represented as:

$$y = 1.0039\ x + 2.0879$$

The regression lines for both precipitation estimates are located barely above a 1:1 line. The correlation coefficient of determination $R^2$ for the 144-month regression is 0.983, and RMSE is 9.1 mm month$^{-1}$ (figure omitted). Over the study area, the TMPA product slightly overestimates the precipitation recorded by gauges, but the mean bias (2.4±8.8) is well within the range (from -1.0 to 1.0 mm day$^{-1}$, or -30.0 to 30.0 mm month$^{-1}$) noted by Tian et al. [2007]. When grouping the 144 months into four seasons, the correlations are still high, although a little lower than before. Fig. 4.3 is the scatter plot of satellite versus gauge precipitation estimates for the four seasons in the study area. The regression line and its corresponding equation and $R^2$ value are shown for each of the four seasons of 36-month pairs. TMPA overestimates precipitation compared with gauge estimates in all seasons but winter.

### 4.2.2 *EOF Analysis*

The temporal and spatial variations of mean annual precipitation in the study area are analyzed by the EOF method. Fig. 4.4 shows the first and second leading modes of the EOF, including their spatial patterns. The results indicate that the first EOF mode (Fig. 4.4(a)) accounts for 46.8% of the total variance while the second mode (Fig. 4.4(b)) explains 30.0% of the total variance. The spatial and temporal patterns obtained from the TMPA data are similar with the EOF results presented by Xiao et al. [2010] in

Fig. 4.5 (note the similarity of the time variance curves from 1998 to 2005). The EOF analysis shows that the dominating factor of precipitation has some consistency throughout the region (same sign for the first mode). The time variances (Fig. 4.4(c, d)) show that large scale patterns are not fluctuating severely in the 12-year study period, which sets a good stage for an epoch analysis. Based on the north-south pattern from the second mode, the region is divided into north and south sub-regions. No further dividing is necessary as any mode other than the first two explains less than 10% of the total variance.

4.2.3 *Sub-regional Validation*

The correlations over 144 months for both the north and south sub-region are still high (regression lines close to 1:1, $R^2$ = 0.9771 for north and 0.9737 for south, RMSE = 11.5 for north and 12.3 mm $month^{-1}$ for the south sub-region, figures omitted). Over the north sub-region, the TMPA product overestimates the precipitation recorded by gauges, the mean bias (5.2±10.3 mm $month^{-1}$) is larger than averaging over the whole study area, but still well within the range of ±30.0 mm $month^{-1}$ noted by Tian et al. [2007]. Over the south sub-region, TMPA only slightly overestimates the precipitation with a lower overall bias (0.6±12.3 mm $month^{-1}$). When examined in four seasons, winter is found to have the lowest $R^2$ values in both sub-regions (Fig. 4.6, Fig. 4.7). Overall, the correlation results suggest that while averaging over a smaller region does make the correlations a little lower with larger biases and RMSE errors, it is not substantial enough to conclude that TMPA performs poorly when validated with smaller regions.

4.2.4 *Daily Scale Validation*

The distribution of TMPA is also correlated with gauge data at daily scale for over 4, 000 days, and the correlation coefficient is found to be significantly lower ($R^2$=0.4594), as one might expect because the 3B43 monthly data are aggregated. The daily cumulative rainfall curves of TMPA and gauge data show close resemblance (Fig. 4.8). They have similar annual cycles where TMPA data are lower than gauge data in most of the first half years, and catch up in most of the second halves. In the end, the accumulated rainfall for 12 years of TMPA is only slightly higher than gauge (13,307.6 mm versus 13,293.0 mm).

4.2.5 *Frequency Analysis*

The frequency distribution of occurrence of daily rainfall totals in the ranges 0–0.005 (trace), 0.005–0.1 (very low), 0.1–1 (low), 1-5 (moderately low), 5-10 (moderately high), 10-25 (high) and >25 (extreme) mm is produced. The results from both satellite and gauge estimates show that the area-averaged high and extreme rain days (area-averaged daily rainfall totals exceed 10 mm) occur less than 9% of the time. The two estimates have good consistency for occurrence of rainfall in the categories over 1 mm $day^{-1}$. This indicates that TMPA does not bias the rainfall distribution of moderate or higher intensity. Below this threshold, TMPA has much fewer days with <0.005 mm $d^{-1}$ precipitation, and compensate in the other two categories. This is probably because the rain gauges are confined by minimum measurement, thus having much more "0" readings. Note that this precipitation region is not likely to be substantial and useful for agricultural production, and it is unlikely to influence the conclusion of this study.

4.3 TMPA Spatial Validation

Mean monthly (averaging from 1998 to 2009) rainfall estimates from the aggregated TMPA 1°×1° grid cells are compared with the corresponding estimates (area-weighted conversion from the Thiessen Polygons) from the gauge estimates to determine how well the rainfall distribution from the TMPA data correlates with the gauge data. TMPA is found to be spatially correlated well with gauge data. The correlation coefficient is $R^2$=0.91 annually and the bias is 3.3±5.6 mm $month^{-1}$ with a RMSE of 6.5 mm $month^{-1}$. Spatial correlations are not as high in summer and fall ($R^2$=0.8054 and 0.8498, respectively) compared with spring and winter ($R^2$=0.9387 and 0.9536, respectively). The scatterplots for all monthly 1-degree matchups between the gridded gauge data and the aggregated TMPA estimates for the four seasons from 1998 to 2009 are shown in Fig. 4.10. The regression line and its corresponding equation and $R^2$ value are shown for each panel. TMPA overestimates precipitation compared with gauge estimates in all seasons, and the overestimation is smallest in winter (note that winter precipitation is the lowest of all seasons). Fig. 4.11 presents the spatial difference maps for four seasons (TMPA - Gauge). Less than 1/3

of the whole area is found to have a difference higher than 15 or lower than -10 mm month$^{-1}$ in any season. The quality of TMPA data is found to be more satisfactory in fall and winter (although the difference is small in winter, it is probably due to low winter precipitation in this region). Overall, there are much more positive biases, and they are mostly seen over mountainous regions near the reservoir. All the results of the verifications suggest that the TMPA estimate of precipitation is quite robust in this area. Although rain gauges data are used as a reference (ground truth), they do have some biases of their own. Additional weaknesses are inevitable when converting point-source data to data grids, as noted in a precipitation analysis over Australia converting from up to 6000 gauges to 25 km grids [*Weymouth et al.*, 1999]. The quality of the analysis depends on the density of gauge reports (sparse data imply larger errors), the complexity of the local terrain (because gauges in mountain areas are generally sited in valleys and, therefore, underreport the true areal average rainfall), and undercatch [*Huffman et al.*, 2007]. Because gauges are spatially less dense and tend to be located on relatively low and flat ground in the study area, it is likely that many topographically induced precipitation events will not be captured by the rain gauges. Therefore, the point-source gauge data might underestimate precipitation in the mountainous regions. The large positive "bias" of TMPA might represent the true precipitation conditions.

## 4.4 Epoch Analysis

Epoch analysis yields daily rainfall composites which represents an "average" heavy or moderate rain day. They show general patterns of a certain intensity of rainfall under normal synoptic condition. The monthly epoch analysis (April–October) results for heavy precipitation (top 25 percentile, usually above 10 mm d$^{-1}$) indicate that high precipitation values are found along the transmeridional rain belt which is associated with the position of subtropical high (refer to Fig. 3.1). This is further supported by the north-south pattern that the EOF analysis revealed. These patterns suggest that the concentrated high precipitation areas as illustrated in Fig. 4.12 (July composite is given as an example here, other months show similar pattern of rain belt north or south of that in July) are most likely governed by large-scale atmosphere factors such as the position and strength of the subtropical high. In July, the rain belt is

approximately located over the central latitudes of this region. The areas with high values of rain rate might result from multiple mesoscale convective systems embedded in the transmeridional rain belt. It would be difficult to for the mesoscale factors like the influence of the reservoir to be observed when synoptic scale forces are dominant.

Compared with heavy precipitation days, moderate precipitation days (usually 1-10mm $d^{-1}$) appear to be less influenced by large-scale forces. Epoch analyses results for composites of moderate precipitation (mid 50 percentile) days reveal clear differences between "pre dam" and two "post dam" epochs in summer months. Fig. 4.13 and 4.14 shows the contrast of July as an example (similar patterns are displayed for June and August, although July is most revealing). The patterns suggests that rainfall in moderate rain days are suppressed in the area adjacent to the reservoir, while there are increases for regions away from the reservoir on both sides (north and south). Given that the large-scale settings are similar, the most significant difference among the epochs is the change of the reservoir surface area.

The patterns observed are not exactly as hypothesized. Although rainfall does decrease in the vicinity of the dam, it does not just increase in the downwind direction (primary wind direction is approximately south-southwest in July, as estimated from the 850 hPa GPH), but increases on both sides away from the reservoir. It was previously assumed that the evaporation and extra moisture from the reservoir would be brought downwind and contributed to more precipitation there. However, it seems that the evaporation part from the reservoir is not as important as some other mechanisms. This might be partly due to the shape of the reservoir (i.e., it is not wide enough to induce strong evaporation, but might be long enough for mechanisms such as "lake breeze" to occur). The evaporation differences among the epochs might not be significant enough for precipitation changes to occur. However, this warrants further study.

Moderate precipitation constitutes about a third of the total precipitation, and the patterns found have significant implications for the region. In most of the moderate rain days (1-10mm $d^{-1}$), rainfall would be effectively absorbed by soil and used by crops. Under average large-scale atmospheric conditions, a decrease of moderate rainfall would further decrease the crop yield for the farmers who stay in the region and work on steeper and less fertile hillside farms. While the government might have

subsidized them for losing their old farms, their losses due to rainfall change, which might be associated with the reservoir, are probably unaccounted. On the other hand, for the regions with increases in moderate rainfall, some are mountainous areas where landslides are a big problem. The increased moderate rainfall would make the soils more saturated and more prone to landslides. Precautions should be taken in those areas to prevent landslide damages, which might occur more frequently (if frequency of heavy rainfall stays the same) in future. The effects suggested by the results of this study would provide valuable information for the decision-makers on adaptation/hazard-prevention strategies, and this thesis would refrain from that part of discussion.

## 4.5 Possible Mechanisms

One possible explanation for the observed patterns is the reservoir might influence the precipitation with a lake breeze-like mechanism as introduced earlier. The difference in sensible heat flux over water and land results in more precipitation occurring in regions on both sides of the reservoir due to the lake breeze induced fronts. The area adjacent to the reservoir has less precipitation due to the relatively stable condition created by the sinking motion. Mesoscale circulation can be more apparent when weak large-scale forcing is in place [*Shepherd*, 2005; *Mote et al.*, 2007]. This is likely the case for TGR in moderate rain days with large enough land-water temperature contrast (summer months). As suggested from the results of this study, there might be a possible relationship between rainfall intensity and influence of TGR in this region, as proposed in Fig. 4.15. TGR effects are less apparent when there are significant large-scale effects, which might be associated with drought (rain intensity near zero) or high intensity rainfall. In other cases, precipitation patterns might be more likely to represent TGR effect as the rainfall intensity goes down, which is found for June, July and August with July (the hottest month) having the clearest pattern. On the contrary, no such pattern is observed for April, May, September and October, this is probably because in these months, the land-water temperature difference is not large enough to initiate local circulation in this mid-latitude region.

However, it is not clear if the lake breeze mechanism alone would explain the observed patterns. The average reservoir width is below 1.5 km, while the length is above 600 km. It is a unique shape that is different from any of the previously studied irrigated land/lakes/vegetation. The effect of this reservoir might be more close to the "river breeze" effect as noted in Dias et al. [2004] and Fitzjarrald et al. [2008], which is found to influence a more local region (~10km). Although TMPA data seems to be the best choice, there could be a scale mismatch since the resolution of TMPA data is about 25 km. Therefore, the results from the analysis of TMPA data may have inflated the influence range. Also, under some circumstances, the influence of the reservoir might combine with other factors like topography, which is very complex in this region. The expanding of the tributaries in this river basin might make the cool air pool wider in the lower atmosphere, and a large portion of the lake-breeze affected precipitation may as well be enhanced by favorable topography and synoptic conditions. Examples of combined effects include river breeze-sea breeze interactions [*Rao et al.*, 1999; *Outlaw and Murphy*, 2000] and urban-topography interactions [*Shepherd*, 2006].

A third possible mechanism is the change of anthropogenic aerosols among the epochs. Aerosols serve as cloud condensation nuclei (CCN) and thus have a substantial effect on cloud properties and the initiation of precipitation (see Rosenfeld et al. [2008] for more information). The question is whether aerosol has changed over the epochs in this region. A quick composite analysis on aerosol optical depth (AOI) at 550nm for three periods (2000.4-2003.4, 2003.4-2006.4, 2006.4-2009.4) using MODIS monthly data seems to suggest otherwise (Fig. 4.16, generated from http://gdata1.sci.gsfc.nasa.gov/daac-bin/G3/gui.cgi?instance_id=MODIS_MONTHLY_L3), as the spatial patterns of the AOI are similar for the three periods, and the trend of changes from the first period to the second and third are different (decrease and increase, respectively), whereas the precipitation changes from "pre dam" to the two "post dam" epochs are similar.

There could also be other possible mechanisms for the patterns observed, and a more in-depth mesoscale modeling approach would be necessary to understand the physical processes better, and it

would be desirable to create series of sensitivity experiments to tease out the effects of the reservoir, topography, aerosol, etc. It is not within the scope of this thesis to further discussing this topic.

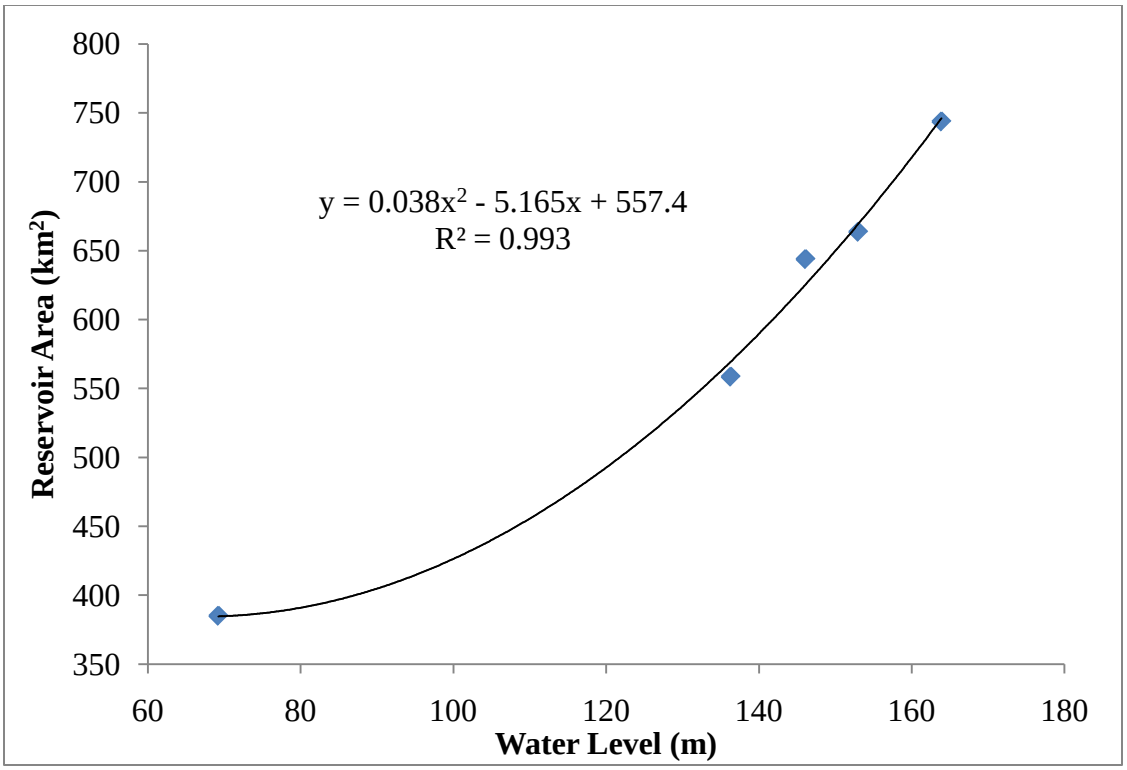


**Fig. 4.1**. Relationship between water level (m) upstream of the dam (above sea level) and the reservoir water surface area ($km^2$).

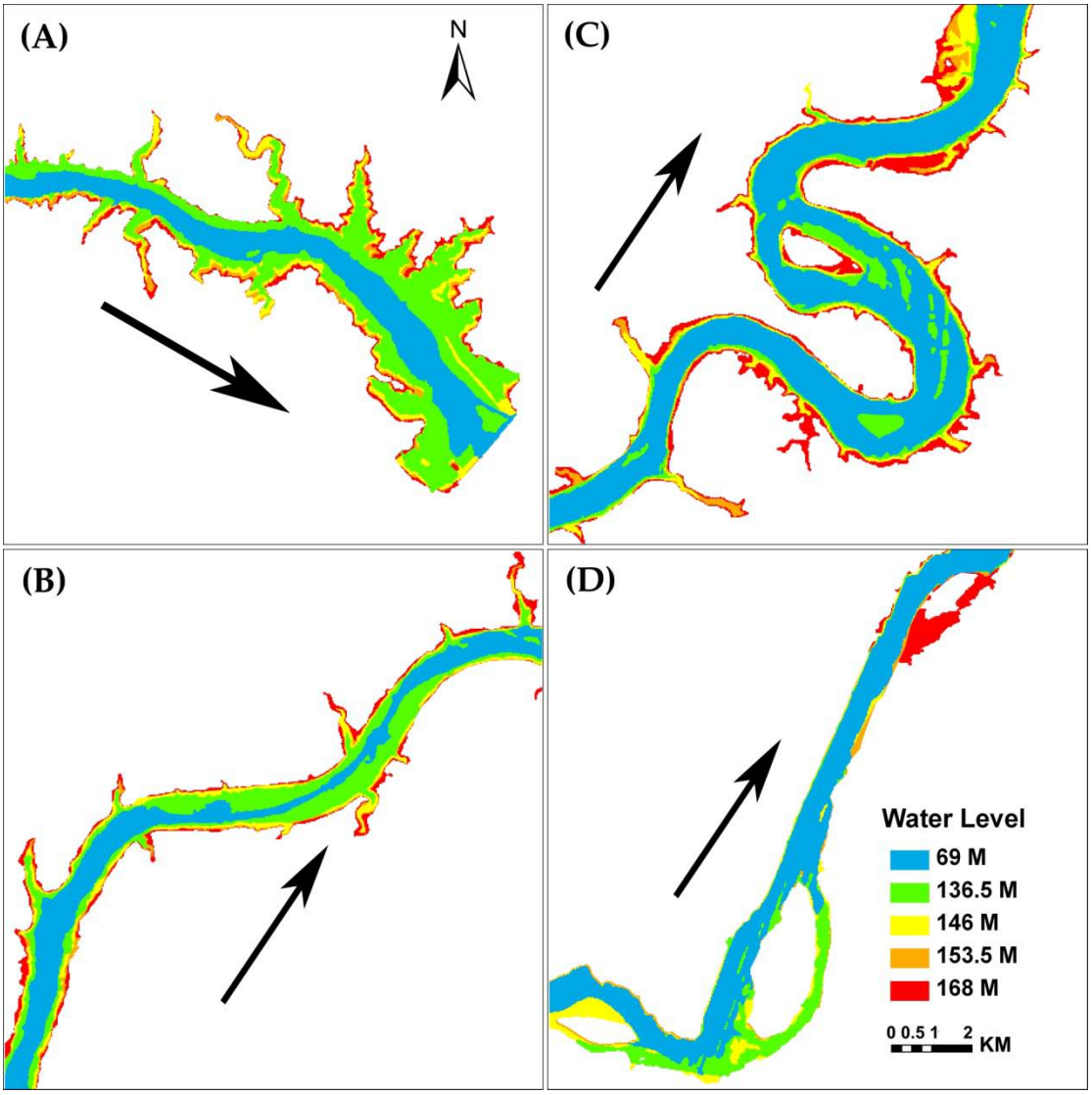


**Fig. 4.2**. Reservoir expansion at different positions as the water level upstream of the dam rises: (A) at the dam; (B) about 260 km upstream; (C) about 360 km upstream; and (D) about 530 km upstream. The black arrows show the direction of the flow.

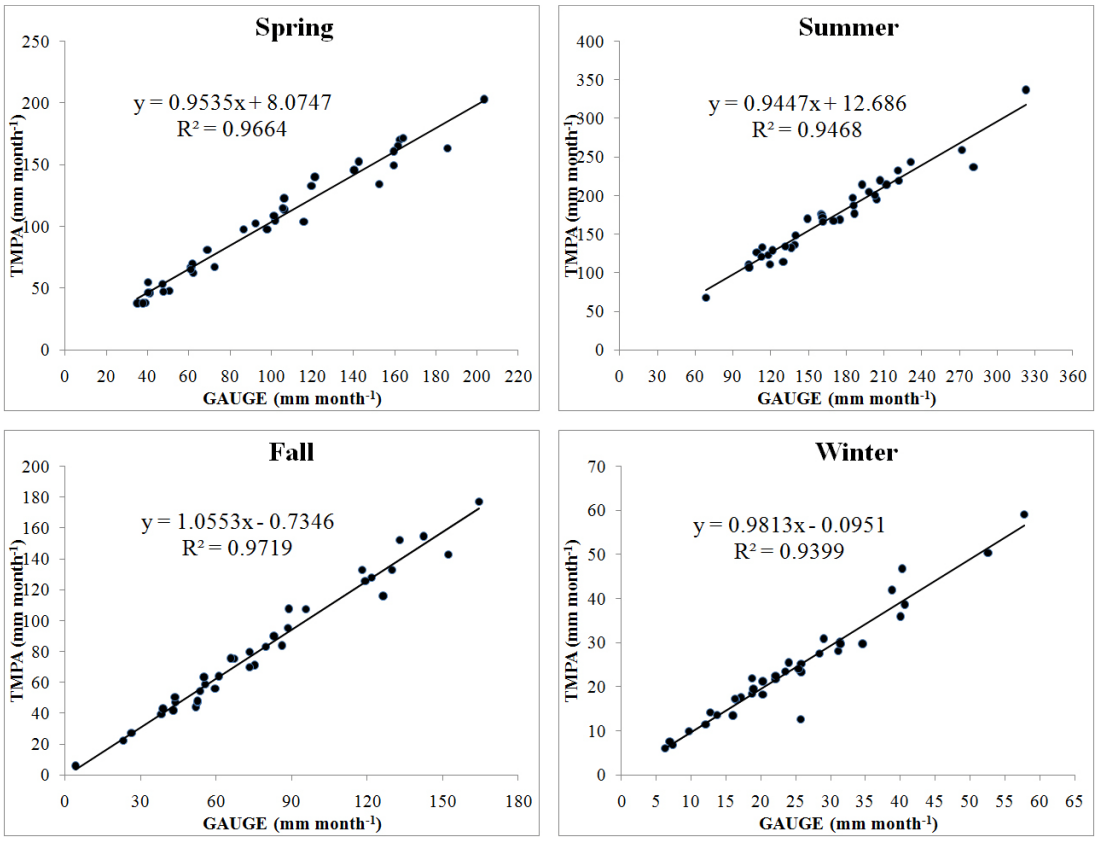


**Fig. 4.3**. Scatter plots of areal average satellite rainfall estimates versus gauge (reference) values (mm month$^{-1}$) for all seasons (36 months each). The linear regression line, formula and $R^2$ are shown. Biases are 3.5±8.9 (spring), 3.3±12.7 (summer), 3.5±7.3 (fall) and -0.6±3.0 (winter) mm month$^{-1}$, RMSE are 9.5(spring), 13.0 (summer), 8.0 (fall) and 3.0 (winter) mm month$^{-1}$. The sample size is 576 grids for all panels.

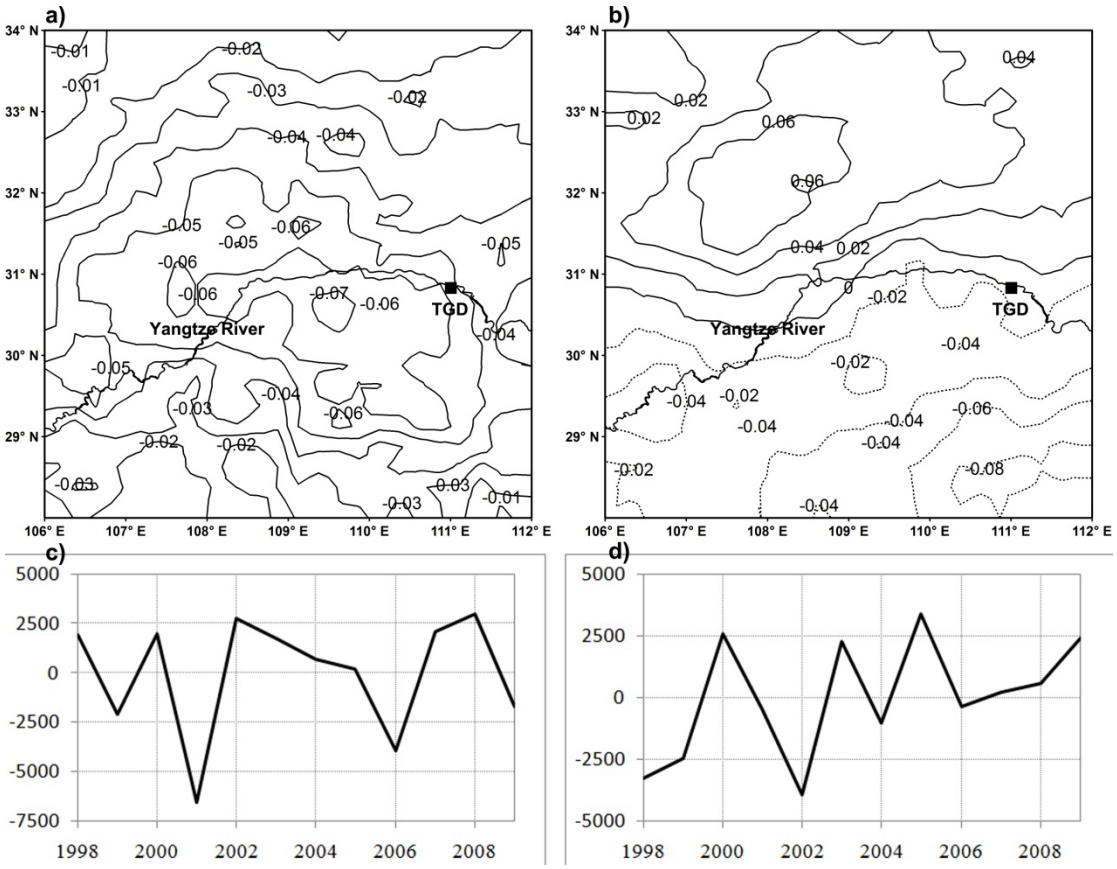


**Fig. 4.4**. The spatial pattern of the EOF's leading modes and the corresponding spatiotemporal variability of mean annual precipitation anomaly in the vicinity of the TGD from 1998 to 2009 (using TMPA estimates). (a) Spatial pattern of the first mode; (b) spatial pattern of the second mode; (c) time variance of the first mode; and (d) time variance of the second mode.

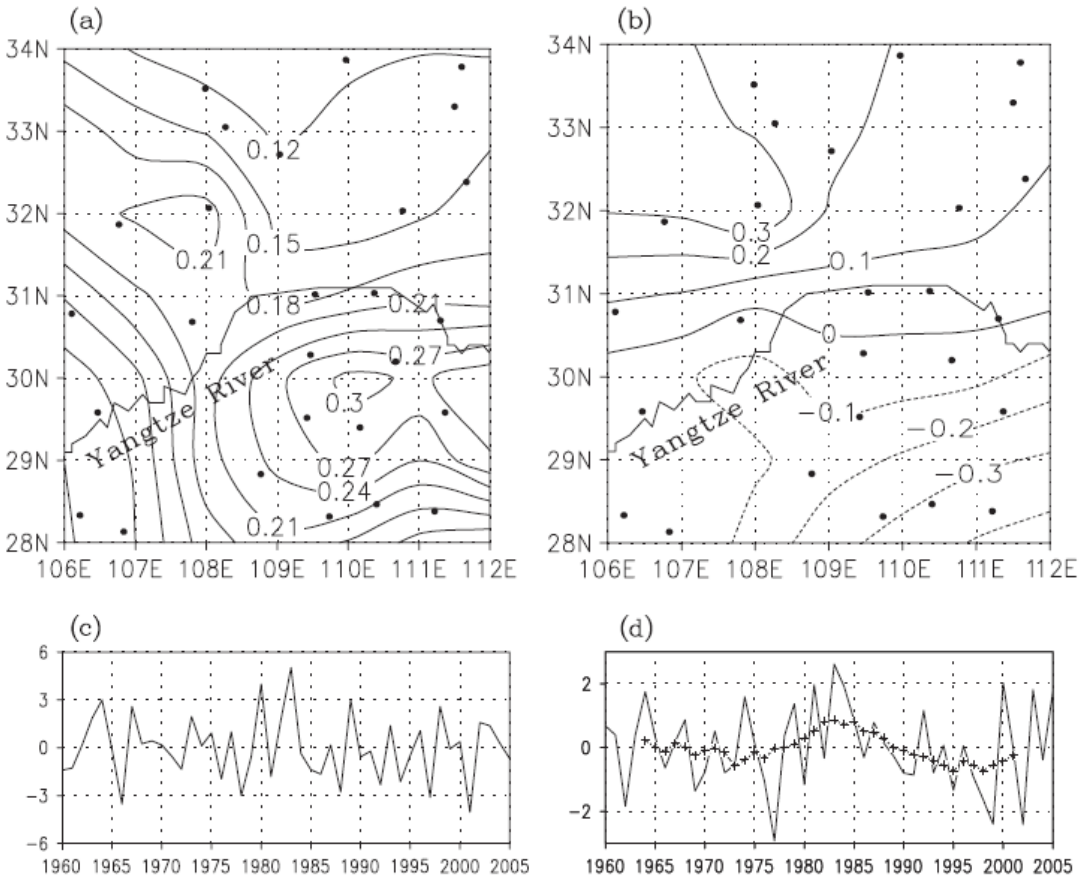


**Fig. 4.5**. The spatial pattern of the EOF's leading modes and the corresponding spatiotemporal variability of mean annual precipitation (mm $d^{-1}$) in the vicinity of the TGD from 1960 to 2005. (a) Spatial pattern of the first mode; (b) spatial pattern of the second mode; (c) time variance of the first mode; and (d) time variance of the second mode and its 9-year moving smoothed time series (crossed line). Black dots denote station locations (from Xiao et al. 2010).

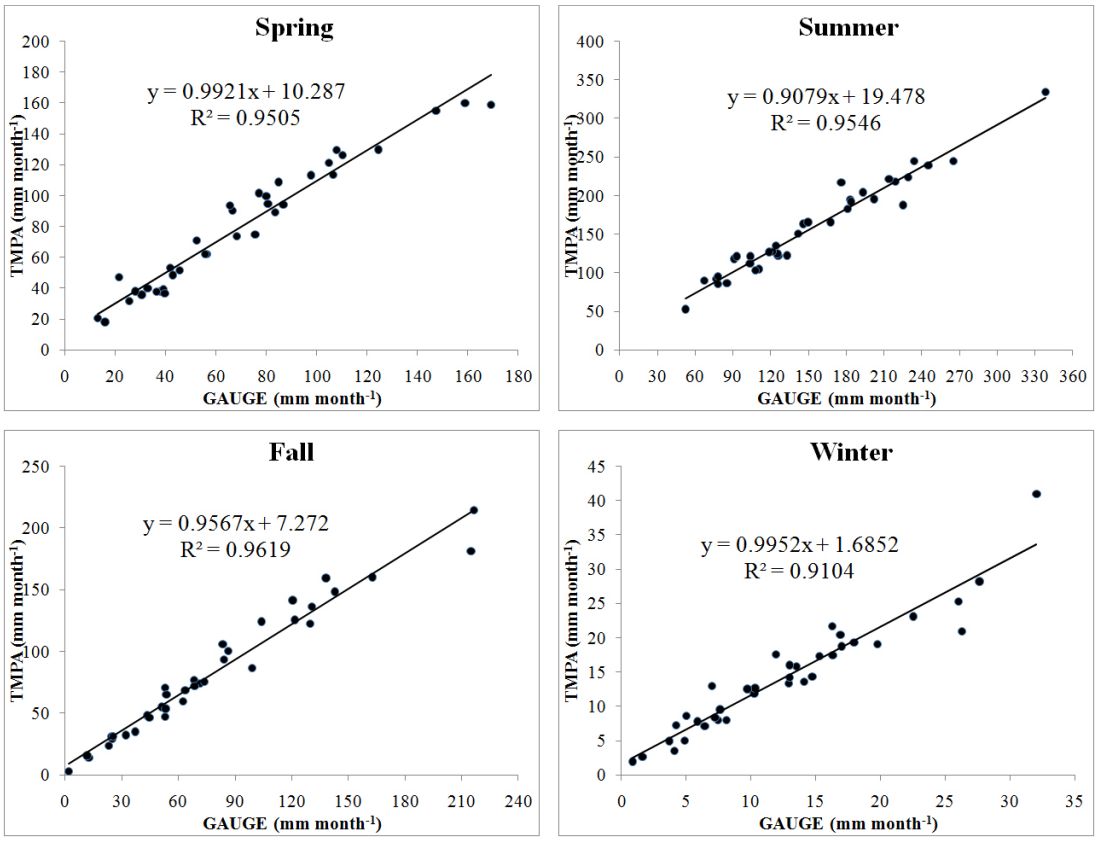


**Fig. 4.6**. Scatter plots of areal average satellite rainfall estimates versus gauge (reference) values (mm month$^{-1}$) for all seasons (36 months each) in the north sub-region. The linear regression line, formula and $R^2$ are shown. Biases are 9.7±9.1 (spring), 5.4±14.2 (summer), 3.9±10.4 (fall) and 1.6±2.4 (winter) mm month$^{-1}$, RMSE are 13.2 (spring), 15.1 (summer), 11.0 (fall) and 2.9 (winter) mm month$^{-1}$. The sample size is 576 grids for all panels.

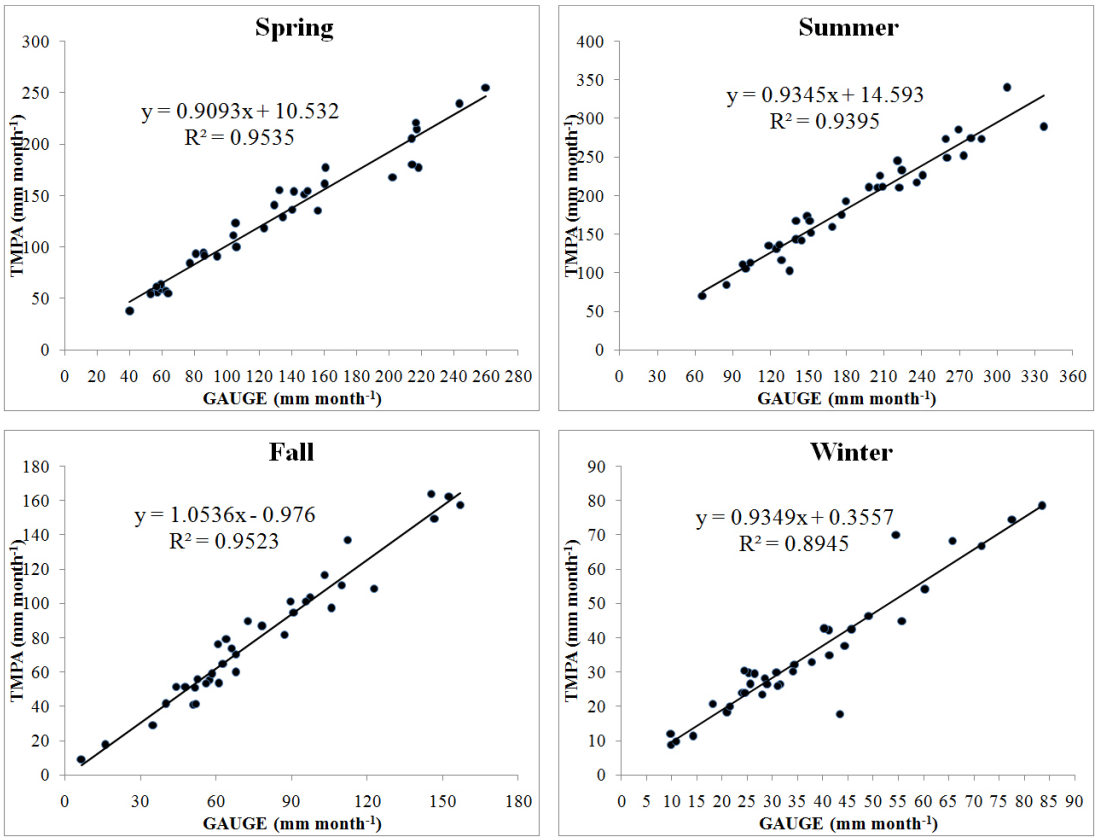


**Fig. 4.7**. Scatter plots of areal average satellite rainfall estimates versus gauge (reference) values (mm month$^{-1}$) for all seasons (36 months each) in the south sub-region. The linear regression line, formula and $R^2$ are shown. Biases are -1.0±13.8 (spring), 2.4±17.0 (summer), 3.2±8.9 (fall) and -2.0±6.1 (winter) mm month$^{-1}$, RMSE are 13.7 (spring), 17.0 (summer), 9.3 (fall) and 6.3 (winter) mm month$^{-1}$. The sample size is 576 grids for all panels.

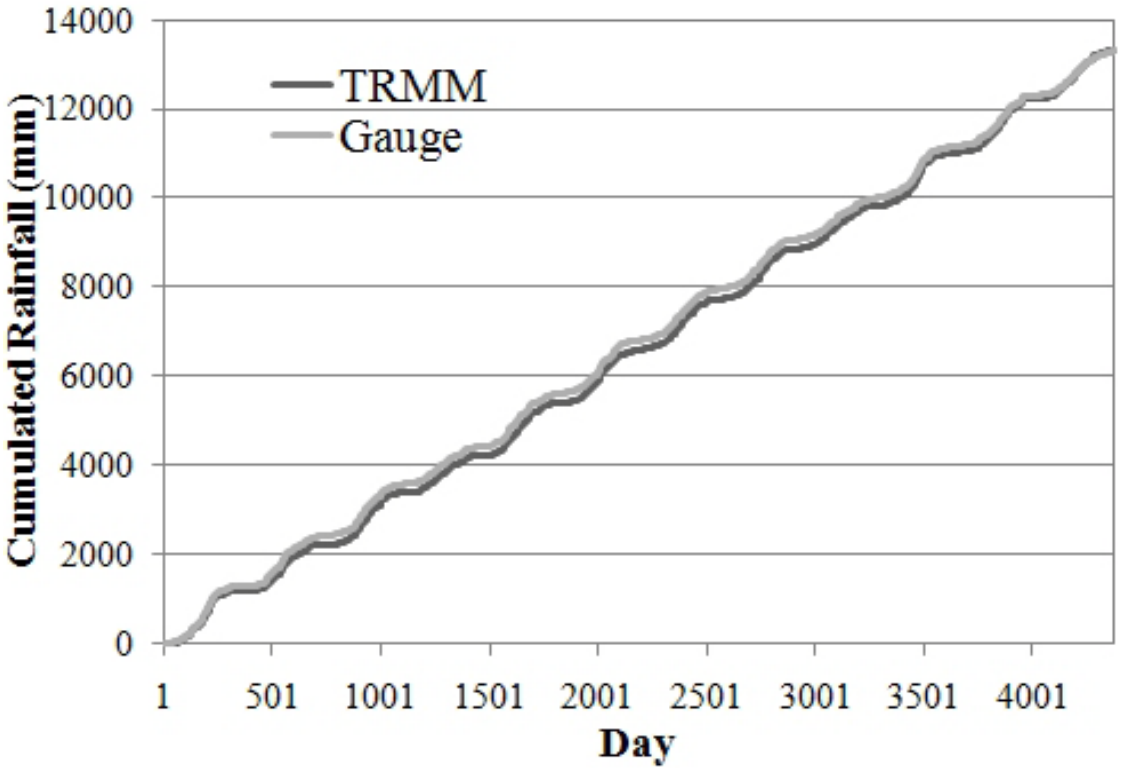


**Fig. 4.8**. Daily cumulative rainfall (area-averaged) curves for the TMPA (black) and gauge (grey) estimates from Jan 1, 1998 to Dec 31, 2009.

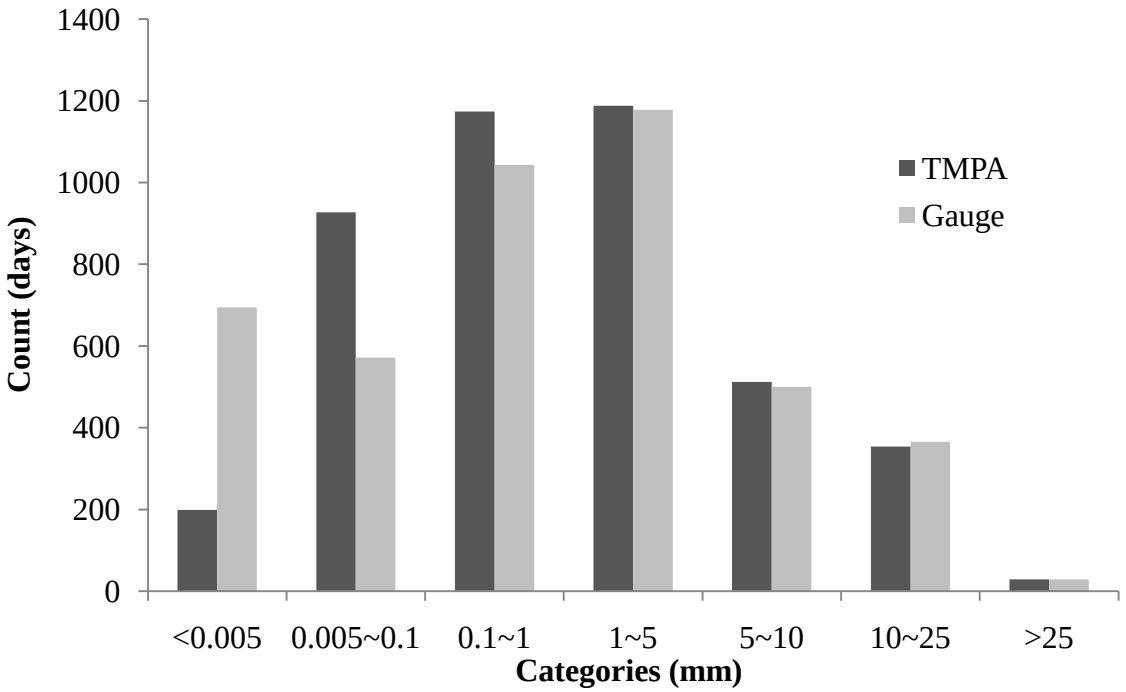


**Fig. 4.9**. Frequency distribution of both TMPA (dark grey) and gauge (light grey) area-averaged daily rainfall estimates from Jan 1, 1998 to Dec 31, 2009.

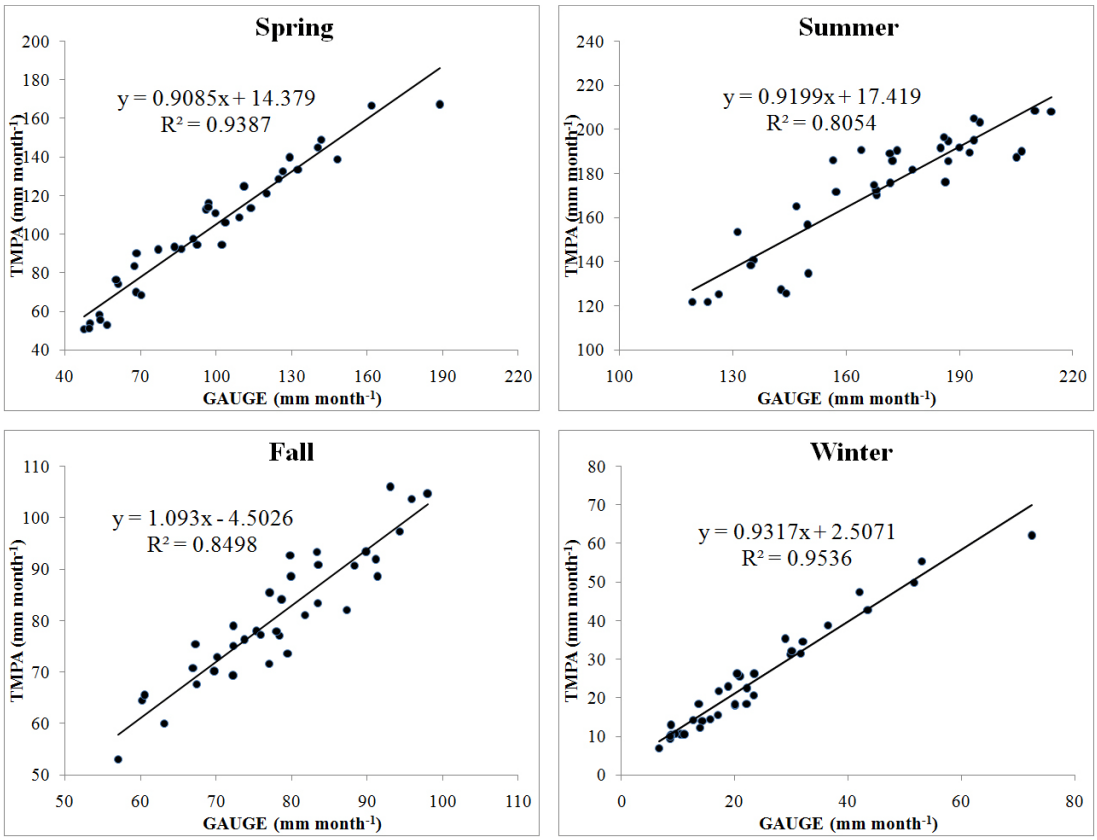


**Fig. 4.10**. Scatter plots of monthly mean satellite rainfall estimates versus gauge (reference) values (mm month$^{-1}$) for all 36 1° aggregated grids in the study area (four seasons, respectively). The linear regression line, formula and $R^2$ are shown. Biases are 5.5±8.6 (spring), 3.9±11.8 (summer), 2.8±4.9 (fall) and 0.9±3.2 (winter) mm month$^{-1}$, RMSE are 10.3 (spring), 12.5 (summer), 5.6 (fall) and 3.3 (winter) mm month$^{-1}$. The sample size is 36 months for all panels.

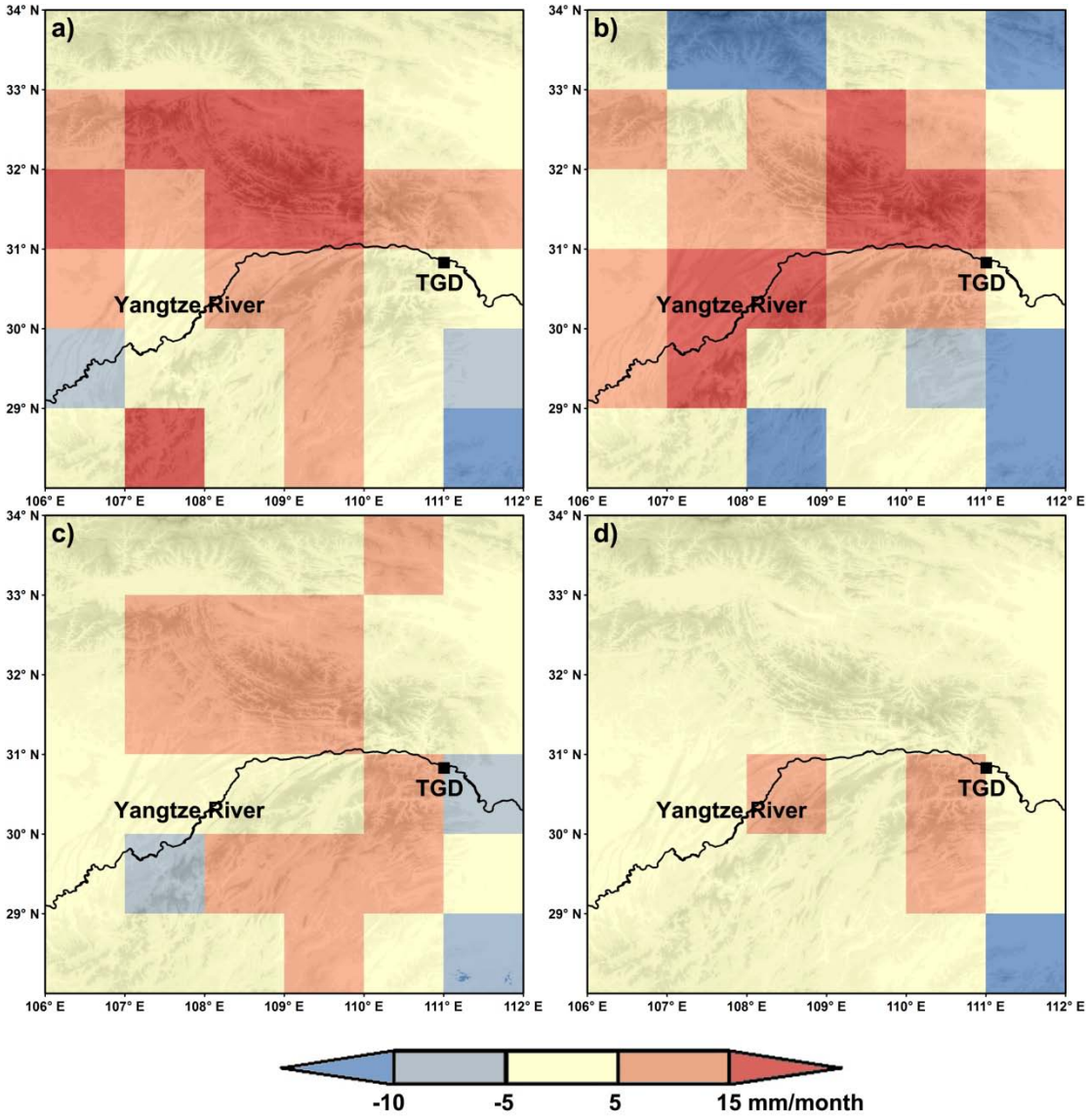


**Fig. 4.11**. Spatial differences (TMPA-GAUGE) overlaid with topography in a) spring, b) summer, c) fall and d) winter. Red indicates overestimations, blue indicates underestimations, and light yellow indicates areas with little differences.

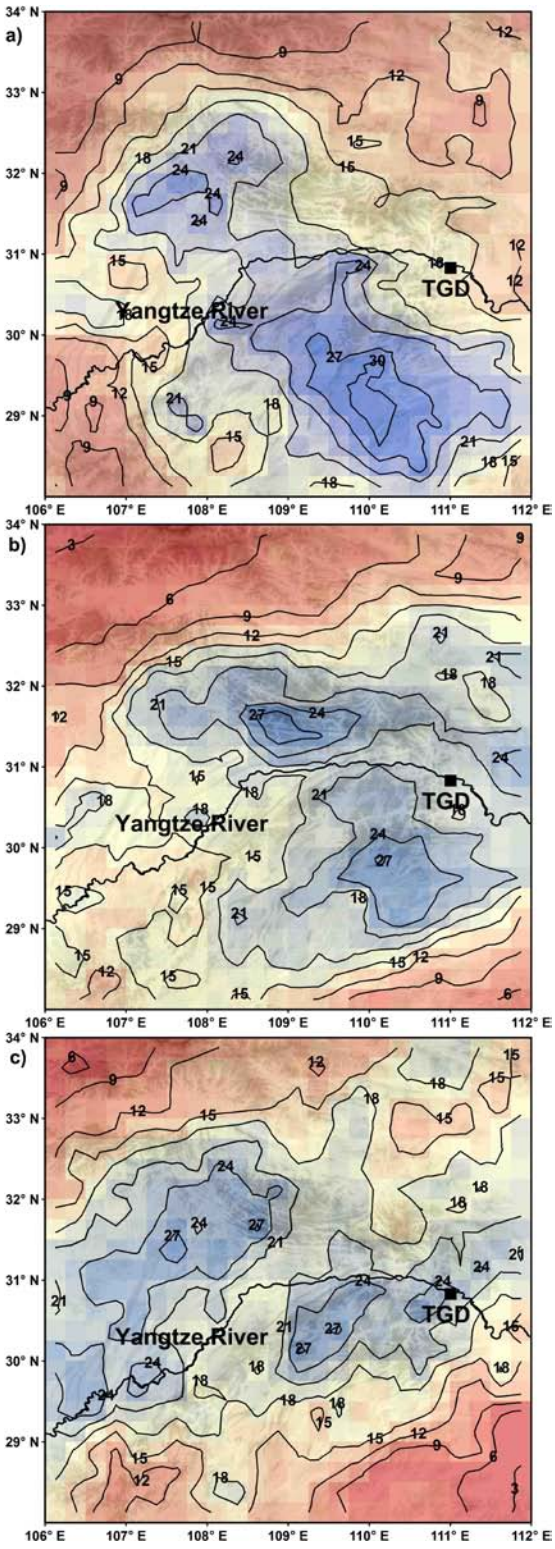


**Fig. 4.12**. Composites of heavy precipitation days (top 25 percentile, mm day$^{-1}$) in July for the three epochs: a) “pre dam”; b) “post dam”; c) “post dam II”.

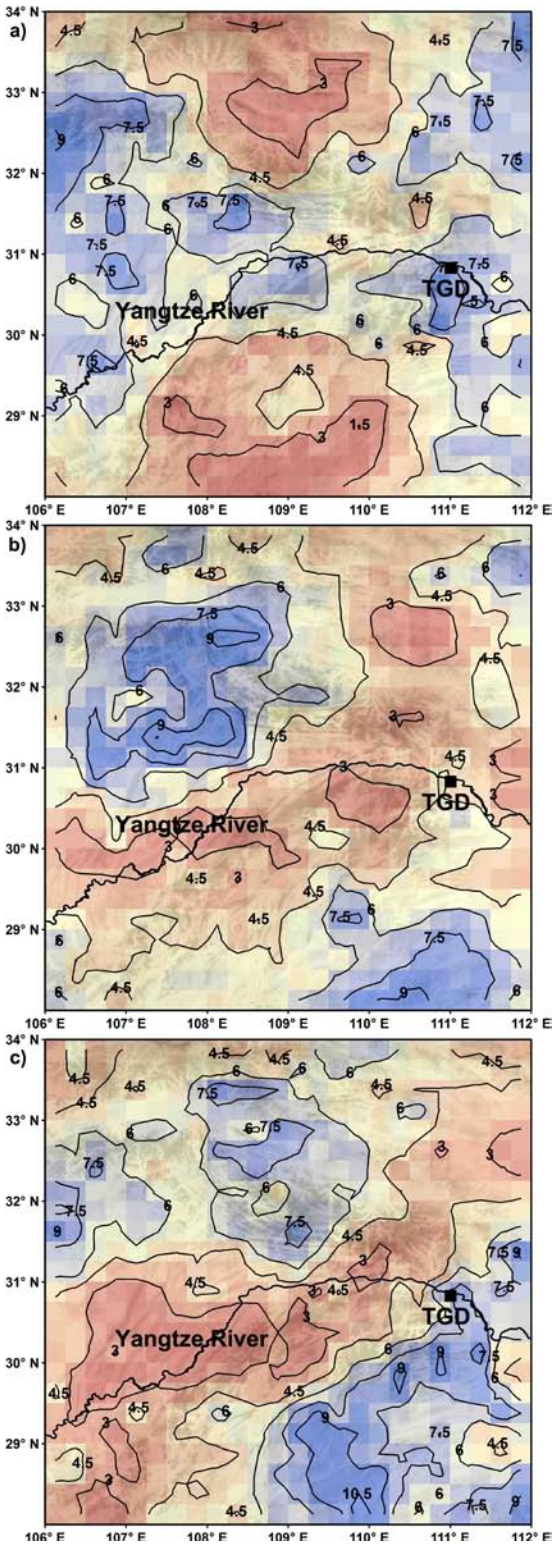


**Fig. 4.13**. Composites of moderate precipitation days (mid 50 percentile, mm day$^{-1}$) in July for the three epochs: a) “pre dam”; b) “post dam”; c) “post dam II”.

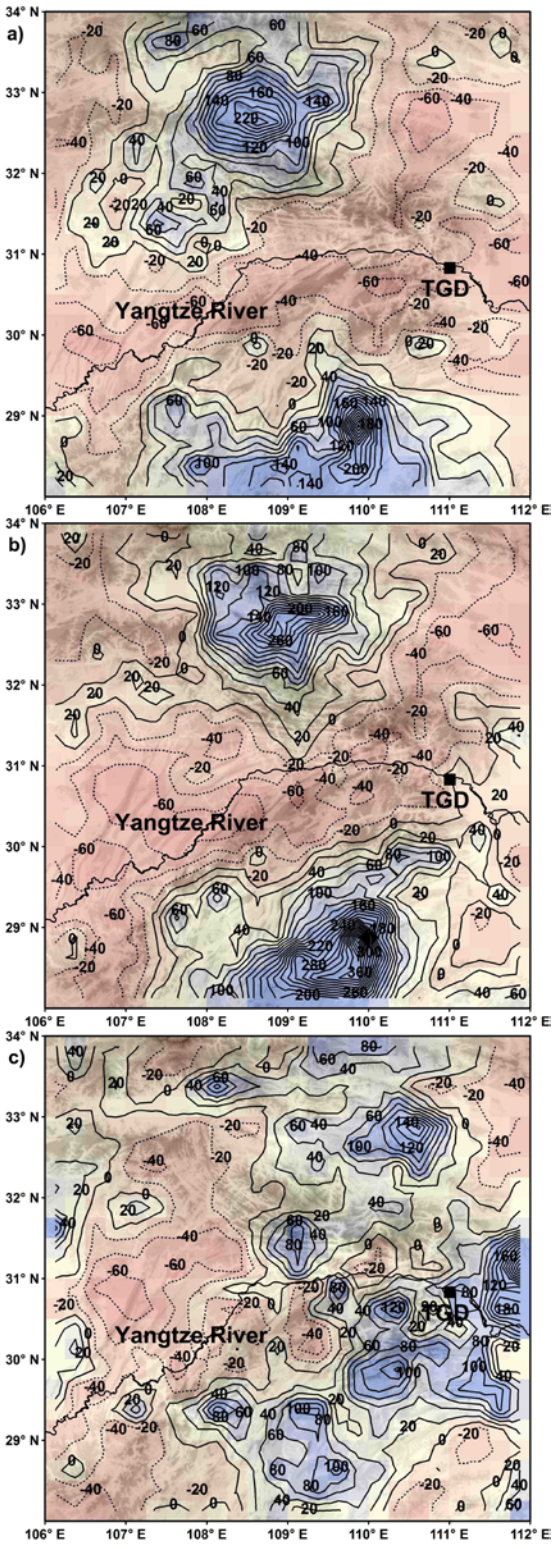


**Fig. 4.14**. Difference maps of composites of moderate precipitation days (Fig. 4.13) between epochs in July (%). a) “post dam”-“pre dam”; b) “post dam II”-“pre dam”; c) “post dam II”-“post dam”.

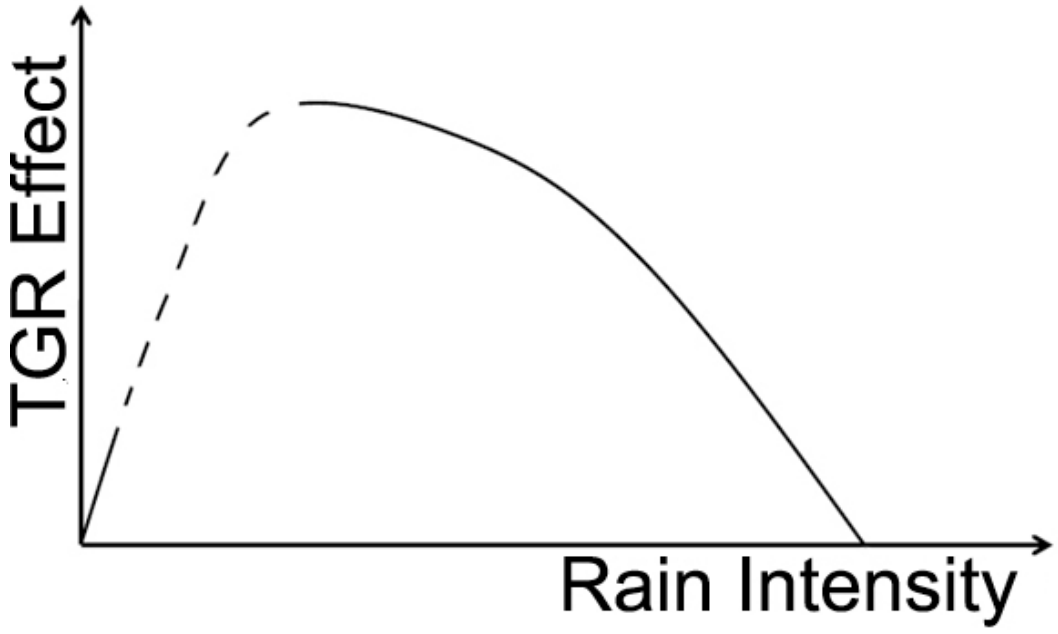


**Fig. 4.15**. A schematic diagram of the relationship between the magnitude of TGR effect and rainfall intensity.

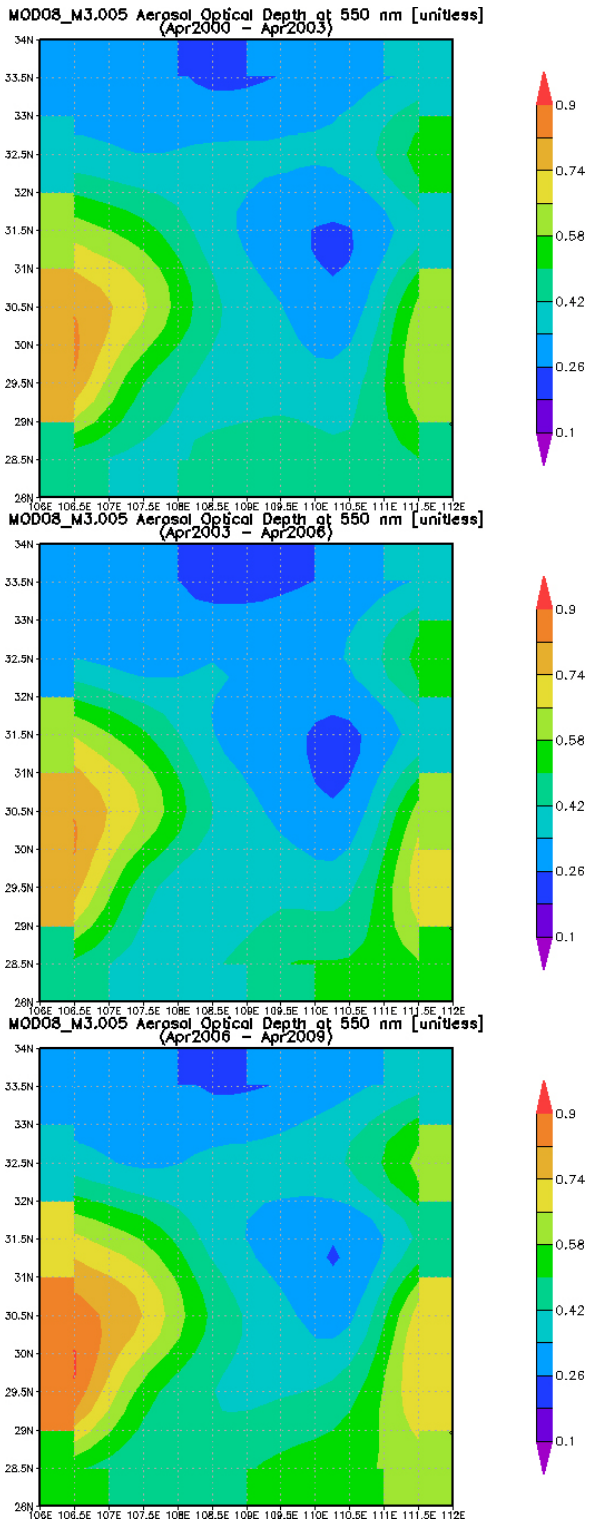


**Fig. 4.16**. Composites of MODIS08_M3.005 Aerosol Optical Depth at 550 nm for the three periods (similar with the epochs): Apr 2000-Apr 2003, Apr 2003-Apr 2006 and Apr 2006-Apr 2009.

# CHAPTER 5

# CONCLUSIONS

## 5.1 Summary

The land surface interacts with the atmosphere through energy and moisture transfers. Sensible heat flux difference over large water body and adjacent land creates local circulation which would alter precipitation patterns in its vicinity in summer. The Three Gorges Dam (TGD) built on the main stream of the Yangtze River has become the largest hydroelectric project in the world, and it has attracted a lot studies on various fields associated with dam. However, little literature exists on the hydroclimate aspect of the project. Miller el al. [2005] found no significant change in precipitation through modeling simulations. However, the simulation period is too short, and they acknowledged that the model they used might not resolve the processes well enough in this region. Wu et al. [2006] concluded that the effects of the dam are significant enough to create a north-south pattern, that is, the precipitation is reduced in the vicinity of the dam, and increased in the mountainous regions in the north. A recent study by Xiao et al. [2010]) refutes Wu et al. [2006]'s conclusion by revealing a similar north-south pattern around 1980. They argue that the pattern Wu et al. observed is more likely to be natural variation. The precipitation changes associated with large hydrological projects have significant implications for agricultural adaptation and natural hazards prevention, and it is useful to perform an epoch analysis on precipitation patterns. The research herein has provided a better understanding as well as directed future research of the effects of large reservoir on local/regional precipitation. The following sections describe the major findings, conclusions, and future directions of the thesis.

## 5.2 Major Findings

The major findings of this thesis are:

- The five stages of water level and reservoir surface area are best fit with a second-order polynomial relationship, and reservoir area at a certain time could be estimated from the derived formula and measured hourly water level data.
- An extensive validation process of TMPA rain rate data shows it has good quality in the study area. Areal average TMPA rain rate data correlate well with the areal average gauge data in all seasons. EOF analysis of the TMPA data yields a similar pattern with the result from Xiao et al. [2010]. The study area is divided into north and south parts, and correlations between TMPA and gauge data in each part are high in all seasons. TMPA estimates are less well correlated with gauge estimates in winter than other seasons.
- TMPA rainfall at daily scale is less correlated with gauge data, although the cumulative curves are similar. A closer examination of the daily rainfall frequency distribution reveals that the discrepancy is mostly due to the mismatches for very light rain days ($< 1$ mm $d^{-1}$).
- Spatial validations of TMPA rainfall through the Thiessen polygon approach also found high correlations, although the spatial differences are more noticeable than temporal ones. Larger spatial discrepancy between TMPA and gauge data is found in summer and fall, and noticeable overestimates are seen in some mountainous regions near the reservoir especially in spring and summer. No more than one third of the whole area is revealed to have a difference higher than 15 or lower than -10 mm $month^{-1}$ in any season.
- Epoch analysis is carried out for both composites of heavy rain days (top 25 percentile) and composites of moderate rain days (mid 50 percentile). While no major distinguishable changes are found for the heavy rain days, it is indicated that in the “post dam” periods, moderate precipitation, which accounts for one third of the total rainfall, is greatly reduced in the vicinity of the reservoir, while increased on both sides 50-100 km (distance is probably inflated due to the resolution of TMPA data) away from the reservoir. Local circulation pattern driven by sensible heat flux difference

over reservoir water surface and surrounding land in summer (a “lake breeze” like mechanism) interacting with favorable topographical and atmospheric conditions is speculated to be the most likely cause.

## 5.3 Conclusions

This research introduced a method to estimate the surface area of the Three Gorges Reservoir from measured hourly water level data upstream of the dam. This may be utilized in future modeling studies. The method to establish the water level-reservoir area relationship by simple interpretation of Landsat images illustrates an easy, quick, practical and efficient way of quantifying the expansion/contraction of reservoir/lake that takes place during a certain period. This is especially useful when field survey data of reservoir/lake surface area is unavailable for the region of study.

Multiple correlation analyses indicate TMPA rainfall has good quality in the study area. Overall, TMPA tends to overestimate rainfall by about 3 mm per month. Temporally, TMPA estimates correlate less well with gauge data in winter. Spatially, compared with gauge data, noticeable TMPA overestimates are found in some mountainous regions adjacent the reservoir especially in spring and summer. A closer examination at the daily scale shows that the TMPA estimates have a similar daily cumulative rainfall curve with that of the rain gauges. The relatively low correlation between TMPA rainfall and gauge data at the daily scale is mostly due to large discrepancy in the frequency of very light rain days ($<1 mm\ d^{-1}$). Similar frequencies are found for other categories with rainfall greater than $1 mm\ d^{-1}$, where the rainfall is more agriculturally/economically meaningful.

Epoch analysis reveals that under similar large scale conditions indicated by 700 and 850hPa geopotential height fields, while there seem to be no major distinguishable changes in heavy precipitation, moderate rainfall is greatly reduced in the vicinity of the reservoir after the abrupt water level shift in 2003. An increase is found on both sides 50-100 km (probably inflated) away from the reservoir. This pattern seems to be associated with the local circulation created by the large sensible heat flux contrast over the reservoir surface and surrounding land interacting with favorable topographical and atmospheric

conditions in summer, as the inundation process is the most prominent land cover change from “pre dam” to “post dam” epochs.

## 5.4 Future Directions

The research presented in this paper has implications for agricultural adaptation and natural hazards prevention. More knowledge on future large-scale circulation changes would provide further guidance for this region, which has a weak economical and ecological status. One limitation of this study is the length of each epoch, even though it is already the longest study period to date. Future work may use up-to-date mesoscale models to simulate the “dam” and “no dam” scenario. Also, it would be useful to tease out the possible influencing mechanisms by investigating other factors like topography through a series of sensitivity modeling simulations. Miller et al [2005]’s suggestion of using fine scale (1 km) multiyear simulations is confirmed herein. After an investigation or literature review of large-scale forces, the methodology used in this study is replicable in other regions where hydroelectric projects have caused huge debates. The procedures to establish water level-reservoir area relationship would be helpful to estimate the change of water surface in areas where survey data are not available. For Three Gorges, after more cloud-free scenes are generated (probably several years later), a revisit of the water level-reservoir area relationship using the same reservoir definition as in [*Wang et al.*, 2005] would allow a direct comparison of accuracy between the two methods. In the survey reports on many Western U.S. reservoirs, the second-order polynomial curve fit the data well. Although five water level-reservoir area pairs are enough to solve the curve, more pairs would allow a more robust regression. It would also be interesting to study the expansion/contraction of more lakes, especially in the tropical regions where the sensible heat flux difference is prominent throughout the year.

# APPENDIX A

Every rain gauge has an inner diameter of 20 cm. The most common type of rain gauges is SM1 made in Shanghai. Rainfall is collected in a glass container through a funnel, which can reduce evaporation. Moreover, an extra observation is done after heavy rainfall in the warm season to minimize the effect of evaporation. In the snowy season, the funnel is removed and snow can fall directly into the container, and it is brought indoors to make the snow melt, then the amount of resulting water is measured. The collecting surface of rain gauges is 70 cm over the ground, and they are installed in open ground. Such location can reach satisfying accuracy as indicated by 'Experimental Research on Rain Gauges Installation Location', which is a national wind tunnel test carried by 16 provincial hydrological stations (National Hydraulic and Hydroelectric Industry Standard of China SL21, 2005). In the late 1980s manual reading procedure has started to be continuously changed to automatic one by installation of siphoning type of rain gauges. The most common type is SJ1 made in Shanghai. The inner diameter is unchanged, the installation locations are chosen in the same manner as previous ones, and the new gauges can measure rainfall INT within the range of 0.05–4 mm/min. The accuracy of precipitation measurements is 0.05 mm. Implementation of this transformation of the reading did not implement change of time to which the reading is attributed.

Precipitation measure occurs daily at 08:00 Beijing time (UTC +8). All data undergo strict quality control by CMA NCC. Errors from relocation, measurement and other reasons are corrected, and the datasets are homogenized. The stations we chose are all in the first level of national meteorological observation where the quality of data is highest, and the data source is the same as many other studies in China. However, the corrections applied did not include wind correction. The uncertainty caused has a smaller impact on extreme precipitation studied in our work, and the error is less than 3% as indicated by the result of experiment.

APPENDIX B

Divisions of epochs for each month (April-October) are listed below. There are 60 (September, "post dam II") to 180 (April, "pre dam") days in each epoch.

| | Pre Dam | Post Dam | Post Dam II |
|---|---|---|---|
| April | 1998-2003 | 2004-2006 | 2008, 2009 |
| May | 1998-2000 | 2004-2006 | 2007-2009 |
| June | 1998-2000, 2002 | 2003-2006 | 2007-2009 |
| July | 1998, 2000 | 2003-2005 | 2007-2009 |
| August | 1999-2001 | 2003-2005 | 2008, 2009 |
| September | 1999-2001 | 2003-2006 | 2008, 2009 |
| October | 1998-2002 | 2003-2005 | 2007-2009 |

REFERENCES


Abbs, D. J. (1986), Sea-breeze interactions along a concave coastline in southern Australia-observations and numerical modeling study, *Monthly Weather Review*, *114*(5), 831-848.

Abbs, D. J., and W. L. Physick (1992), Sea-breeze observations and modelling: a review, *Australian Meteorological Magazine*, *41*, 7-19.

Alexander, L. V., et al. (2006), Global observed changes in daily climate extremes of temperature and precipitation, *Journal of Geophysical Research-Atmospheres*, *111*(D5), D05109.

Anyah, R. O., F. H. M. Semazzi, and L. Xie (2006), Simulated physical mechanisms associated with climate variability over Lake Victoria basin in East Africa, *Monthly Weather Review*, *134*(12), 3588-3609.

Arritt, R. W. (1987), The effect of water-surface temperature on lake breezes and thermal internal boundary-layers, *Boundary-Layer Meteorology*, *40*(1-2), 101-125.

Arritt, R. W. (1993), Effects of the large-scale flow on characteristic features of the sea breeze, *Journal of Applied Meteorology*, *32*(1), 116-125.

Atkinson, B. W. (1981), *Meso-scale atmospheric circulations*, 495 pp., Academic Press, London.

Avissar, R., and Y. Q. Liu (1996), Three-dimensional numerical study of shallow convective clouds and precipitation induced by land surface forcing, *Journal of Geophysical Research-Atmospheres*, *101*(D3), 7499-7518.

Barnston, A. G., and P. T. Schickedanz (1984), The effect of irrigation on warm season precipitation in southern Great Plains, *Journal of Climate and Applied Meteorology*, *23*(6), 865-888.

Barrett, E., J. Dodge, M. Goodman, J. Janowiak, C. Kidd, and E. Smith (1994), The first WETNET intercomparison project (PIP-1), *Remote Sensing Reviews*, *11*, 49-60.

Bedient, P. B., and W. C. Huber (2002), *Hydrology and floodplain analysis, 3rd edition*, 35-36 pp, Prentice Hall, Inc., Upper Saddle River, NJ.

Bounoua, L., G. J. Collatz, S. O. Los, P. J. Sellers, D. A. Dazlich, C. J. Tucker, and D. A. Randall (2000), Sensitivity of climate to changes in NDVI, *Journal of Climate*, *13*(13), 2277-2292.

Camberlin, P. (1997), Rainfall anomalies in the source region of the Nile and their connection with the Indian summer monsoon, *Journal of Climate*, *10*(6), 1380-1392.

Chang, C. P., Y. S. Zhang, and T. Li (2000), Interannual and interdecadal variations of the East Asian summer monsoon and tropical Pacific SSTs. Part I: Roles of the subtropical ridge, *Journal of Climate*, *13*(24), 4310-4325.

Chase, T. N., R. A. Pielke, T. G. F. Kittel, J. S. Baron, and T. J. Stohlgren (1999), Potential impacts on Colorado Rocky Mountain weather due to land use changes on the adjacent Great Plains, *Journal of Geophysical Research-Atmospheres*, *104*(D14), 16673-16690.

Chau, K. C. (1995), Three Gorges Project of China: Resettlement prospects and problems, *Ambio*, *24*(2), 98-102.

Cheng, Y. Y., and D. W. Byun (2008), Application of high resolution land use and land cover data for atmospheric modeling in the Houston-Galveston metropolitan area, Part I: Meteorological simulation results, *Atmospheric Environment*, *42*(33), 7795-7811.

Crosman, E. T., and J. D. Horel (2010), Sea and lake breezes: a review of numerical studies, *Boundary-Layer Meteorology*, *137*(1), 1-29.

Dandou, A., M. Tombrou, and N. Soulakellis (2009), The Influence of the City of Athens on the Evolution of the Sea-Breeze Front, *Boundary-Layer Meteorology*, *131*(1), 35-51.

De Fries, R. S., M. Hansen, J. R. G. Townshend, and R. Sohlberg (1998), Global land cover classifications at 8 km spatial resolution: the use of training data derived from Landsat imagery in decision tree classifiers, *International Journal of Remote Sensing*, *19*(16), 3141-3168.

DeAngelis, A., F. Dominguez, Y. Fan, A. Robock, M. D. Kustu, and D. Robinson (2010), Evidence of enhanced precipitation due to irrigation over the Great Plains of the United States, *Journal of Geophysical Research-Atmospheres*, *115*, D15115.

Degu, A. M., F. Hossain, D. Niyogi, R. Pielke, J. M. Shepherd, N. Voisin, and T. Chronis (2011), The influence of large dams on surrounding climate and precipitation patterns, *Geophysical Research Letters*, *38* (In Press).

Dias, M., P. L. S. Dias, M. Longo, D. R. Fitzjarrald, and A. S. Denning (2004), River breeze circulation in eastern Amazonia: observations and modelling results, *Theoretical and Applied Climatology*, *78*(1-3), 111-121.

Ding, Y. H., Z. Y. Wang, and Y. Sun (2008), Inter-decadal variation of the summer precipitation in East China and its association with decreasing Asian summer monsoon. Part I: Observed evidences, *International Journal of Climatology*, *28*(9), 1139-1161.

Ding, Y. H., Y. J. Liu, Y. Sun, and Y. F. Song (2010), Weakening of the Asian summer monsoon and its impact on the precipitation pattern in China, *International Journal of Water Resources Development*, *26*(3), 423-439.

Ding, Y. H., Y. Sun, Z. Y. Wang, Y. X. Zhu, and Y. F. Song (2009), Inter-decadal variation of the summer precipitation in China and its association with decreasing Asian summer monsoon Part II: Possible causes, *International Journal of Climatology*, *29*(13), 1926-1944.

Easterling, D. R., T. W. R. Wallis, J. H. Lawrimore, and R. R. Heim (2007), Effects of temperature and precipitation trends on US drought, *Geophysical Research Letters*, *34*(20).

Easterling, D. R., J. L. Evans, P. Y. Groisman, T. R. Karl, K. E. Kunkel, and P. Ambenje (2000), Observed variability and trends in extreme climate events: A brief review, *Bulletin of the American Meteorological Society*, *81*(3), 417-425.

Edmonds, R. L. (1992), The Sanxia (3 Gorges) project-the environmental argument surrounding China super dam, *Global Ecology and Biogeography Letters*, *2*(4), 105-125.

Eltahir, E. A. B., and R. L. Bras (1996), Precipitation recycling, *Reviews of Geophysics*, *34*(3), 367-378.

Fang, Z., D. Hang, and Z. Xinyi (2010), Rainfall regime in Three Gorges area in China and the control factors, *International Journal of Climatology*, *30*(9), 1396-1406.

Feddema, J. J., K. W. Oleson, G. B. Bonan, L. O. Mearns, L. E. Buja, G. A. Meehl, and W. M. Washington (2005), The importance of land-cover change in simulating future climates, *Science*, *310*(5754), 1674-1678.

Fitzjarrald, D. R., R. K. Sakai, O. L. L. Moraes, R. C. de Oliveira, O. C. Acevedo, M. J. Czikowsky, and T. Beldini (2008), Spatial and temporal rainfall variability near the Amazon-Tapajos confluence, *Journal of Geophysical Research-Biogeosciences*, *113*, G00B11.

Førland, E. J., H. Alexandersson, A. Drebs, H. Hanssen-Bauer Vedin, and O. E. Tveito (1998), Trends in maximum 1-day precipitation in the Nordic region, DNMI Report 14/98 klima, 1-55 pp, Norwegian Meteorological Institute, Oslo.

Freitas, E. D., C. M. Rozoff, W. R. Cotton, and P. L. S. Dias (2007), Interactions of an urban heat island and sea-breeze circulations during winter over the metropolitan area of Sao Paulo, Brazil, *Boundary-Layer Meteorology*, *122*(1), 43-65.

Fuhrer, J., M. Beniston, A. Fischlin, C. Frei, S. Goyette, K. Jasper, and C. Pfister (2006), Climate risks and their impact on agriculture and forests in Switzerland, *Climatic Change*, *79*(1-2), 79-102.

Gao, F., and G. Chen (1987), *Some analyses of environmental capacity for migration in the reservoir area*, In: Studies on the Ecological and Environmental Impacts of The Three Gorges Project and the Remedies. The Three Gorges Project Ecology and Environment Study Group, Chinese Academy of Science, Science Publication Institute, Beijing (In Chinese).

Garbrecht, G. (1986), Wasserspeicher (Talsperren) in der Antike, *Antike Welt. 2nd special edition: Antiker Wasserbau*, 51-64 pp (*52*).

Groisman, P. Y., T. R. Karl, D. R. Easterling, R. W. Knight, P. F. Jamason, K. J. Hennessy, R. Suppiah, C. M. Page, J. Wibig, K. Fortuniak, V. N. Razuvaev, A. Douglas, E. Forland, and P. M. Zhai (1999), Changes in the probability of heavy precipitation: Important indicators of climatic change, *Climatic Change*, *42*(1), 243-283.

Groisman, P. Y., R. W. Knight, D. R. Easterling, T. R. Karl, G. C. Hegerl, and V. A. N. Razuvaev (2005), Trends in intense precipitation in the climate record, *Journal of Climate*, *18*(9), 1326-1350.

Gwynne, P., and Y. Q. Li (1992), China-Yangtze project dammed with faint praise, *Nature*, *356*(6372), 736-736.

Han, W., S. Burian, and J. M. Shepherd (2010), Assessment of satellite-based rainfall estimates in urban areas in different geographic and climatic regions, *Natural Hazards* (In Press).

Hand, L. M., and J. M. Shepherd (2009), An investigation of warm-season spatial rainfall variability in Oklahoma City: possible linkages to urbanization and prevailing wind, *Journal of Applied Meteorology and Climatology*, *48*(2), 251-269.

Hannachi, A., I. Joliffe, and D. Stephenson (2007), Empirical orthogonal functions and related techniques in atmospheric science: A review. *International Journal of Climatology*, *27*, 1119–1152.

Holzman, B. (1937), Sources of moisture for precipitation in the United States, *Technical Bulletin 589, U.S. Department of Agriculture.*, *589*, 41.

Horton, R. (1943), Hydrologic interrelations between lands and oceans, *EOS Transactions (AGU)*, *24*, 753-764.

Hossain, F., I. Jeyachandran, and R. Pielke (2009), Have large dams altered extreme precipitation patterns?, *EOS Transactions (AGU)*, *90* (48), 453-454.

Hossain, F., I. Jeyachandran, and R. Pielke (2010), Dam safety effects due to human alteration of extreme precipitation, *Water Resources Research*, *46*, W03301.

Hu, Z. Z. (1997), Interdecadal variability of summer climate over East Asia and its association with 500 hPa height and global sea surface temperature, *Journal of Geophysical Research-Atmospheres*, *102*(D16), 19403-19412.

Huffman, G. J., R. F. Adler, D. T. Bolvin, G. J. Gu, E. J. Nelkin, K. P. Bowman, Y. Hong, E. F. Stocker, and D. B. Wolff (2007), The TRMM multisatellite precipitation analysis (TMPA): Quasi-global, multiyear, combined-sensor precipitation estimates at fine scales, *Journal of Hydrometeorology*, *8*(1), 38-55.

Huntley, B., R. Baxter, K. J. Lewthwaite, S. G. Willis, and J. K. Adamson (1998), Vegetation responses to local climatic changes induced by a water-storage reservoir, *Global Ecology and Biogeography Letters*, *7*(4), 241-257.

Iwashima, T., and R. Yamamoto (1993), A statistical-analysis of the extreme events-long-term trend of heavy daily precipitation, *Journal of the Meteorological Society of Japan*, *71*(5), 637-640.

Jackson, R. B., E. G. Jobbagy, R. Avissar, S. B. Roy, D. J. Barrett, C. W. Cook, K. A. Farley, D. C. le Maitre, B. A. McCarl, and B. C. Murray (2005), Trading water for carbon with biological sequestration, *Science*, *310*(5756), 1944-1947.

Jensen, J. C. (1935), The relation between surface evaporation from lakes and ponds to precipitation from local thunderstorms in the drought area, *Bulletin of American Meteorological Society*, *16*, 142-145.

Jiang, T., B. Su, and H. Hartmann (2007), Temporal and spatial trends of precipitation and river flow in the Yangtze River Basin, 1961-2000, *Geomorphology*, *85*(3-4), 143-154.

Ju, J. H., and J. Slingo (1995), The Asian summer monsoon and ENSO, *Quarterly Journal of the Royal Meteorological Society*, *121*(525), 1133-1168.

Jung, H. S., Y. Choi, J. H. Oh, and G. H. Lim (2002), Recent trends in temperature and precipitation over South Korea, *International Journal of Climatology*, *22*(11), 1327-1337.

Kalnay, E., M. Kanamitsu, R. Kistler, W. Collins, D. Deaven, L. Gandin, M. Iredell, S. Saha, G. White, J. Woollen, Y. Zhu, M. Chelliah, W. Ebisuzaki, W. Higgins, J. Janowiak, K. C. Mo, C. Ropelewski, J. Wang, A. Leetmaa, R. Reynolds, R. Jenne, and D. Joseph (1996), The NCEP/NCAR 40-year reanalysis project, *Bulletin of the American Meteorological Society*, *77*(3), 437-471.

Karl, T. R., and R. W. Knight (1998), Secular trends of precipitation amount, frequency, and intensity in the United States, *Bulletin of the American Meteorological Society*, *79*(2), 231-241.

Karl, T. R., R. W. Knight, and N. Plummer (1995), Trends in high-frequency climate variability in the 20th-century, *Nature*, *377*(6546), 217-220.

Kiage, L. M., K. B. Liu, N. D. Walker, N. Lam, and O. K. Huh (2007), Recent land-cover/use change associated with land degradation in the Lake Baringo catchment, Kenya, East Africa: evidence from Landsat TM and ETM, *International Journal of Remote Sensing*, *28*(19), 4285-4309.

Kunkel, K. E., R. A. Pielke, and S. A. Changnon (1999), Temporal fluctuations in weather and climate extremes that cause economic and human health impacts: A review, *Bulletin of the American Meteorological Society*, *80*(6), 1077-1098.

Kusaka, H., F. Kimura, H. Hirakuchi, and M. Mizutori (2000), The effects of land-use alteration on the sea breeze and daytime heat island in the Tokyo metropolitan area, *Journal of the Meteorological Society of Japan*, *78*(4), 405-420.

Lemonsu, A., S. Bastin, V. Masson, and P. Drobinski (2006), Vertical structure of the urban boundary layer over Marseille under sea-breeze conditions, *Boundary-Layer Meteorology*, *118*(3), 477-501.

Liu, H. Q., Z. B. Sun, and W. J. Zhu (2003), Relationship of inter-decadal variations of snow over the Tibetan plateau and the Asian summer monsoon circulation, *Journal of Nanjing Institute of Meteorology*, *26*, 734-739 (In Chinese).

Liu, H. Q., Z. B. Sun, J. Wang, and J. Z. Min (2004), A modeling study of the effects of anomalous snow cover over the Tibetan Plateau upon the South Asian summer monsoon, *Advances in Atmospheric Sciences*, *21*(6), 964-975.

Lohar, D., and B. Pal (1995), The effect of irrigation on premonsoon season precipitation over South-West Bengal, India, *Journal of Climate*, *8*(10), 2567-2570.

Mahmood, R., R. A. Pielke, K. G. Hubbard, D. Niyogi, G. Bonan, P. Lawrence, R. McNider, C. McAlpine, A. Etter, S. Gameda, B. D. Qian, A. Carleton, A. Beltran-Przekurat, T. Chase, A. I. Quintanar, J. O. Adegoke, S. Vezhapparambu, G. Conner, S. Asefi, E. Sertel, D. R. Legates, Y. L. Wu, R. Hale, O. W. Frauenfeld, A. Watts, M. Shepherd, C. Mitra, V. G. Anantharaj, S. Fall, R. Lund, A. Trevino, P. Blanken, J. Y. Du, H. I. Chang, R. E. Leeper, U. S. Nair, S. Dobler, R. Deo, and J. Syktus (2010), Impacts of land use/land cover change on climate and future research priorities, *Bulletin of the American Meteorological Society*, *91*(1), 37-46.

Mason, S. J., P. R. Waylen, G. M. Mimmack, B. Rajaratnam, and J. M. Harrison (1999), Changes in extreme rainfall events in South Africa, *Climatic Change*, *41*(2), 249-257.

May, W. (2008), Potential future changes in the characteristics of daily precipitation in Europe simulated by the HIRHAM regional climate model, *Climate Dynamics*, *30*(6), 581-603.

Miller, N. L., J. M. Jin, and C. F. Tsang (2005), Local climate sensitivity of the Three Gorges Dam, *Geophysical Research Letters*, *32*(16).

Mote, T. L., M. C. Lacke, and J. M. Shepherd (2007), Radar signatures of the urban effect on precipitation distribution: A case study for Atlanta, Georgia, *Geophysical Research Letters*, *34, L20710*.

Murphy, B. F., and B. Timbal (2008), A review of recent climate variability and climate change in southeastern Australia, *International Journal of Climatology*, *28*(7), 859-879.

Nair, U. S., D. K. Ray, R. O. Lawton, R. M. Welch, R. A. S. Pielke, and co-authors (2006), *Impact of deforestation on orographic cloud formation in a complex tropical environment*, In: Mountains in the Mist, Science for conserving and managing Tropical Montane Cloud Forest. (eds. L. A. Bruijnzeel, J. Juvik, F. Scatena, L. Hamilton and P. Bubb), University of Hawaii Press, Hawaii.

National Climate Center (NCC) (1998), *Heavy Flooding and Climate Anomalies in China in 1998*, China Meteorological Press, Beijing (In Chinese).

National Research Council (2005), *Radiative forcing of climate change: Expanding the concept and addressing uncertainties*, 208 pp., The National Academies Press, Washington, D.C.

Ogawa, S., W. M. Sha, T. Iwasaki, and Z. F. Wang (2003), A numerical study on the interaction of a sea-breeze front with convective cells in the daytime boundary layer, *Journal of the Meteorological Society of Japan*, *81*(4), 635-651.

Ohashi, Y., and H. Kida (2002), Local circulations developed in the vicinity of both coastal and inland urban areas: A numerical study with a mesoscale atmospheric model, *Journal of Applied Meteorology*, *41*(1), 30-45.

Ohashi, Y., and H. Kida (2004), Local circulations developed in the vicinity of both coastal and inland urban areas. Part II: Effects of urban and mountain areas on moisture transport, *Journal of Applied Meteorology*, *43*(1), 119-133.

Outlaw, D. E., and M. P. Murphy (2000), A Radar-based climatology of July convective initiation in Georgia and surrounding area. *Eastern Region Technical Attachment.* NO. 2000-04.

Peng, W., C. F. Shuai, and X. Xin (2010), Yangtze River: China's golden waterway, *Proceedings of the Institution of Civil Engineers-Civil Engineering*, *163*(5), 15-18.

Physick, W. (1976), Numerical-model of sea-breeze phenomenon over a lake or gulf, *Journal of the Atmospheric Sciences*, *33*(11), 2107-2135.

Pielke, R. A., T. J. Lee, J. H. Copeland, J. L. Eastman, C. L. Ziegler, and C. A. Finley (1997), Use of USGS-provided data to improve weather and climate simulations, *Ecological Applications*, *7*(1), 3-21.

Pielke, R. A., R. L. Walko, L. T. Steyaert, P. L. Vidale, G. E. Liston, W. A. Lyons, and T. N. Chase (1999), The influence of anthropogenic landscape changes on weather in south Florida, *Monthly Weather Review*, *127*(7), 1663-1673.

Pielke, R. A., J. Adegoke, A. Beltran-Przekurat, C. A. Hiemstra, J. Lin, U. S. Nair, D. Niyogi, and T. E. Nobis (2007), An overview of regional land-use and land-cover impacts on rainfall, *Tellus Series B-Chemical and Physical Meteorology*, *59*(3), 587-601.

Plank, C., and B. Shuman (2009), Drought-driven changes in lake areas and their effects on the surface energy balance of Minnesota's Lake-dotted landscape, *Journal of Climate*, *22*(15), 4055-4065.

Porson, A., D. G. Steyn, and G. Schayes (2007a), Sea-breeze scaling from numerical model simulations, part II: Interaction between the sea breeze and slope flows, *Boundary-Layer Meteorology*, *122*(1), 31-41.

Porson, A., D. G. Steyn, and G. Schayes (2007b), Sea-breeze scaling from numerical model simulations, Part I: Pure sea breezes, *Boundary-Layer Meteorology*, *122*(1), 17-29.

Qian, Y. F., Y. Q. Zheng, Y. Zhang, and M. Q. Miao (2003), Responses of China's summer monsoon climate to snow anomaly over the Tibetan Plateau, *International Journal of Climatology*, *23*(6), 593-613.

Ramos, M. C., and J. A. Martinez-Casasnovas (2006), Trends in precipitation concentration and extremes in the Mediterranean Penedes-Anoia region, NE Spain, *Climatic Change*, *74*(4), 457-474.

Rao, P. A., H. E. Fuelberg, and K. K. Droegemeier (1999), High-resolution modeling of the Cape Canaveral area land-water circulations and associated features, *Monthly Weather Review, 127*(8), 1808-1821.

Ray, D. K., R. A. Pielke, U. S. Nair, R. M. Welch, and R. O. Lawton (2009), Importance of land use versus atmospheric information verified from cloud simulations from a frontier region in Costa Rica, *Journal of Geophysical Research-Atmospheres, 114*, D08113.

Rocha, A., P. Melo-Goncalves, C. Marques, J. Ferreira, and J. M. Castanheira (2008), High-frequency precipitation changes in southeastern Africa due to anthropogenic forcing, *International Journal of Climatology, 28*(9), 1239-1253.

Rosenfeld, D., U. Lohmann, G. B. Raga, C. D. O'Dowd, M. Kulmala, S. Fuzzi, A. Reissell, and M. O. Andreae (2008), Flood or drought: How do aerosols affect precipitation?, *Science, 321*(5894), 1309-1313.

Rotstayn, L. D., M. D. Keywood, B. W. Forgan, A. J. Gabric, I. E. Galbally, J. L. Gras, A. K. Luhar, G. H. McTainsh, R. M. Mitchell, and S. A. Young (2009), Possible impacts of anthropogenic and natural aerosols on Australian climate: a review, *International Journal of Climatology, 29*(4), 461-479.

Rotunno, R. (1983), On the linear-theory of the land and sea breeze, *Journal of the Atmospheric Sciences, 40*(8), 1999-2009.

Rudolf, B., H. Hauschild, R. W., and U. Schneider (1994), Terrestrial precipitation analysis: Operational method and required density of point measurements. Global Precipitation and Climate Change. NATO ASI Series *I*(26), 173-186 pp, Springer, Verlag Berin Heidelberg.

Ruelland, D., A. Dezetter, C. Puech, and S. Ardoin-Bardin (2008), Long-term monitoring of land cover changes based on Landsat imagery to improve hydrological modelling in West Africa, *International Journal of Remote Sensing, 29*(12), 3533-3551.

Scho¨nwiese, C. D., and J. Rapp (1997), *Climate trend atlas of Europe based on observations 1891-1990*, Kluwer Academic Publishers, Dordrecht.

Scott, R. W., and F. A. Huff (1996), Impacts of the Great Lakes on regional climate conditions, *Journal of Great Lakes Research, 22*(4), 845-863.

Segal, M., and R. W. Arritt (1992), Nonclassical mesoscale circulations caused by surface sensible heat-flux gradients, *Bulletin of the American Meteorological Society, 73*(10), 1593-1604.

Segal, M., Y. Mahrer, and R. A. Pielke (1983), A study of meteorological patterns associated with a lake confined by mountains-the dead-sea case, *Quarterly Journal of the Royal Meteorological Society*, *109*(461), 549-564.

Segal, M., M. Leuthold, R. W. Arritt, C. Anderson, and J. Shen (1997), Small lake daytime breezes: Some observational and conceptual evaluations, *Bulletin of the American Meteorological Society*, *78*(6), 1135-1147.

Semenov, V. A., and L. Bengtsson (2002), Secular trends in daily precipitation characteristics: greenhouse gas simulation with a coupled AOGCM, *Climate Dynamics*, *19*(2), 123-140.

Shen, G. Z., and Z. Q. Xie (2004), Three Gorges Project: Chance and challenge, *Science*, *304*(5671), 681-681.

Shepherd, J. M. (2005), A review of current investigations of urban-induced rainfall and recommendations for the future, *Earth Interactions*, *9*(12), 1-27.

Shepherd, J. M. (2006), Evidence of urban-induced precipitation variability in arid climate regimes, *Journal of Arid Environments*, *67*(4), 607-628.

Shepherd, J. M., M. Carter, M. Manyin, D. Messen, and S. Burian (2010), The impact of urbanization on current and future coastal precipitation: a case study for Houston, *Environment and Planning B-Planning & Design*, *37*(2), 284-304.

Sills, D. M. L. (1998), Lake and land breezes in southwestern Ontario: observations, analyses and numerical modeling, 338 pp, York University, York.

Simpson, J. E., D. A. Mansfield, and J. R. Milford (1977), Inland penetration of sea-breeze fronts, *Quarterly Journal of the Royal Meteorological Society*, *103*(435), 47-76.

Stidd, C. K. (1975), Irrigation increases rainfall, *Science*, *188*(4185), 279-280.

Stivari, S. M. S., A. P. De Oliveira, and J. Soares (2005), On the climate impact of the local circulation in the Itaipu Lake area, *Climatic Change*, *72*(1-2), 103-121.

Stivari, S. M. S., A. P. de Oliveira, H. A. Karam, and J. Soares (2003), Patterns of local circulation in the Itaipu Lake area: Numerical simulations of lake breeze, *Journal of Applied Meteorology*, *42*(1), 37-50.

Tan, Y., and F. J. Yao (2006), Three Gorges project: Effects of resettlement on the environment in the reservoir area and countermeasures, *Population and Environment*, *27*(4), 351-371.

Taschetto, A. S., and M. H. England (2009), An analysis of late twentieth century trends in Australian rainfall, *International Journal of Climatology*, *29*(6), 791-807.

Thiessen, A. H. (1911), Precipitation averages for large areas, *Monthly Weather Review*, *39*(7), 1082-1084.

Thompson, W. T., T. Holt, and J. Pullen (2007), Investigation of a sea breeze front in an urban environment, *Quarterly Journal of the Royal Meteorological Society*, *133*, 579-594.

Tian, Y. D., C. D. Peters-Lidard, B. J. Choudhury, and M. Garcia (2007), Multitemporal analysis of TRMM-based satellite precipitation products for land data assimilation applications, *Journal of Hydrometeorology*, *8*(6), 1165-1183.

Tian, Y. D. and C. D. Peters-Lidard (2010), A global map of uncertainties in satellite-based precipitation measurements, *Geophysical Research Letters*, *37*, L24407.

Tijm, A. B. C., A. J. Van Delden, and A. A. M. Holtslag (1999), The inland penetration of sea breezes, *Contributions to Atmospheric Physics*, *72*, 317-328.

Tomassetti, B., F. Giorgi, M. Verdecchia, and G. Visconti (2003), Regional model simulation of the hydrometeorological effects of the Fucino Lake on the surrounding region, *Annales Geophysicae*, *21*(11), 2219-2232.

Trenberth, K. E. (1998), Atmospheric moisture residence times and cycling: Implications for rainfall rates and climate change, *Climatic Change*, *39*(4), 667-694.

Trenberth, K.E., P.D. Jones, P. Ambenje, R. Bojariu, D. Easterling, A. Klein Tank, D. Parker, F.Rahimzadeh, J.A. Renwick, M. Rusticucci, B. Soden, and P. Zhai (2007), Observations: Surface and atmospheric climate change, In S. Solomon et al. (ed.) Climate Change 2007: The physical science basis. Contribution of Working Group I to the Fourth Assessment Report of the Intergovernmental Panel on Climate Change, Cambridge Univ. Press, Cambridge, UK.

Vogelmann, J. E., T. L. Sohl, P. V. Campbell, and D. M. Shaw (1998), Regional land cover characterization using Landsat thematic mapper data and ancillary data sources, *Environmental Monitoring and Assessment*, *51*(1-2), 415-428.

Walsh, J. E. (1974), Sea breeze theory and applications, *Journal of the Atmospheric Sciences*, *31*(8), 2012-2026.

Wang, H. J. (2001), The weakening of the Asian monsoon circulation after the end of 1970's, *Advances in Atmospheric Sciences*, *18*(3), 376-386.

Wang, J. Z. (2002), Three Gorges Project: The largest water conservancy project in the world, *Public Administration and Development*, *22*(5), 369-375.

Wang, Y., M. Liao, G. Sun, and J. Gong (2005), Analysis of the water volume, length, total area and inundated area of the Three Gorges Reservoir, China using the SRTM DEM data, *International Journal of Remote Sensing*, *26*(18), 4001-4012.

World Commission on Dams (2000), Dams and development: A new framework for decision making, World Commission on Dams Report, Nov. 16.

Weng, H. Y., K. M. Lau, and Y. K. Xue (1999), Multi-scale summer rainfall variability over China and its long-term link to global sea surface temperature variability, *Journal of the Meteorological Society of Japan*, *77*(4), 845-857.

Weymouth, G., G. A. Mills, D. Jones, E. E. Ebert, and M. J. Manton (1999), A continental-scale daily rainfall analysis system, *Australian Meteorological Magazine*, *48*(3), 169-179.

Wu, J., C. Fu, Y. Xu, J. P. Tang, W. Wang, and Z. Wang (2008), Simulation of direct effects of black carbon aerosol on temperature and hydrological cycle in Asia by a Regional Climate Model, *Meteorology and Atmospheric Physics*, *100*(1-4), 179-193.

Wu, J., C. B. Fu, Y. Y. Xu, J. P. Tang, Z. W. Han, and R. H. Zhang (2009), Effects of total aerosol on temperature and precipitation in East Asia, *Climate Research*, *40*(1), 75-87.

Wu, L. G., Q. Zhang, and Z. H. Jiang (2006), Three Gorges Dam affects regional precipitation, *Geophysical Research Letters*, *33*(13).

Wu, T. W., and Z. A. Qian (2003), The relation between the Tibetan winter snow and the Asian summer monsoon and rainfall: An observational investigation, *Journal of Climate*, *16*(12), 2038-2051.

Xian, G., C. Homer, and J. Fry (2009), Updating the 2001 National Land Cover Database land cover classification to 2006 by using Landsat imagery change detection methods, *Remote Sensing of Environment*, *113*(6), 1133-1147.

Xiao, C., R. C. Yu, and Y. F. Fu (2010), Precipitation characteristics in the Three Gorges Dam vicinity, *International Journal of Climatology*, *30*(13), 2021-2024.

Yan, H., and R. A. Anthes (1987), The effect of latitude on the sea breeze, *Monthly Weather Review*, *115*(5), 936-956.

Yang, F. L., and K. M. Lau (2004), Trend and variability of China precipitation in spring and summer: Linkage to sea-surface temperatures, *International Journal of Climatology*, *24*(13), 1625-1644.

Yoshikado, H. (1990), Vertical structure of the sea breeze penetrating through a large urban complex, *Journal of Applied Meteorology*, *29*(9), 878-891.

Yoshikado, H. (1992), Numerical study of the daytime urban effect and its interaction with the sea breeze, *Journal of Applied Meteorology*, *31*(10), 1146-1164.

Zhai, P. M., X. B. Zhang, H. Wan, and X. H. Pan (2005), Trends in total precipitation and frequency of daily precipitation extremes over China, *Journal of Climate*, *18*(7), 1096-1108.

Zhang, Y. S., T. Li, and B. Wang (2004), Decadal change of the spring snow depth over the Tibetan Plateau: The associated circulation and influence on the East Asian summer monsoon, *Journal of Climate*, *17*(14), 2780-2793.

Zhong, S. Y., J. M. Leone, and E. S. Takle (1991), Interaction of the sea breeze with a river breeze in an area of complex coastal heating, *Boundary-Layer Meteorology*, *56*(1-2), 101-139.

Zhu, X. H. (1999), The research on characteristics of flood from 1840 to 1996 in China, *Journal of Catastrophology*, *14*(2), 7-12 (In Chinese).

Zwiers, F. W. (1993), Simulation of the Asian summer monsoon with the CCC GCM-1, *Journal of Climate*, *6*(3), 470-486.